

Electronic Supplementary Information (ESI) for:

Blended Vinyllogous Urethane/Urea Vitrimers Derived from Aromatic Alcohols

Philipp Haida,^a

Gloria Signorato,^a and Volker Abetz^{a,b*}

^aInstitute of Physical Chemistry, Universität Hamburg, Martin-Luther-King-Platz 6, 20146 Hamburg, Germany

^bHelmholtz-Zentrum Hereon, Institute of Membrane Research, Max-Planck-Straße 1, 21502 Geesthacht, Germany.

E-Mail: volker.abetz@hereon.de

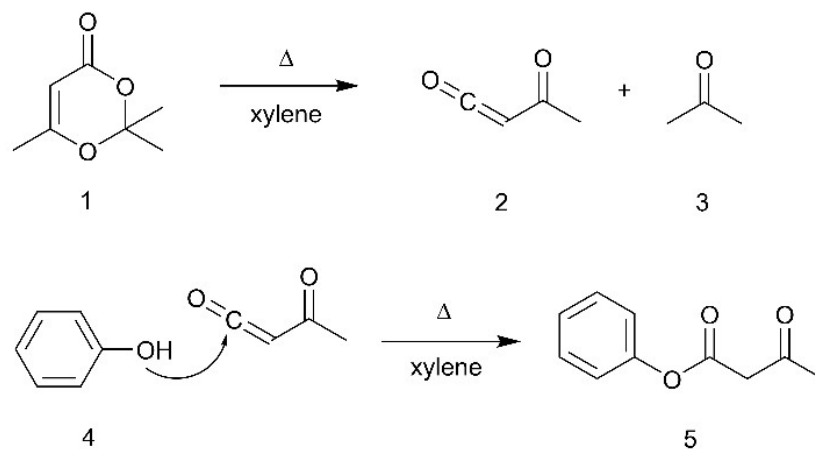


Fig. S1 Schematic representation of the synthesis route for the acetoacetylation of aromatic alcohols using TMDO (1). TMDO undergoes a retro-Diels Alder reaction at temperatures above 110 °C, releasing a reactive acetylketene (2) and acetone (3), while the acetylketene undergoes a fast addition reaction with the aromatic alcohol (4) to give the desired aromatic acetoacetate (5).

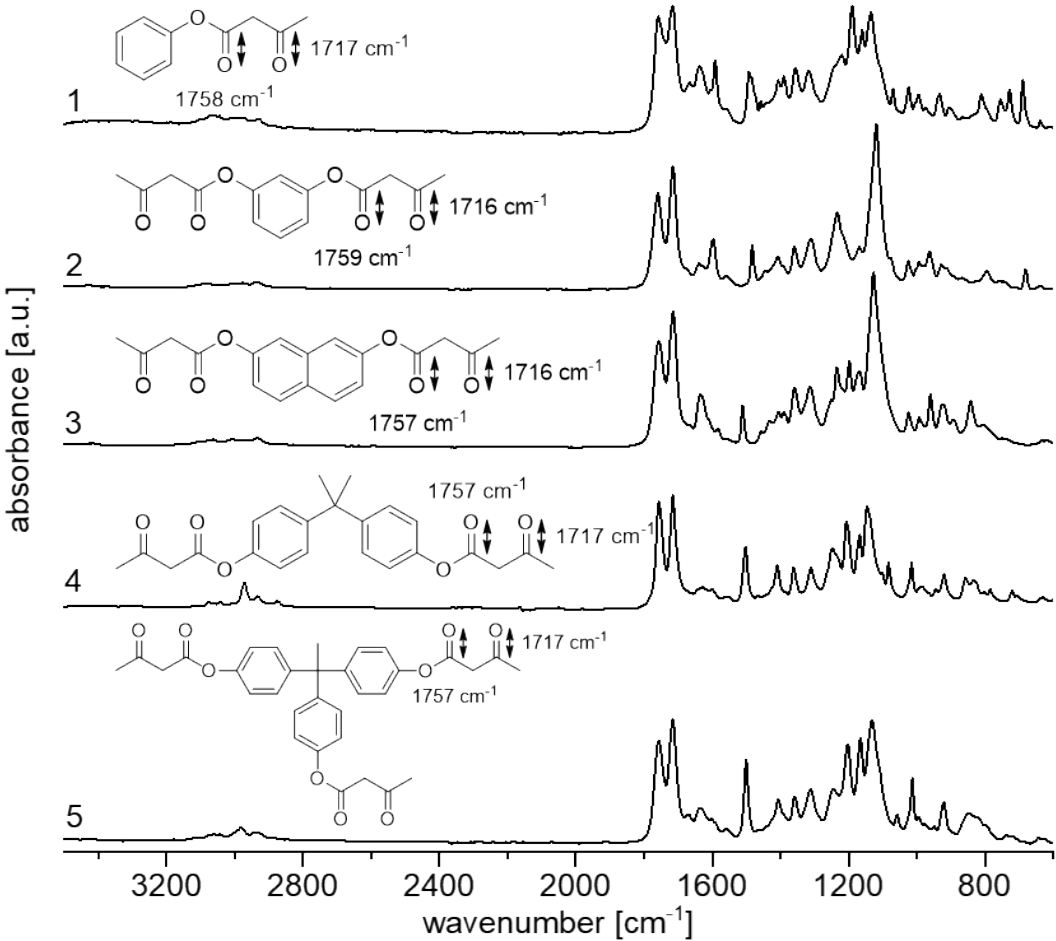


Fig. S2a Full ATR-FT-IR spectra of the synthesized acetoacetate monomers phenyl-3-oxobutanoate (PH)(1), 1,3-phenylene bis(3-oxobutanoate) (RE)(2), naphthalene-2,7-diyl bis(3-oxobutanoate) (NDO)(3), propane-2,2-diylbis(4,1-phenylene) bis(3-oxobutanoate) (BPA)(4) and ethane-1,1,1-triyltris(benzene-4,1-diyl) tris(3-oxobutanoate) (THPE)(5).

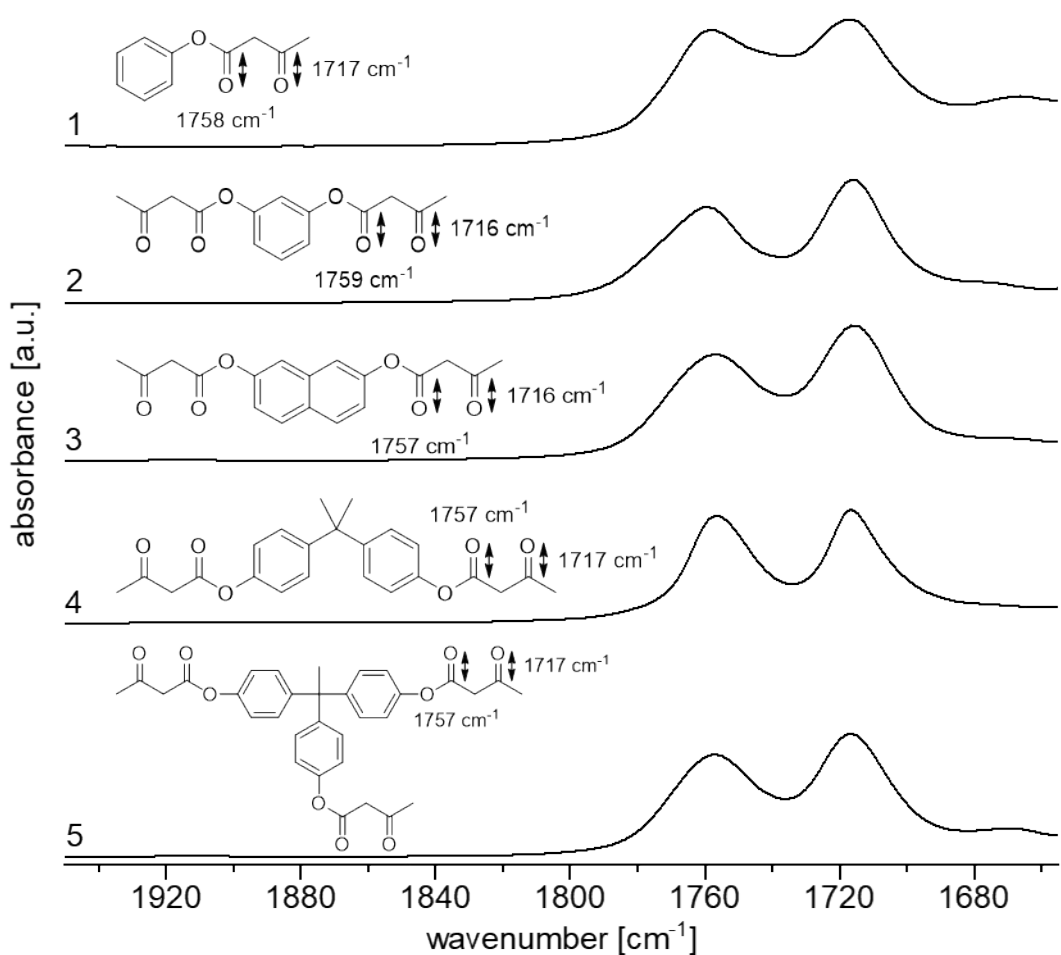


Fig. S2b ATR-FT-IR spectra of the synthesized acetoacetate-monomers PH (1), RE (2), NDO (3), BPA (4) and THPE (5) with the focus on the characteristic C=O ester (1757–1759 cm⁻¹) and C=O ketone bands (1716–1717 cm⁻¹).

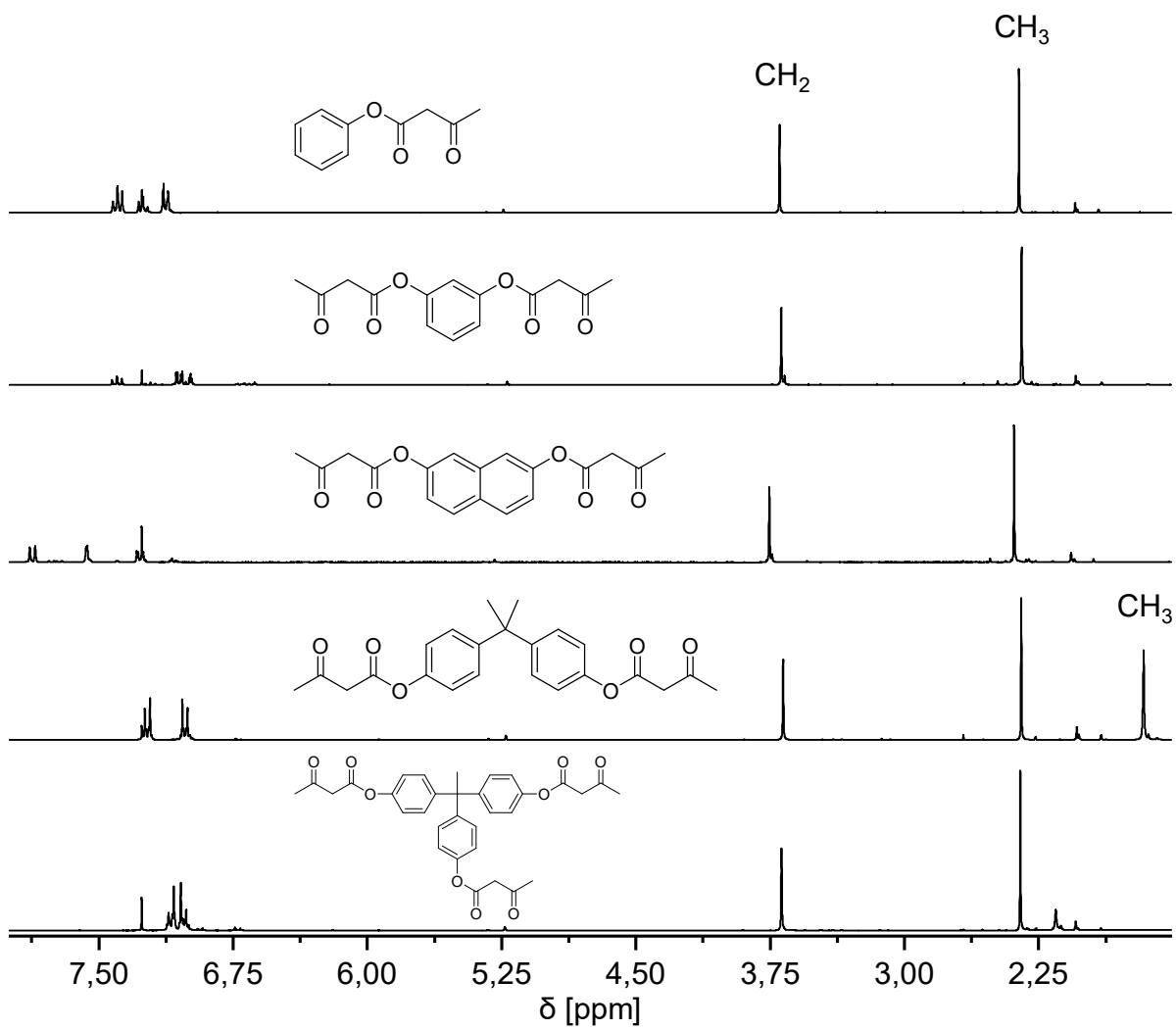


Fig. S3a ^1H NMR (CDCl_3 , 25 °C) spectra of the synthesized acetoacetate monomers PH, RE, NDO, BPA and THPE (from top to bottom). The characteristic CH_2 and CH_3 signals appear at similar chemical shifts. A detailed list of all signals is provided in the experimental section.

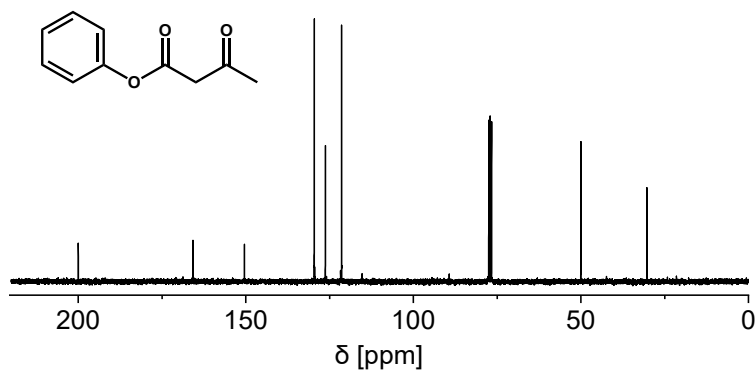


Fig. S3b ^{13}C NMR (broadband decoupled, CDCl_3 , 25 °C) spectrum of the synthesized acetoacetate monomer phenyl-3-oxobutanoate (PH). δC (75 MHz, CDCl_3 , Me_4Si): 200.06 (q, C=O), 165.83 (q, COO), 150.49 (q, Ph), 129.63 (t, Ph), 126.33 (t, Ph), 121.15 (t, Ph), 50.09 (s, CH_2), 30.37 (p, CH_3).

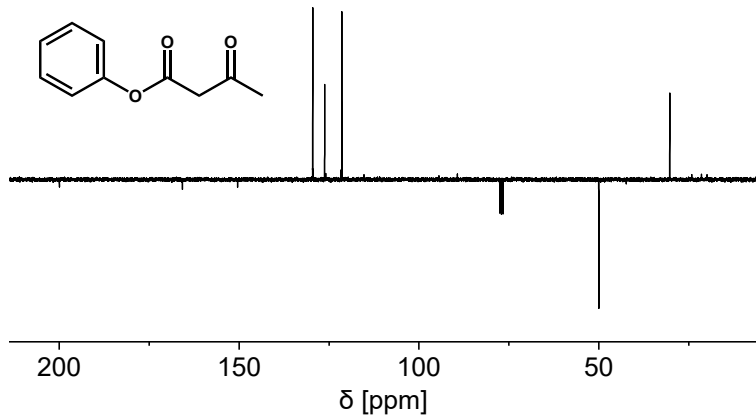


Fig. S3c ^{13}C NMR (DEPTQ-135, CDCl_3 , 25 °C) spectrum of the synthesized acetoacetate monomer phenyl-3-oxobutanoate (PH). δC (75 MHz, CDCl_3 , Me_4Si): 200.06 (q, C=O), 165.83 (q, COO), 150.49 (q, Ph), 129.63 (t, Ph), 126.33 (t, Ph), 121.15 (t, Ph), 50.09 (s, CH_2), 30.37 (p, CH_3).

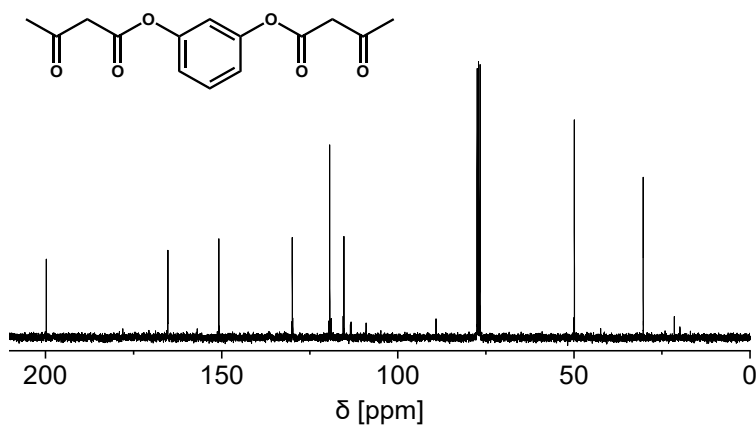


Fig. S3d ^{13}C NMR (broadband decoupled, CDCl_3 , 25 °C) spectrum of the synthesized acetoacetate monomer 1,3-phenylene bis(3-oxobutanoate) (RE). δC (75 MHz, CDCl_3 , Me_4Si): 199.97 (q, C=O), 165.38 (q, COO), 150.90 (q, Ph-O), 130.05 (t, Ph), 119.42 (t, Ph), 115.38 (t, Ph), 49.46 (s, CH_2), 30.41 (p, CH_3).

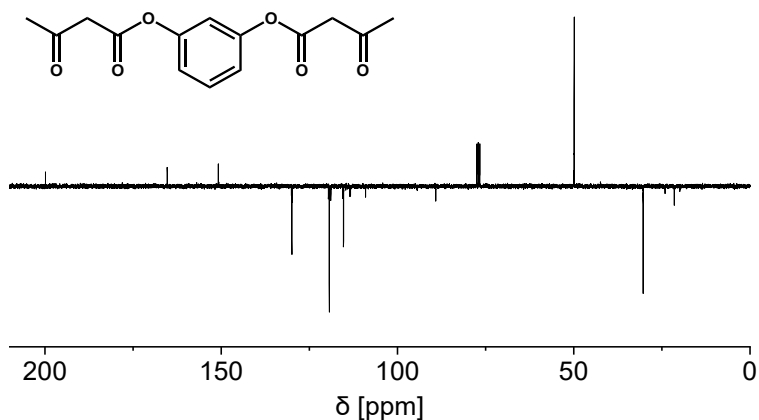


Fig. S3e ^{13}C NMR (DEPTQ-135, CDCl_3 , 25 °C) spectrum of the synthesized acetoacetate monomer 1,3-phenylene bis(3-oxobutanoate) (RE). δC (75 MHz, CDCl_3 , Me₄Si): 199.97 (q, C=O), 165.38 (q, COO), 150.90 (q, Ph-O), 130.05 (t, Ph), 119.42 (t, Ph), 115.38 (t, Ph), 49.46 (s, CH₂), 30.41 (p, CH₃).

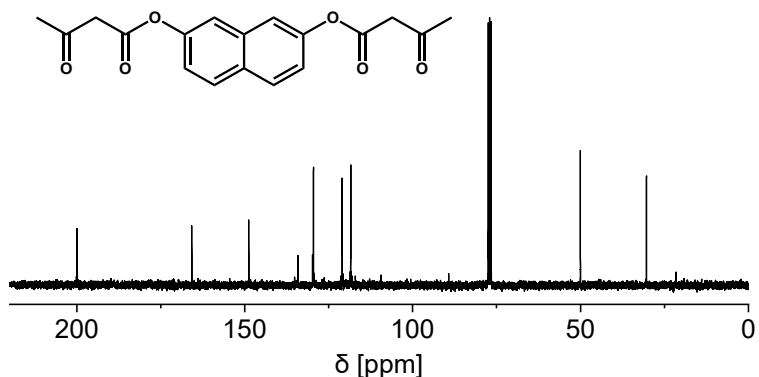


Fig. S3f ^{13}C NMR (broadband decoupled, CDCl_3 , 25 °C) spectrum of the synthesized acetoacetate monomer naphthalene 2,7 diyl bis(3 oxobutanoate) (NDO). δC (75 MHz, CDCl_3 , Me₄Si): 200.03 (q, C=O), 165.86 (q, COO), 148.89 (q, Ph-O), 134.25 (q, Ph), 129.86 (q, Ph), 129.63 (t, Ph), 121.08 (t, Ph), 118.53 (t, Ph), 50.13 (s, CH₂), 30.47 (p, CH₃).

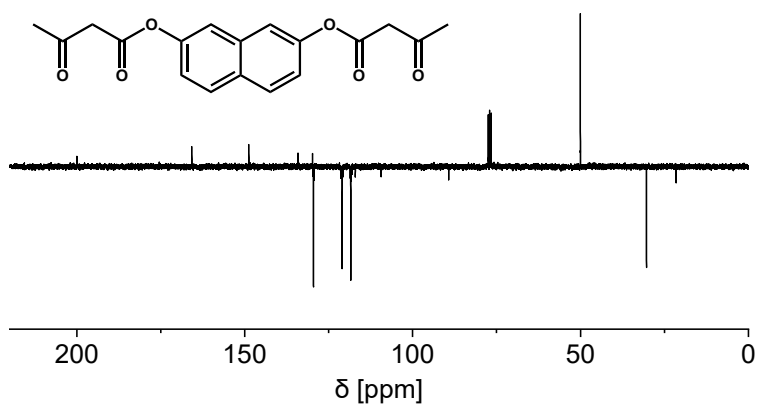


Fig. S3g ^{13}C NMR (DEPTQ-135, CDCl_3 , 25 °C) spectrum of the synthesized acetoacetate monomer naphthalene 2,7 diyl bis(3 oxobutanoate) (NDO). δC (75 MHz, CDCl_3 , Me_4Si): 200.03 (q, C=O), 165.86 (q, COO), 148.89 (q, Ph-O), 134.25 (q, Ph), 129.86 (q, Ph), 129.63 (t, Ph), 121.08 (t, Ph), 118.53 (t, Ph), 50.13 (s, CH_2), 30.47 (p, CH_3).

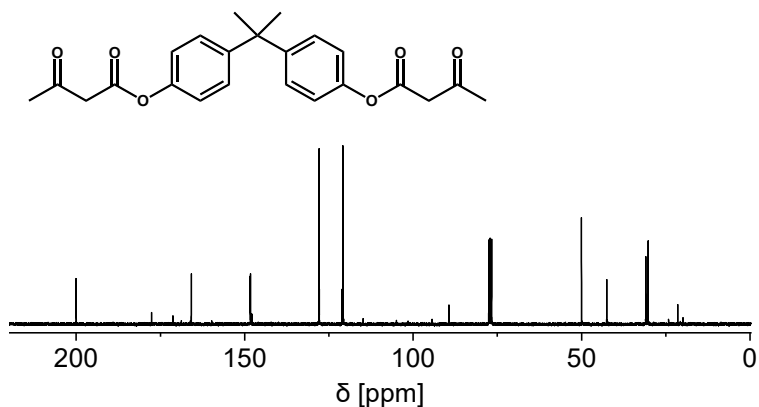


Fig. S3h ^{13}C NMR (broadband decoupled, CDCl_3 , 25 °C) spectrum of the synthesized acetoacetate monomer propane-2,2-diylbis(4,1-phenylene)bis(3-oxobutanoate) (BPA). δC (75 MHz, CDCl_3 , Me_4Si): 200.06 (q, C=O), 165.87 (q, COO), 148.37 (q, Ph), 148.28 (q, Ph-O), 127.96 (t, Ph), 120.86 (t, Ph), 50.06 (s, CH_2), 42.57 (q, C- CH_3), 30.95 (p, CH_3), 30.31 (p, O=C- CH_3).

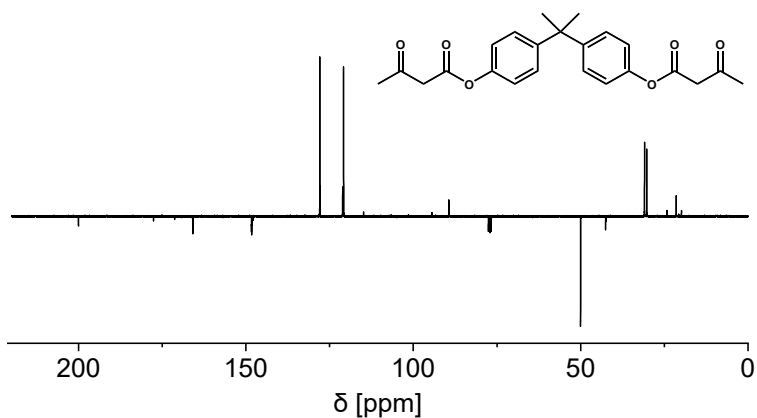


Fig. S3i ^{13}C NMR (DEPTQ-135, CDCl_3 , 25 °C) spectrum of the synthesized acetoacetate monomer propane-2,2-diylbis(4,1-phenylene)bis(3-oxobutanoate) (BPA). δC (75 MHz, CDCl_3 , Me_4Si): 200.06 (q, C=O), 165.87 (q, COO), 148.37 (q, Ph), 148.28 (q, Ph-O), 127.96 (t, Ph), 120.86 (t, Ph), 50.06 (s, CH_2), 42.57 (q, C- CH_3), 30.95 (p, CH_3), 30.31 (p, O=C- CH_3).

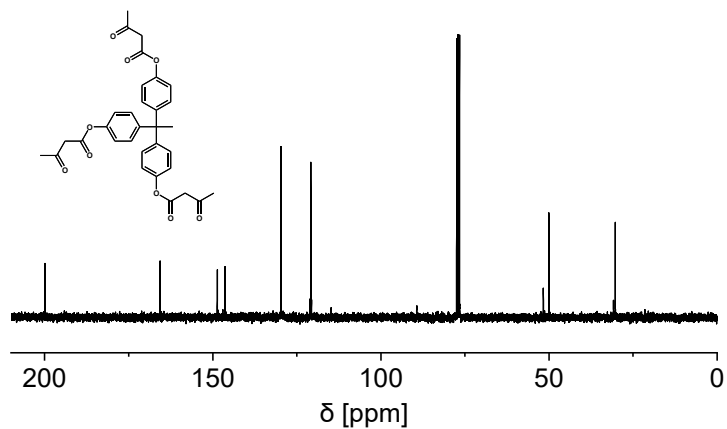


Fig. S3j ^{13}C NMR (broadband decoupled, CDCl_3 , 25 °C) spectrum of the synthesized acetoacetate monomer ethane-1,1,1-triyltris(benzene-4,1-diyl) tris(3-oxobutanoate) (THPE). δC (75 MHz, CDCl_3 , Me_4Si): 200.01 (q, C=O), 165.81 (q, COO), 148.77 (q, Ph-O), 146.48 (q, Ph-C), 129.86 (t, Ph), 120.93 (t, Ph), 51.80 (q, C- CH_3), 50.15 (s, CH_2), 30.95 (p, C- CH_3), 30.40 (p, O=C- CH_3).

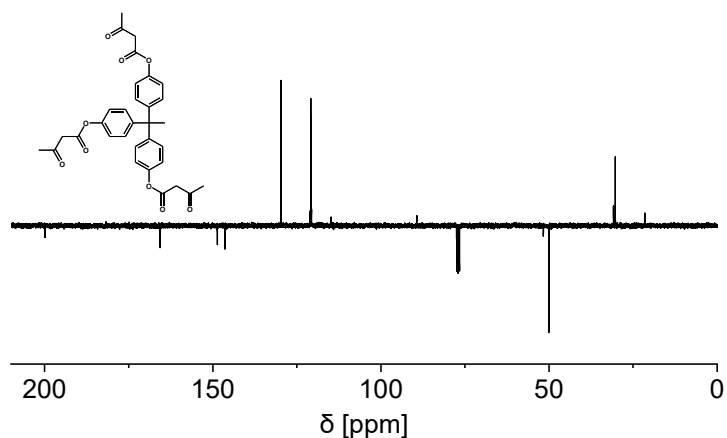


Fig. S3k ^{13}C NMR (DEPTQ-135, CDCl_3 , 25 °C) spectrum of the synthesized acetoacetate monomer ethane-1,1,1-triyltris(benzene-4,1-diyl) tris(3-oxobutanoate) (THPE). δC (75 MHz, CDCl_3 , Me_4Si): 200.01 (q, C=O), 165.81 (q, COO), 148.77 (q, Ph-O), 146.48 (q, Ph-C), 129.86 (t, Ph), 120.93 (t, Ph), 51.80 (q, C-CH₃), 50.15 (s, CH₂), 30.95 (p, C-CH₃), 30.40 (p, O=C-CH₃).

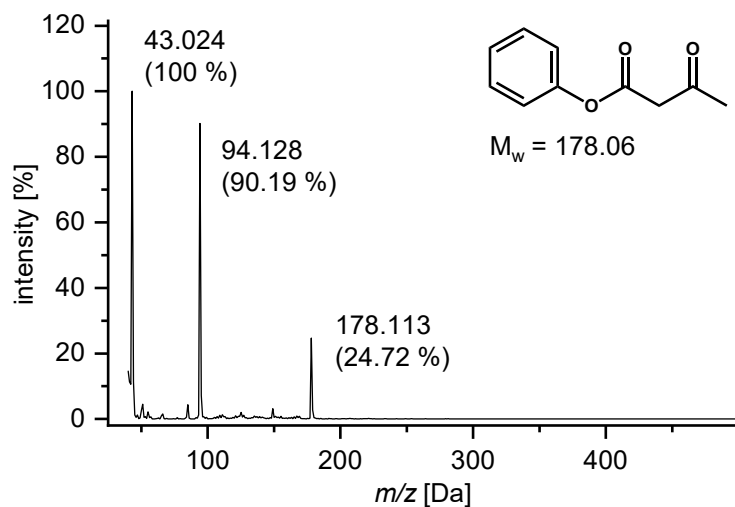


Fig. S4a EI-DIP measurement of phenyl-3-oxobutanoate (PH), showing the characteristic molecule-ion peak and fragmentations. EI-DIP: m/z 179.152 ($\text{M}^+ + 1$, 2.73 %) 178.113 (M^+ , 24.72), 94.128 (90.19), 43.024 (100). Calculated for $\text{C}_{10}\text{H}_{10}\text{O}_3$ (M^+) 178.063, found 178.113.

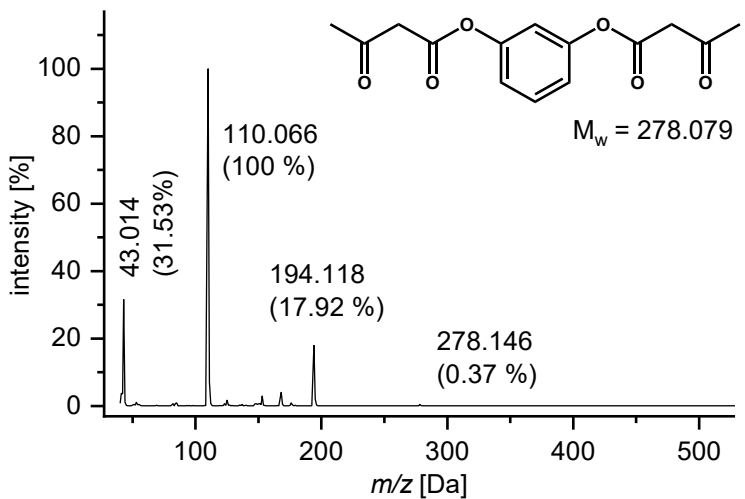


Fig. S4b EI-DIP measurement of 1,3-phenylene bis(3-oxobutanoate) (RE), showing the characteristic molecule-ion peak and fragmentations. EI-DIP: m/z 278.146 (M^+ , 0.37%), 194.118 (17.92), 110.066 (100) 43.014 (31.53). Calculated for $C_{14}H_{14}O_6$ (M^+) 278.079, found 278.146.

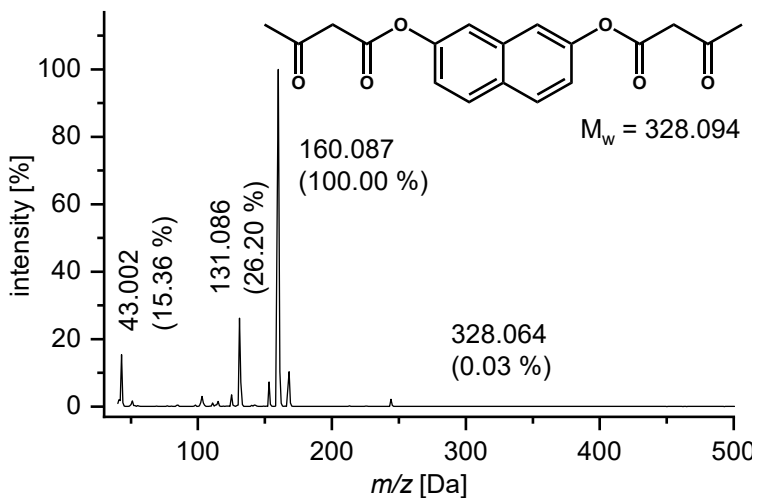


Fig. S4c EI-DIP measurement of naphthalene 2,7 diylbis(3 oxobutanoate)(NDO), showing the characteristic molecule-ion peak and fragmentations. EI-DIP: m/z 178.113 (M , 24.72 %), 94.128 (90.19), 43.024 (100). EI-DIP: m/z 328.064 (M^+ , 0.03%), 160.087 (100.00), 131.086 (26.20), 43.002 (15.06). Calculated for $C_{18}H_{16}O_6$ (M^+) 328.094, found 328.064.

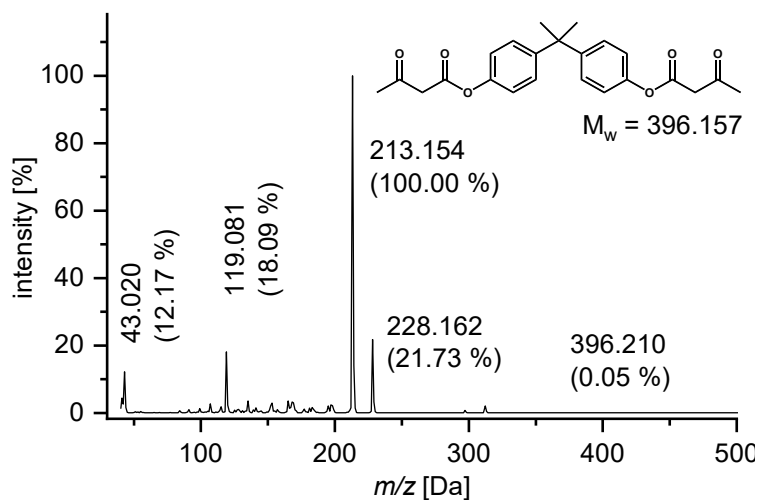


Fig. S4d EI-DIP measurement of propane-2,2-diylbis(4,1-phenylene)bis(3-oxobutanoate) (BPA), showing the characteristic molecule-ion peak and fragmentations. EI-DIP: m/z 396.210 (M^+ , 0.05%), 228.162 (21.73), 213.154 (100.00), 119.081 (18.09), 43.020 (12.17). Calculated for $C_{23}H_{24}O_6$ (M^+) 396.157, found 396.210.

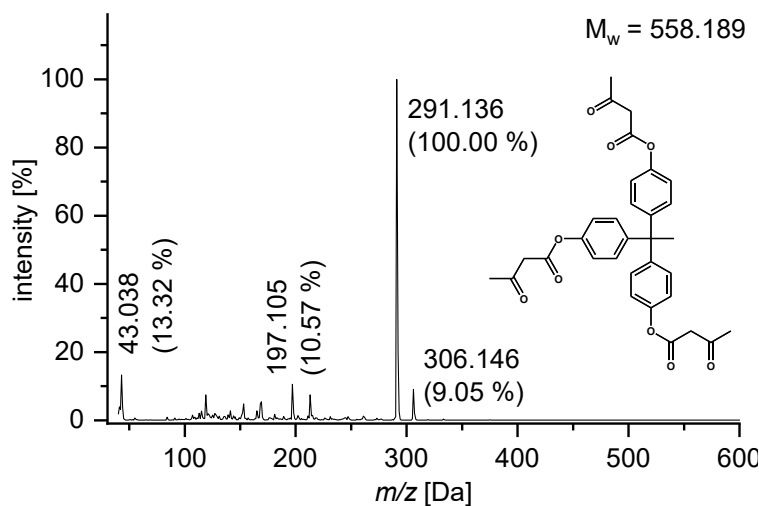


Fig. S4e EI-DIP measurement of ethane-1,1,1-triyltris(benzene-4,1-diyl) tris(3-oxobutanoate) (THPE), showing the characteristic molecule-ion peak and fragmentations. EI-DIP: m/z 558.271 (0.01 %) 306.146 (9.05), 291.136 (100.00), 197.105 (10.57) 43.038 (13.32) ($O=C-CH_3^+$). Calculated for $C_{32}H_{30}O_9$ (M^+) 558.189, found 558.271.

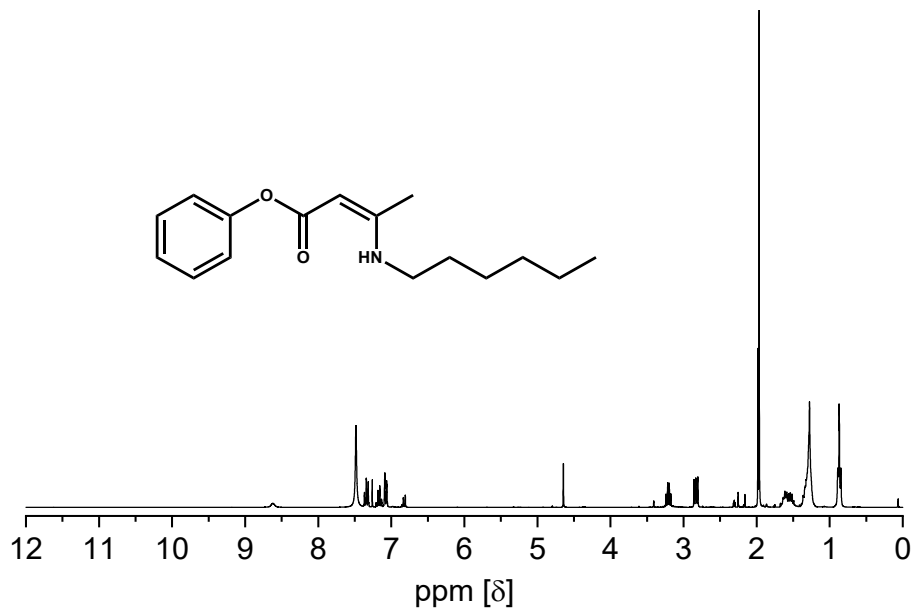


Fig. S5a ^1H NMR spectra (CDCl_3 , 25 °C) of spectrum of the synthesized vinylogous urethane reference compound Phe-VUT-Hex. δH (300 MHz, CDCl_3 , 298 K): 8.62 (1H, s, NH), 7.40–7.30 (2 H, m, Ph), 7.23–7.12 (1H, m, Ph), 7.11–7.05 (2H, m, Ph), 4.65 (s, 1H; CH), 3.20 (2H, m, CH₂) 1.98 (3H, s, CH₃), 1.68–1.47 (2H, m, CH₂), 1.40–1.18 (6H, m, CH₂), 0.93–0.79 (3H, t, CH₃). Acetic acid: 1.97 (3H, s, CH₃)

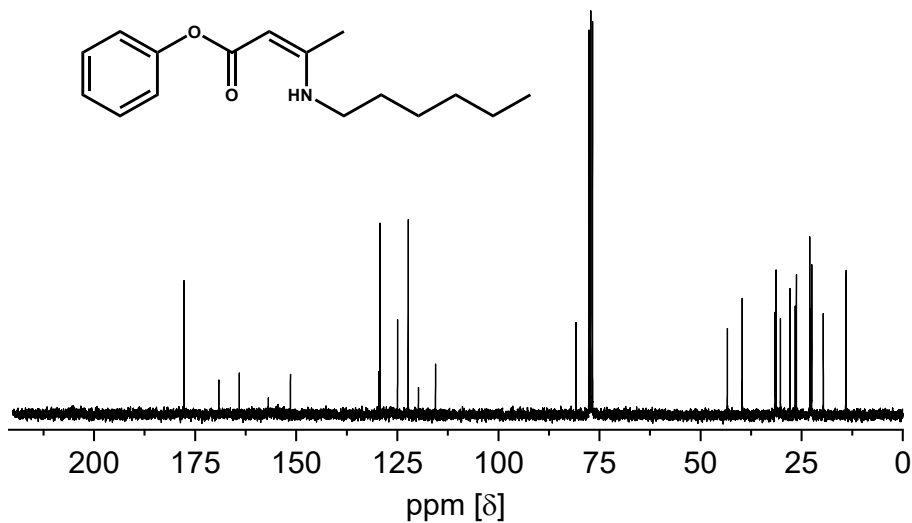


Fig. S5b ^{13}C NMR (broadband decoupled, CDCl_3 , 25 °C) spectrum of the synthesized vinylogous urethane reference compound Phe-VUT-Hex. δC (75 MHz, CDCl_3 , Me_4Si , 298 K): 169.16 (q, COO), 164.08 (q, C=C), 151.54 (q, Ph-O), 129.28 (t, Ph), 124.96 (t, Ph), 122.32 (t, Ph), 80.82 (t, CH), 43.38 (s, CH₂), 31.59 (s, CH₂), 31.32 (s, CH₂), 26.62 (s, CH₂), 22.49 (s, CH₂), 31.6 (p, C-CH₃) 14.11 (p, CH₂-CH₃). Acetic acid: 177.74 (q, COOH), 22.99 (p, CH₃).

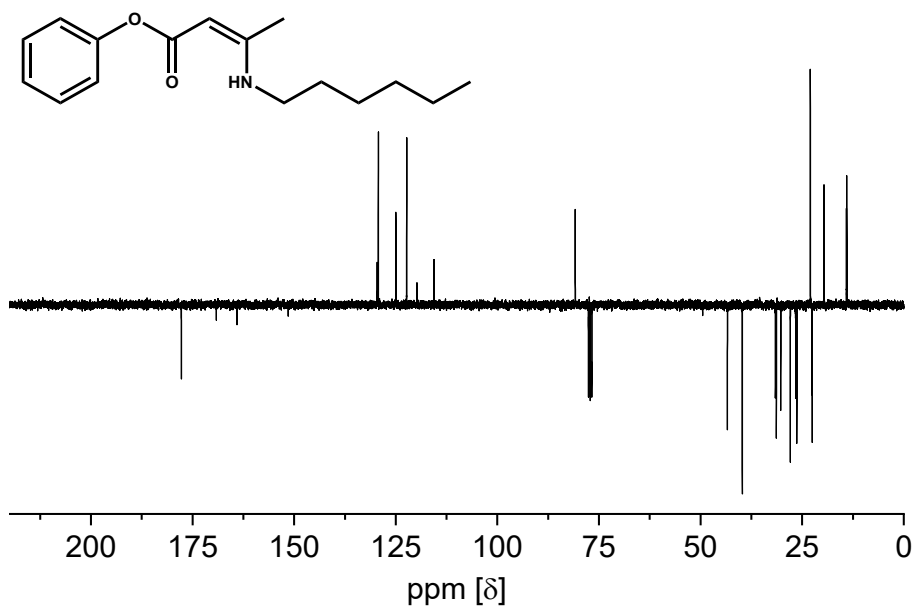


Fig. S5c ^{13}C NMR (DEPTQ-135, CDCl_3 , 25 °C) spectrum of the synthesized vinylogous urethane reference compound Phe-VUT-Hex. δC (75 MHz, CDCl_3 , Me_4Si , 298 K): 169.16 (q, COO), 164.08 (q, C=C), 151.54 (q, Ph-O), 129.28 (t, Ph), 124.96 (t, Ph), 122.32 (t, Ph), 80.82 (t, CH), 43.38 (s, CH_2), 31.59 (s, CH_2), 31.32 (s, CH_2), 26.62 (s, CH_2), 22.49 (s, CH_2), 31.6 (p, C- CH_3) 14.11 (p, $\text{CH}_2\text{-CH}_3$). Acetic acid: 177.74 (q, COOH), 22.99 (p, CH_3).

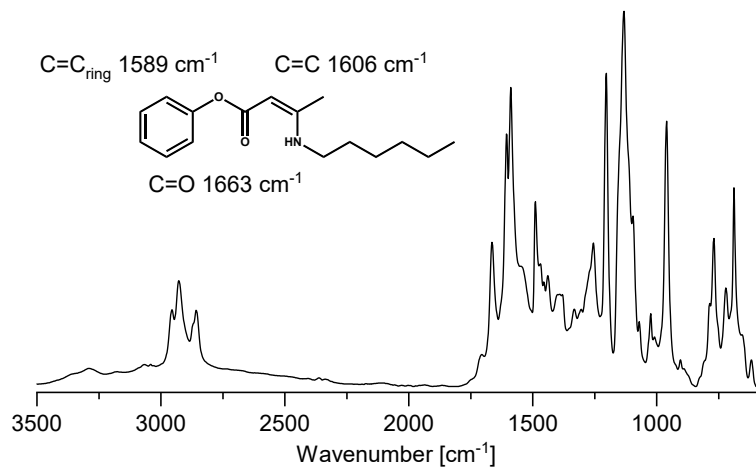


Fig. S6a ATR-FT-IR spectrum of the vinylogous urethane reference compound Phe-VUT-Hex with the characteristic C=O ester band at 1663 cm^{-1} , $\text{C}=\text{C}$ band at 1606 cm^{-1} and $\text{C}=\text{C}$ at 1589 cm^{-1} stretching vibrations of the phenylic unit.

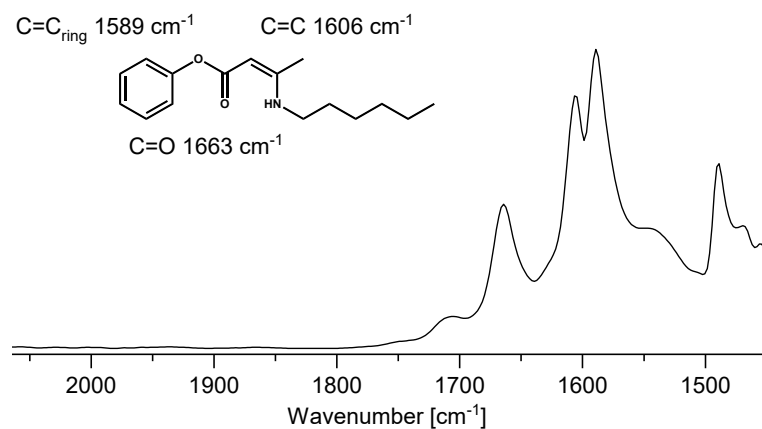


Fig. S6b ATR-FT-IR spectrum of the vinylogous urethane reference compound Phe-VUT-Hex with the characteristic C=O ester band at 1663 cm⁻¹, C=C band at 1606 cm⁻¹ and C=C at 1589 cm⁻¹ stretching vibrations of the phenylic unit proved by measuring ATR-FT-IR-spectra of Phenol (C=C at 1591 cm⁻¹).

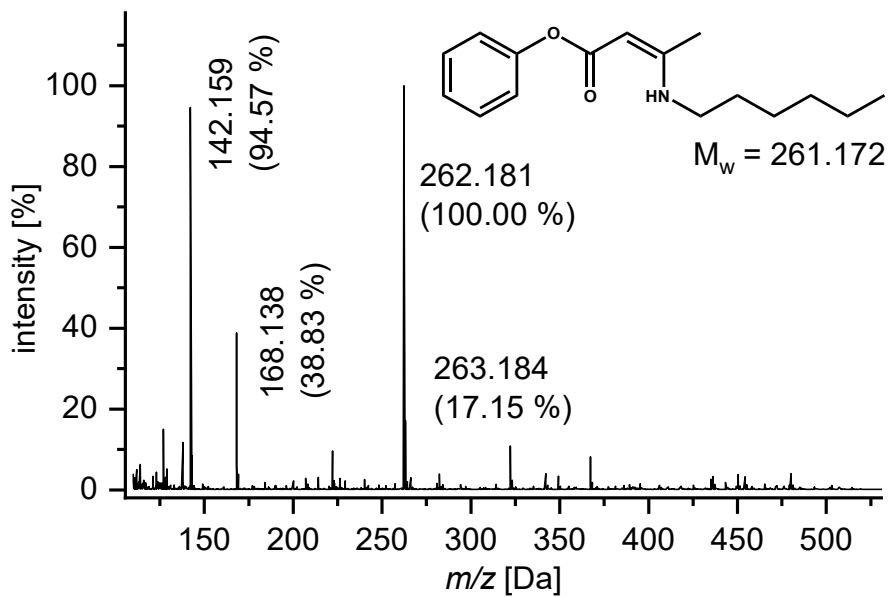


Fig. S7 ESI-MS spectrum of the synthesized vinylogous urethane reference Phe-VUT-Hex showing the characteristic molecule ion peaks 262.181 ($M^+ + 1$) and 263.184 ($M^+ + 2$).

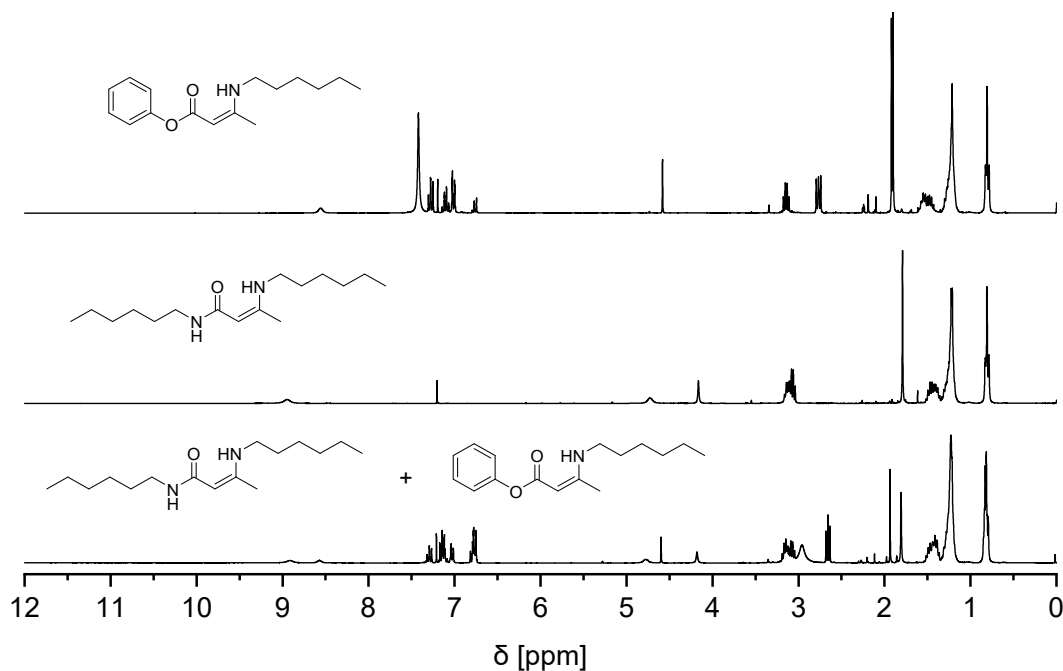


Fig. S8 ¹H NMR spectra (CDCl_3 , 25 °C) of the reference Phe-VUT-Hex (top), Hex-VUA-Hex (middle) and the mixture of both compounds during the synthesis in chloroform (bottom). Hex-VUA-Hex: δH (300 MHz, CDCl_3): 9.00 (1H, s, NH), 4.78 (1H, s, NH), 4.22 (1H, s, CH), 3.18 (2H, d, CH_2), 3.13 (2H, d, CH_2), 1.85 (3H, s, CH_3), 1.60–1.42 (4H, m, CH_2), 1.40–1.20 (12H, m, CH_2), 0.87 (3H, t, CH_3), 0.86 (3H, t, CH_3). Phe-VUT-Hex: δH (300 MHz, CDCl_3 , 298 K): 8.62 (1H, s, NH), 7.40–7.30 (2 H, m, Ph), 7.23–7.12 (1H, m, Ph), 7.11–7.05 (2H, m, Ph), 4.65 (s, 1H; CH), 3.20 (2H, m, CH_2) 1.98 (3H, s, CH_3), 1.68–1.47 (2H, m, CH_2), 1.40–1.18 (6H, m, CH_2), 0.93–0.79 (3H, t, CH_3).

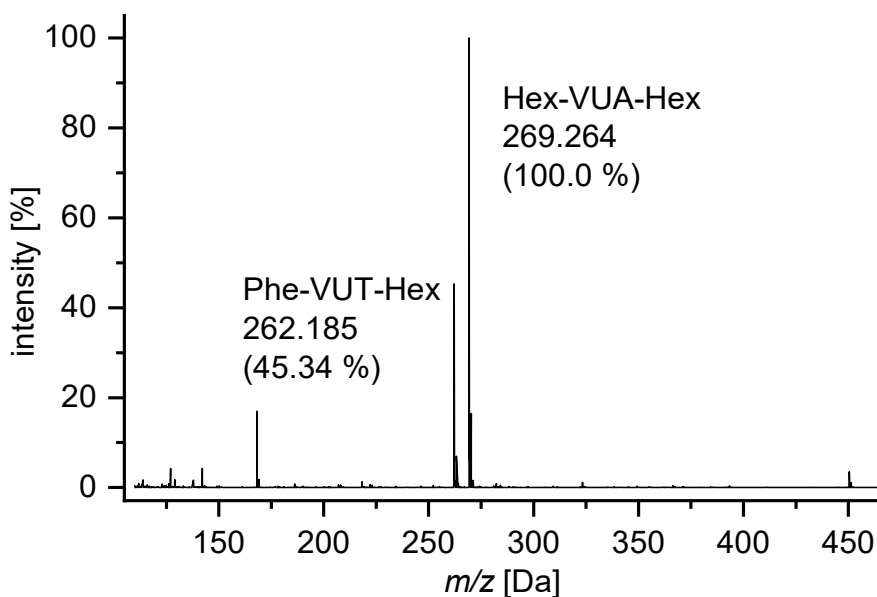


Fig. S9 ESI-MS spectrum of the synthesized mixture of vinylogous urethane Phe-VUT-Hex and Hex-VUA-Hex showing the characteristic molecule ion peaks 269.264 ($\text{M}^+ + 1$) and 262.185 ($\text{M}^+ + 1$).

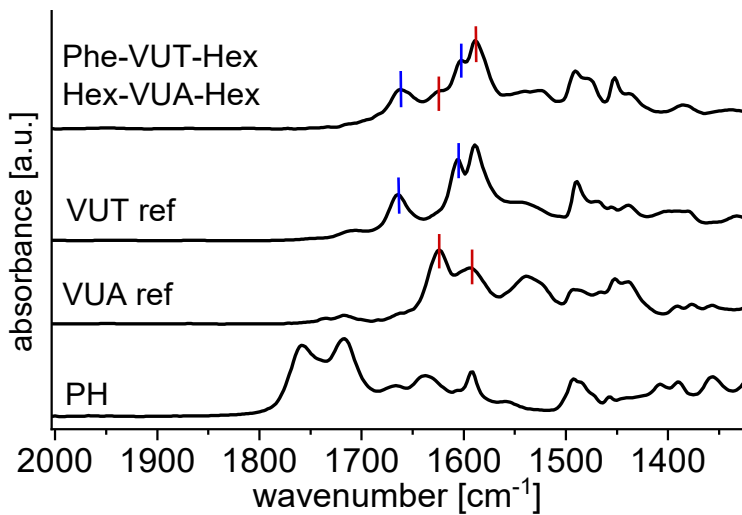


Fig. S10 ATR-FT-IR spectra of the vinylogous urethane and vinylogous urea reference compounds in comparison to the mixture resulted from the condensation/substitution reaction of PH and hexylamine in chloroform. The spectra show the characteristic C=O ester band (1663 cm^{-1}), C=C_{VUT} band (1606 cm^{-1}), C=O amide band (1623 cm^{-1}) and C=C_{VUA} band (1590 cm^{-1})

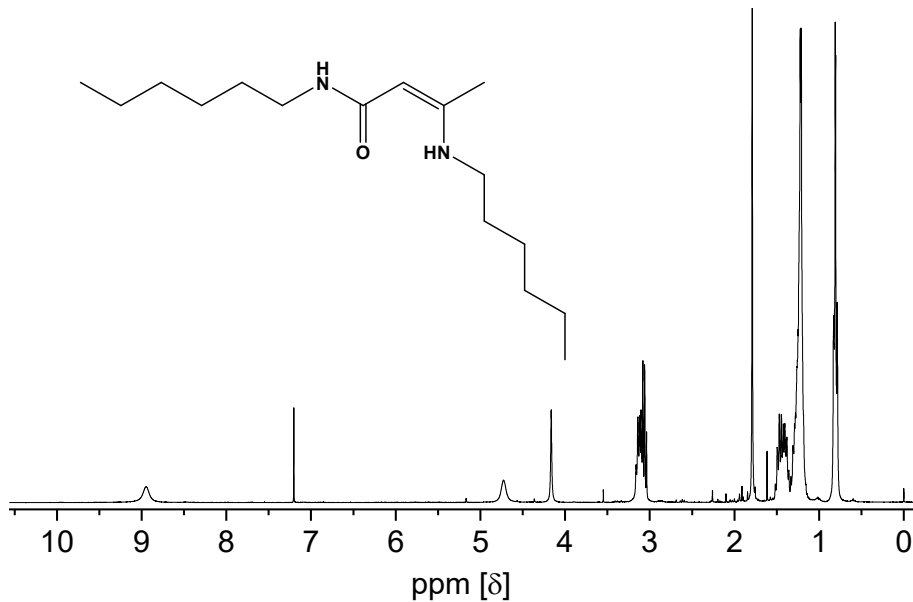


Fig. 11a ^1H NMR spectra (CDCl_3 , 25 °C) of spectrum of the synthesized vinylogous urea reference compound N-hexyl-3-(hexylamino)but-2-enamide (Hex-VUA-Hex). δH (300 MHz, CDCl_3): 9.00 (1H, s, NH), 4.78 (1H, s, NH), 4.22 (1H, s, CH), 3.18 (2H, d, CH_2), 3.13 (2H, d, CH_2), 1.85 (3H, s, CH_3), 1.60–1.42 (4H, m, CH_2), 1.40–1.20 (12H, m, CH_2), 0.87 (3H, t, CH_3), 0.86 (3H, t, CH_3).

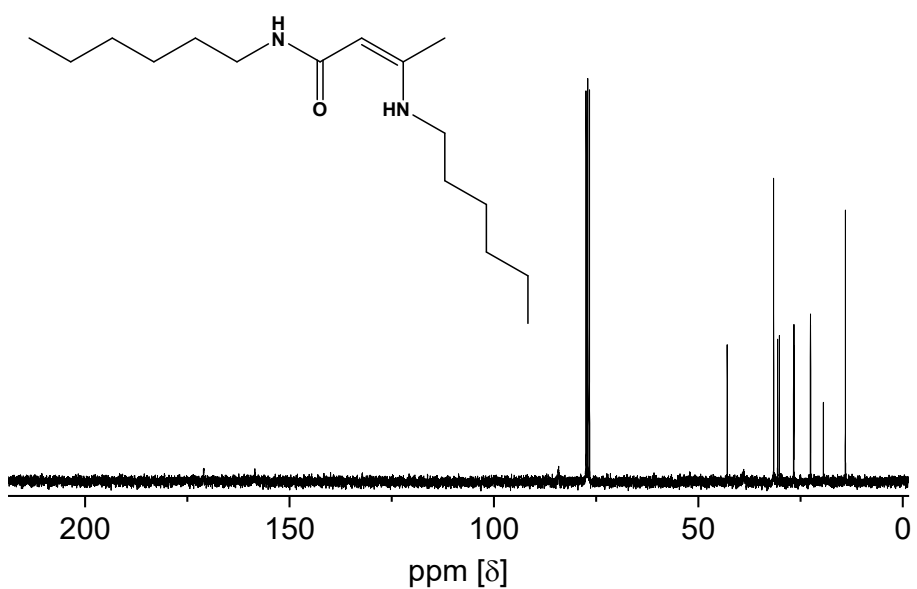


Fig. S11b ^{13}C NMR (broadband decoupled, CDCl_3 , 25 °C) spectrum of the synthesized vinylogous urea reference compound N-hexyl-3-(hexylamino)but-2-enamide (Hex-VUA-Hex). δC (75 MHz, CDCl_3 , 25°C): 171.10 (q, C=O), 158.61 (q, C-CH₃), 84.32 (t, CH), 43.04 (s, CH₂), 31.07 (s, CH₂), 30.73 (s, CH₂), 30.31 (s, CH₂), 26.83 (s, CH₂), 26.75 (s, CH₂), 22.72 (s, CH₂), 22.66 (s, CH₂), 19.53 (p, CH₃). 14.15 (p, CH₃).

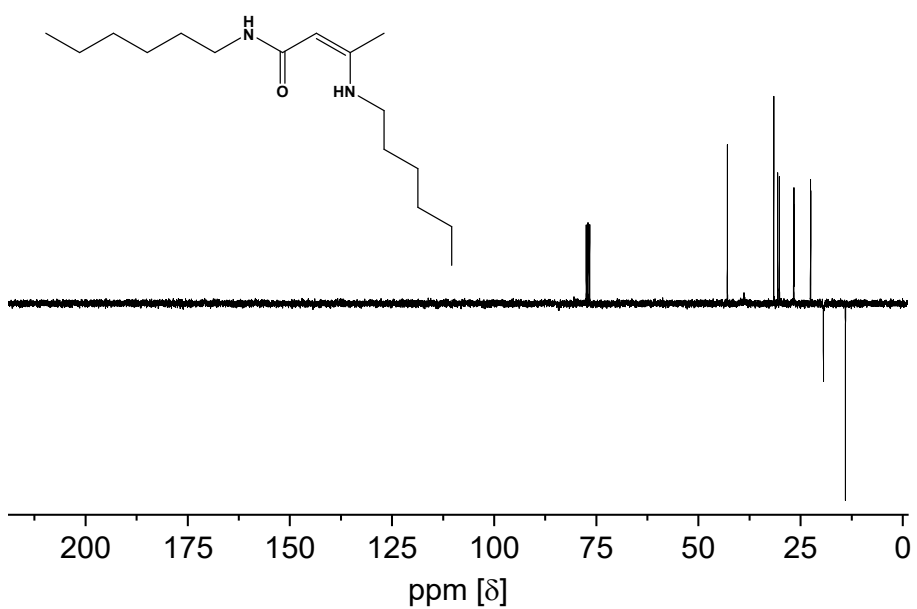


Fig. S11c ^{13}C NMR (DEPTQ-135, CDCl_3 , 25 °C) spectrum of the synthesized vinylogous urea reference compound N-hexyl-3-(hexylamino)but-2-enamide (Hex-VUA-Hex). δC (75 MHz, CDCl_3 , 25°C): 171.10 (q, C=O), 158.61 (q, C-CH₃), 84.32 (t, CH), 43.04 (s, CH₂), 31.07 (s, CH₂), 30.73 (s, CH₂), 30.31 (s, CH₂), 26.83 (s, CH₂), 26.75 (s, CH₂), 22.72 (s, CH₂), 22.66 (s, CH₂), 19.53 (p, CH₃). 14.15 (p, CH₃).

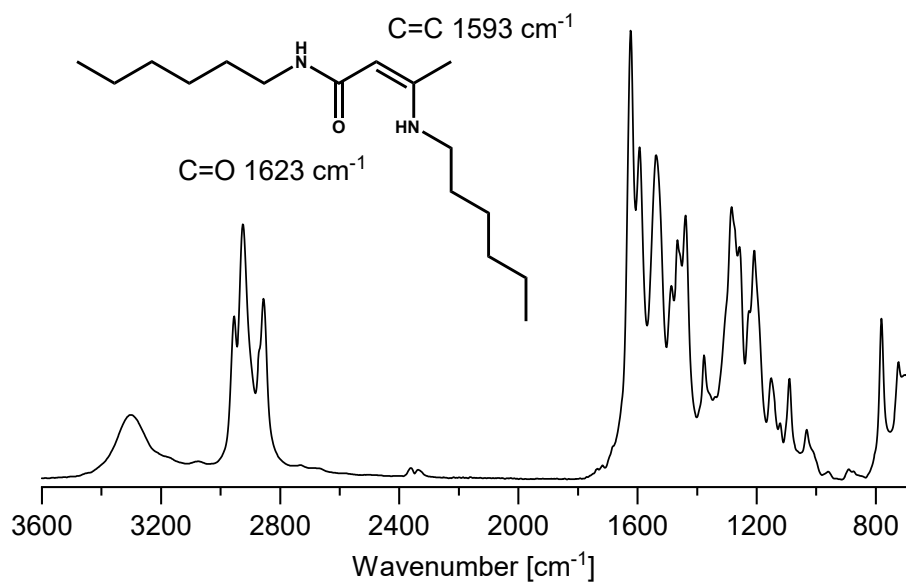


Fig. S12 ATR-FT-IR spectrum of the vinylogous urea reference compound Hex-VUA-Hex with the characteristic C=O amid band at 1623 cm⁻¹ and C=C band at 1593 cm⁻¹.

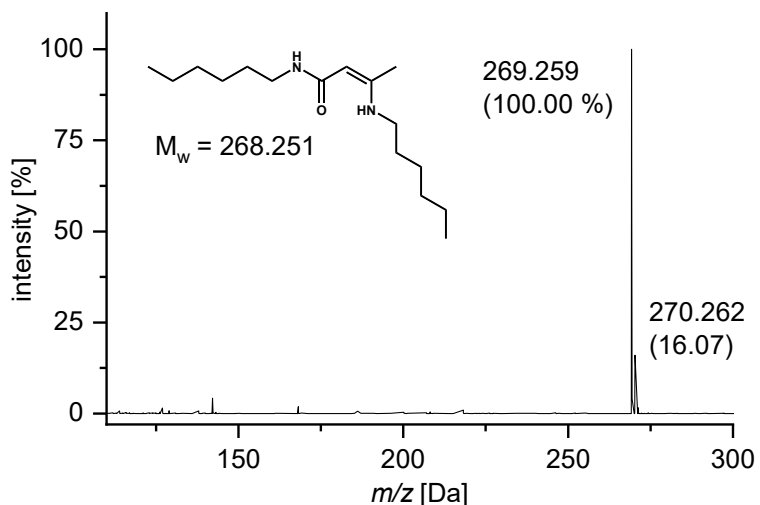


Fig. S13 ESI-MS spectrum of the synthesized vinylogous urea reference compound Hex-VUA-Hex showing the characteristic molecule ion peaks 269.264 ($M^+ + 1$) and 270.262 ($M^+ + 2$).

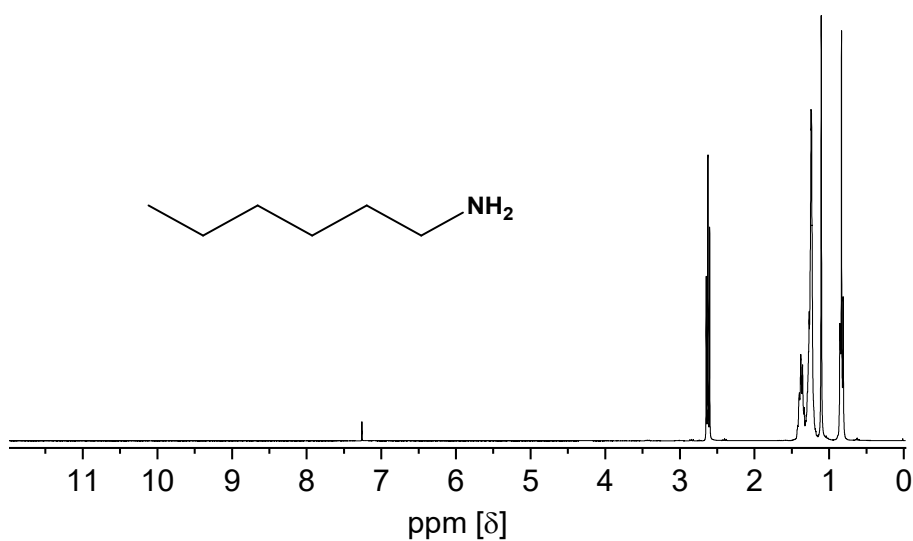


Fig. S14a ^1H NMR spectra (CDCl_3 , 25 °C) of spectrum of hexylamine. δH (300 MHz, CDCl_3): δH (300 MHz, CDCl_3 , 25°C): 2.62 (2H, t, $\text{N}-\text{CH}_2$), 1.43–1.32 (2H, m, CH_2), 1.32–1.17 (6H, m, CH_2), 1.11 (2H, s, NH_2), 0.83 (3H, t, CH_3).

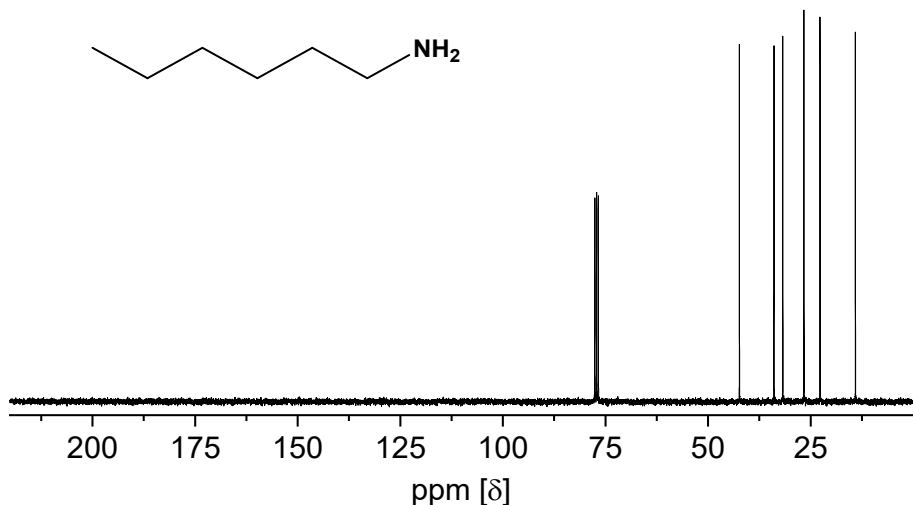


Fig. S14b ^{13}C NMR (broadband decoupled, CDCl_3 , 25 °C) spectrum of hexylamine. δC (75 MHz, CDCl_3): 42.35 (s, CH_2), 33.93 (s, CH_2), 31.78 (s, CH_2), 26.63 (s, CH_2), 22.70 (s, CH_2), 14.08 (s, CH_3).

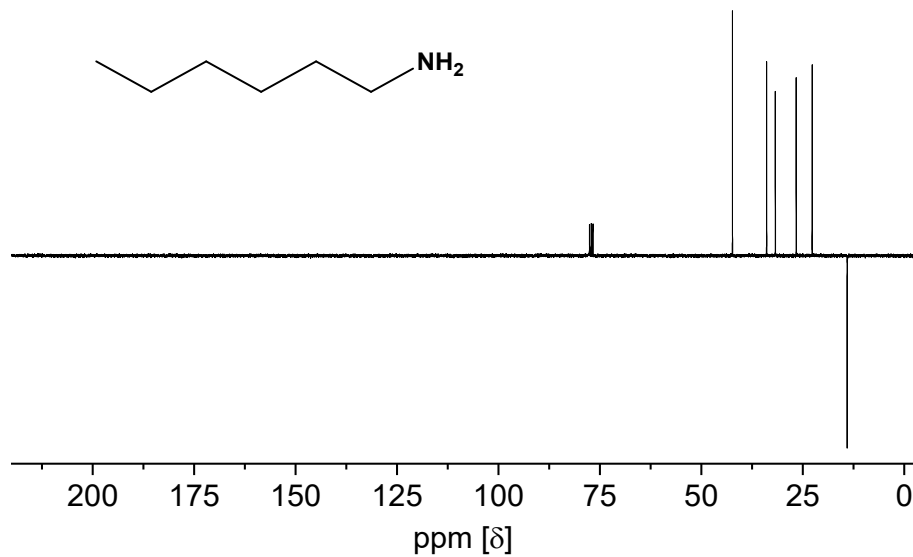


Fig. S14c ^{13}C NMR (DEPTQ-135, CDCl_3 , 25 °C) spectrum of hexylamine. δC (75 MHz, CDCl_3): 42.35 (s, CH_2), 33.93 (s, CH_2), 31.78 (s, CH_2), 26.63 (s, CH_2), 22.70 (s, CH_2), 14.08 (s, CH_3).

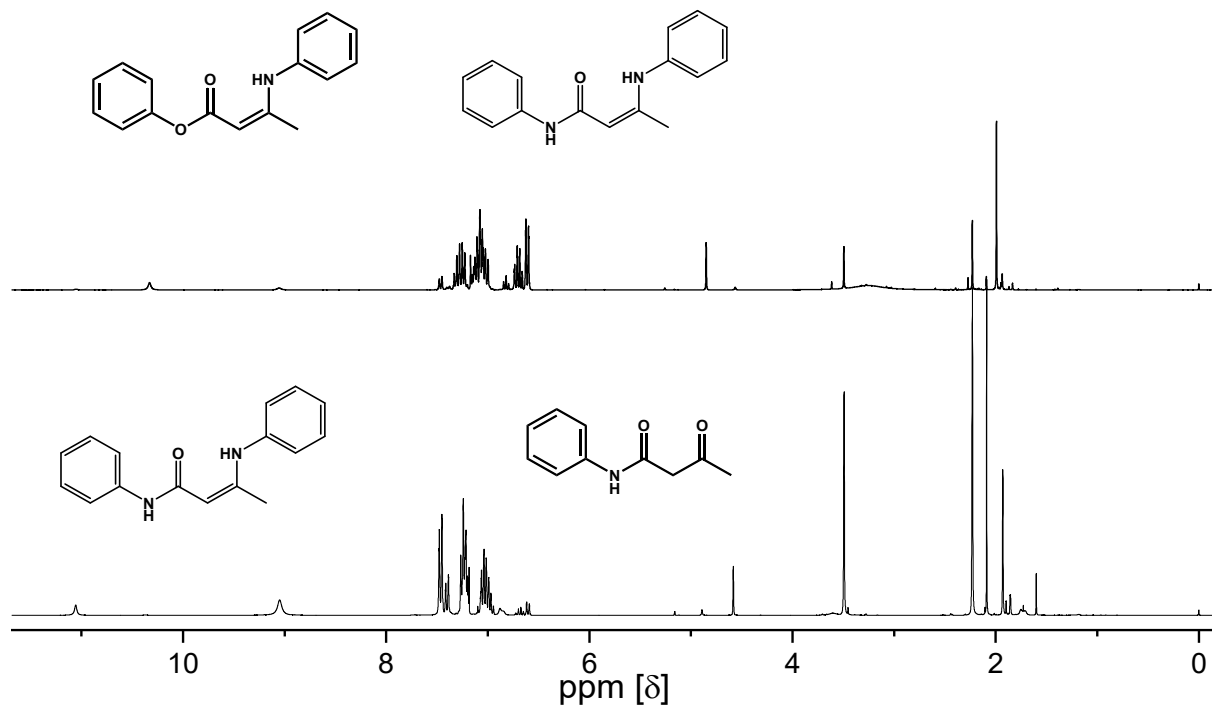


Fig. S15 ^1H NMR spectra (CDCl_3 , 25 °C) of the condensation reaction product Phenyl-3-(phenylamino)but-2-enoate (Phe-VUT-Phe) synthesized by mixing phenylacetoacetate and aniline, producing mainly the vinylogous urethane product (67%) (top). ^1H NMR reference spectra of the vinylogous urea compound N-phenyl-3-(phenylamino)but-2-enamide Phe-VUA-Phe, showing the vinylogous urea compound and the acetoacetamide intermediate product (bottom). Phe-VUA-Phe: δH (300 MHz, CDCl_3): 11.06 (1H, s, NH), 7.43–7.34 (2H, d, Ph), 7.26–7.15 (4H, m, Ph), 7.08–6.91 (4H, m, Ph), 6.85 (1H, s, NH), 4.57 (1H, s, CH), 1.91 (3H, s,

CH_3). Phe-VUT-Phe: δH (300 MHz, CDCl_3 , 298 K): 10.33 (1H, t, NH), 7.50–6.97 (10H, m, Ph), 4.87 (1H, s, CH), 2.02 (3H, s, CH_3).

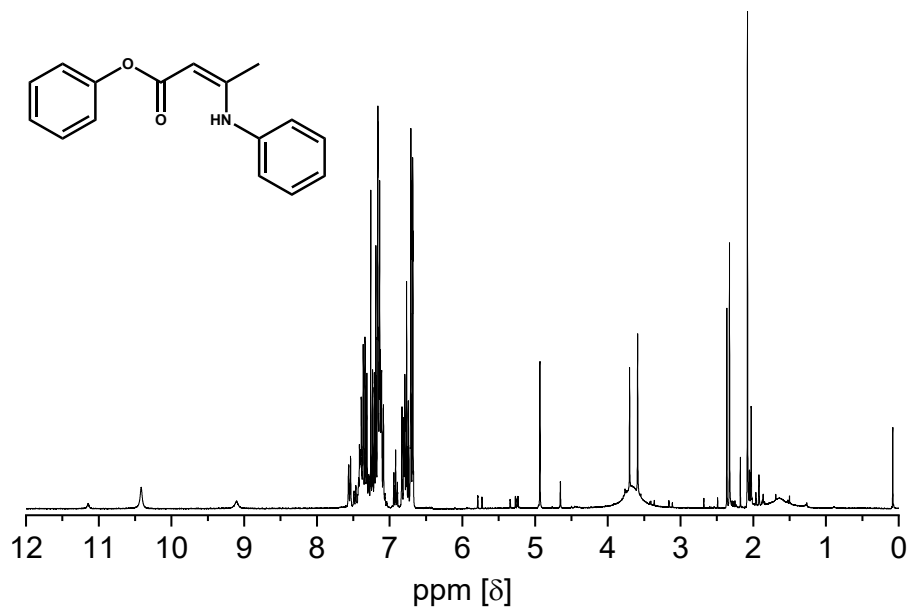


Fig. S16a ^1H NMR spectra (CDCl_3 , 25 °C) of spectrum of the synthesized vinylogous urethane mixture of Phe-VUT-Phe and Phe-VUA-Phe. Phe-VUA-Phe: δH (300 MHz, CDCl_3): 11.06 (1H, s, NH), 7.43–7.34 (2H, d, Ph), 7.26–7.15 (4H, m, Ph), 7.08–6.91 (4H, m, Ph), 6.85 (1H, s, NH), 4.57 (1H, s, CH), 1.91 (3H, s, CH_3). Phe-VUT-Phe: δH (300 MHz, CDCl_3 , 298 K): 10.33 (1H, t, NH), 7.50–6.97 (10H, m, Ph), 4.87 (1H, s, CH), 2.02 (3H, s, CH_3).

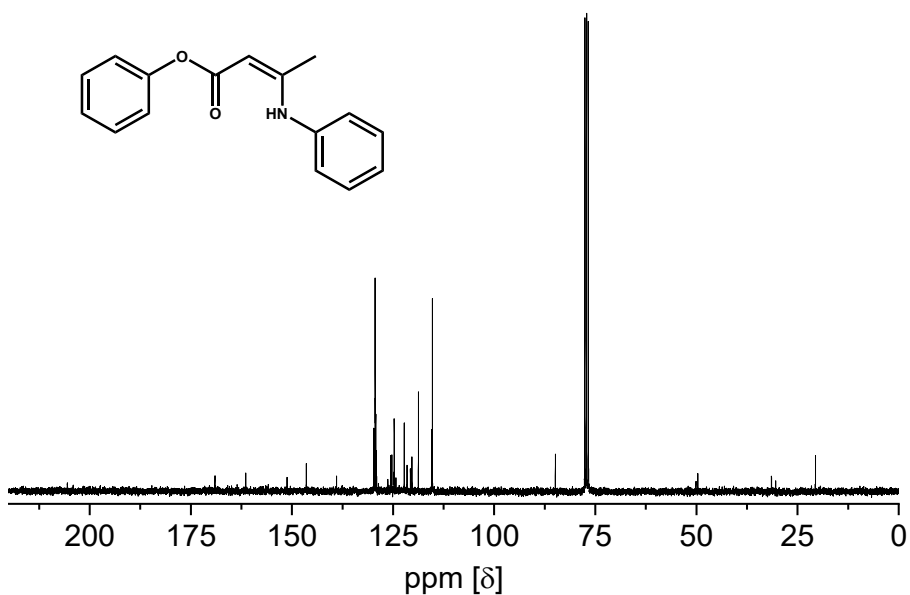


Fig. S16b ^{13}C NMR (broadband decoupled, CDCl_3 , 25 °C) of the synthesized vinylogous urethane mixture of Phe-VUT-Phe and Phe-VUA-Phe. Phe-VUT-Phe: δC (75 MHz, CDCl_3 , Me_4Si): 169.04 (q, COO), 161.42 (q, C=C), 151.21 (q, Ph-O), 129.45 (t, Ph), 129.10 (t, Ph), 124.74 (t, Ph), 122.24 (t, Ph), 118.72 (t, Ph), 84.86 (t, CH), 20.74 (p, CH_3). Phe-VUA-Phe: δC (75 MHz, CDCl_3): 168.85 (q, C=O), 157.38 (q, C- CH_3), 139.71 (q, Ph), 138.91 (q, Ph), 129.08 (t, Ph), 129.00 (t, Ph), 124.56 (t, Ph), 124.18 (t, Ph), 123.37 (t, Ph), 120.11 (t, Ph), 88.66 (t, CH), 20.57 (p, CH_3).

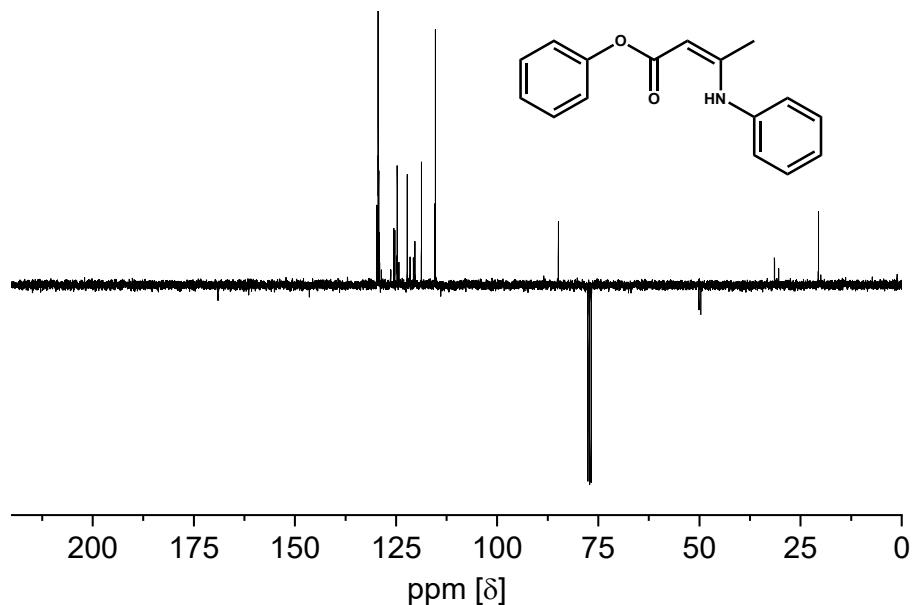


Fig. S16c ^{13}C NMR (DEPTQ-135, CDCl_3 , 25 °C) of the synthesized vinylogous urethane mixture of Phe-VUT-Phe and Phe-VUA-Phe. Phe-VUT-Phe: δC (75 MHz, CDCl_3 , Me_4Si): 169.04 (q, COO), 161.42 (q, C=C), 151.21 (q, Ph-O), 129.45 (t, Ph), 129.10 (t, Ph), 124.74 (t, Ph), 122.24 (t, Ph), 118.72 (t, Ph), 84.86 (t, CH), 20.74 (p, CH_3). Phe-VUA-Phe: δC (75 MHz, CDCl_3): 168.85 (q, C=O), 157.38 (q, C- CH_3), 139.71 (q, Ph), 138.91 (q, Ph), 129.08 (t, Ph), 129.00 (t, Ph), 124.56 (t, Ph), 124.18 (t, Ph), 123.37 (t, Ph), 120.11 (t, Ph), 88.66 (t, CH), 20.57 (p, CH_3).

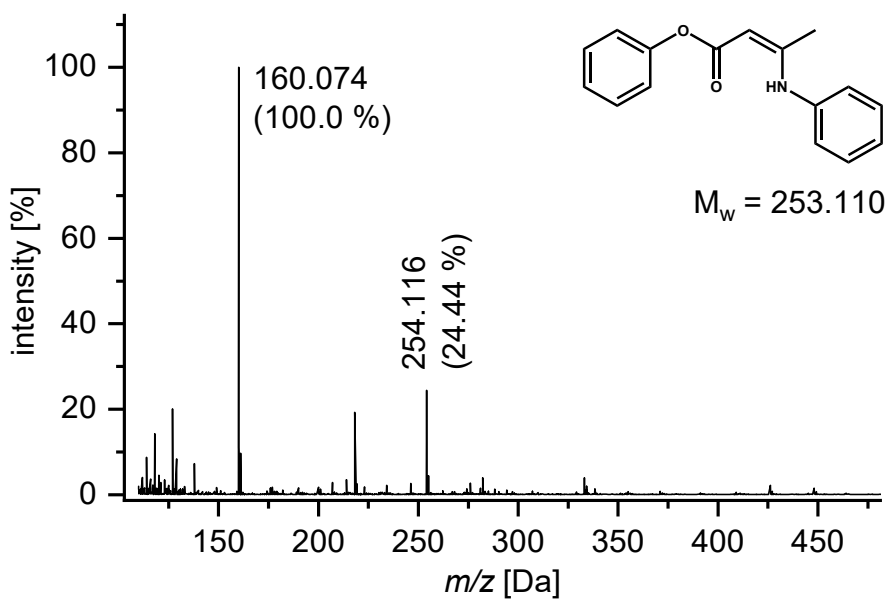


Fig. S17 ESI-MS spectrum of the synthesized vinylogous urethane compound Phe-VUT-Phe showing the characteristic molecule ion peak 254.116 ($M^+ + 1$).

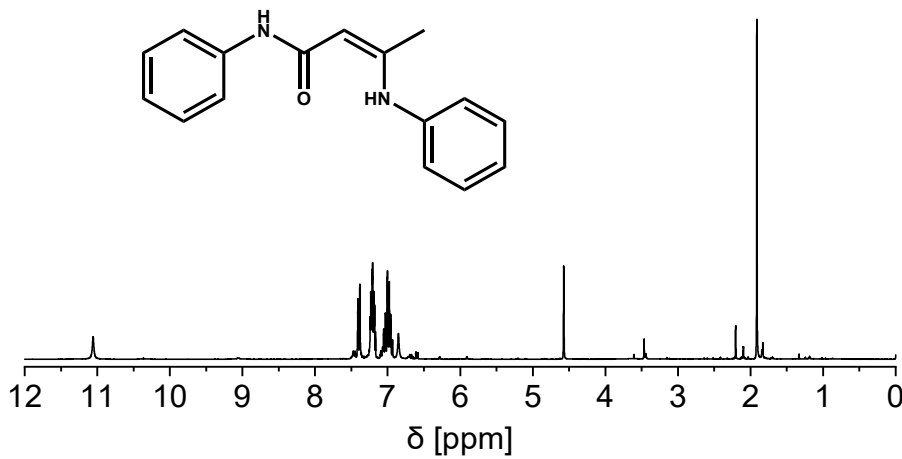


Fig. S18a ^1H NMR spectra (CDCl_3 , 25 °C) of spectrum of the synthesized vinylogous urea reference compound N-phenyl-3-(phenylamino)but-2-enamide (Phe-VUA-Phe). δH (300 MHz, CDCl_3): 11.06 (1H, s, NH), 7.43–7.34 (2H, d, Ph), 7.26–7.15 (4H, m, Ph), 7.08–6.91 (4H, m, Ph), 6.85 (1H, s, NH), 4.57 (1H, s, CH), 1.91 (3H, s, CH₃).

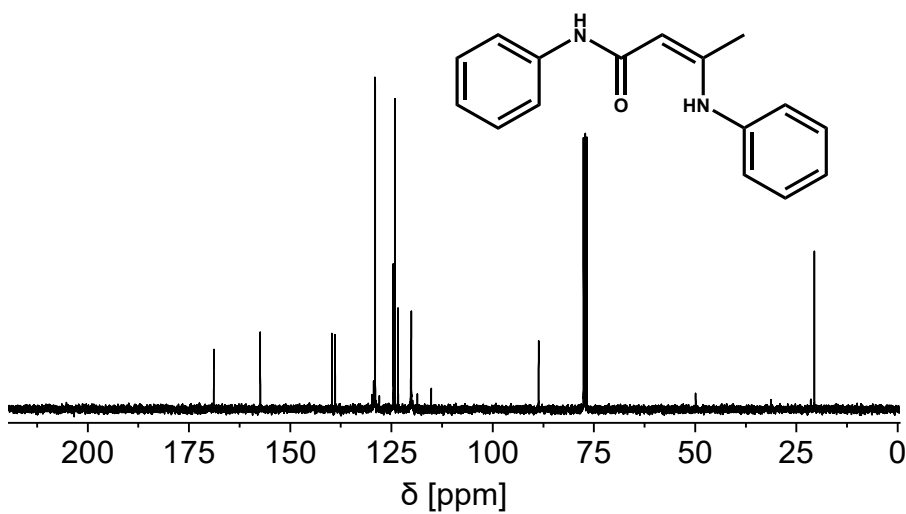


Fig. S18b ^{13}C NMR (broadband decoupled, CDCl_3 , 25 °C) spectrum of the synthesized vinylogous urea reference compound N-phenyl-3-(phenylamino)but-2-enamide (Phe-VUA-Phe). δC (75 MHz, CDCl_3): 168.85 (q, C=O), 157.38 (q, C- CH_3), 139.71 (q, Ph), 138.91 (q, Ph), 129.08 (t, Ph), 129.00 (t, Ph), 124.56 (t, Ph), 124.18 (t, Ph), 123.37 (t, Ph), 120.11 (t, Ph), 88.66 (t, CH), 20.57 (p, CH_3).

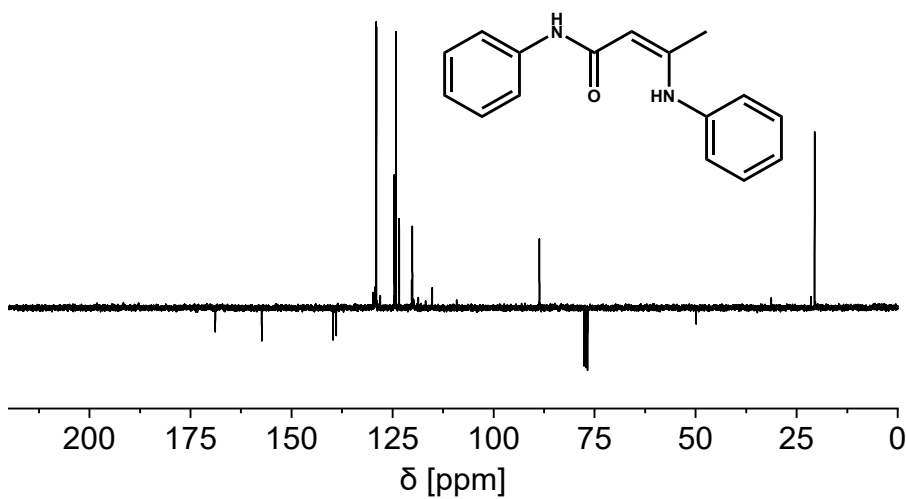


Fig. S18c ^{13}C NMR (DEPTQ-135, CDCl_3 , 25 °C) spectrum of the synthesized vinylogous urea reference compound N-phenyl-3-(phenylamino)but-2-enamide (Phe-VUA-Phe). δC (75 MHz, CDCl_3): 168.85 (q, C=O), 157.38 (q, C- CH_3), 139.71 (q, Ph), 138.91 (q, Ph), 129.08 (t, Ph), 129.00 (t, Ph), 124.56 (t, Ph), 124.18 (t, Ph), 123.37 (t, Ph), 120.11 (t, Ph), 88.66 (t, CH), 20.57 (p, CH_3).

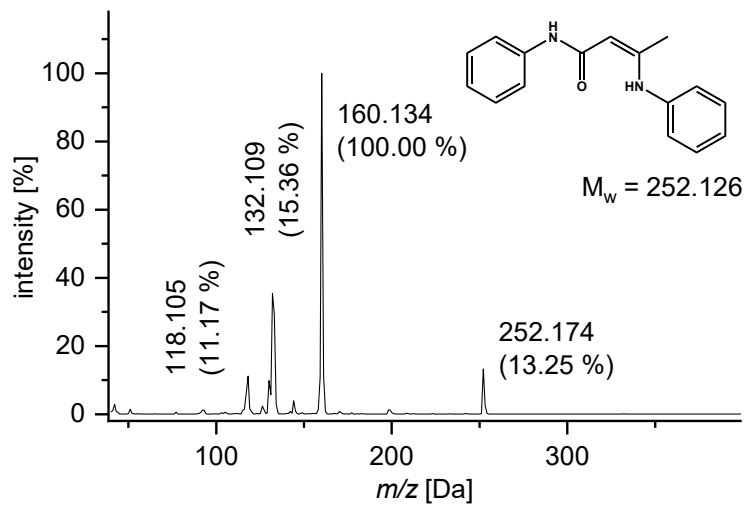


Fig. S19 EI-DIP measurement of N-phenyl-3-(phenylamino)but-2-enamide (Phe-VUA-Phe), showing the characteristic molecule-ion peak and fragmentations. EI-DIP: m/z 252.174 (M^+ , 13.25 %), 160.134 (100.00), 132.109 (15.36), 118.105 (11.17). Calculated for $\text{C}_{16}\text{H}_{16}\text{N}_2\text{O}_6$ (M^+) 252.126, found 252.174.

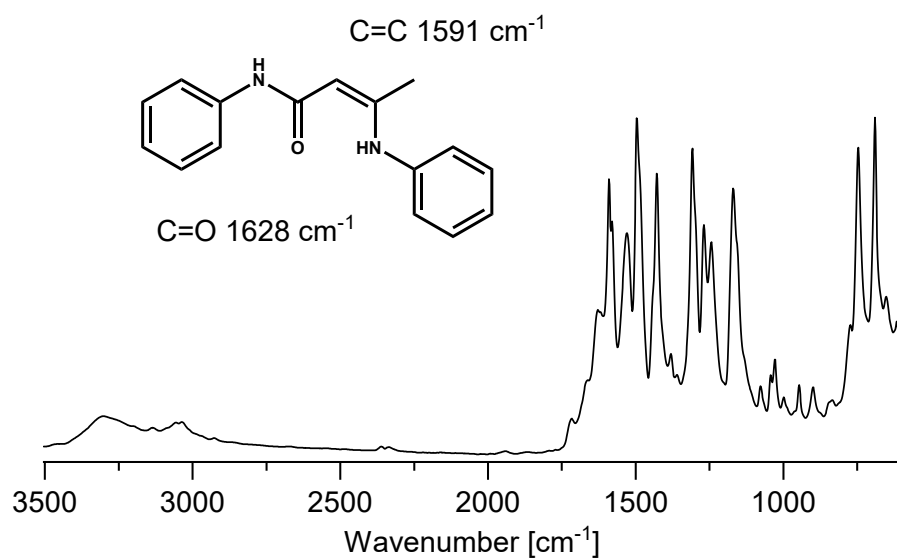


Fig. S20 ATR-FT-IR spectrum of the vinylogous urea compound Phe-VUA-Phe showing the characteristic C=O amid band at 1628 cm^{-1} and C=C band at 1591 cm^{-1} .

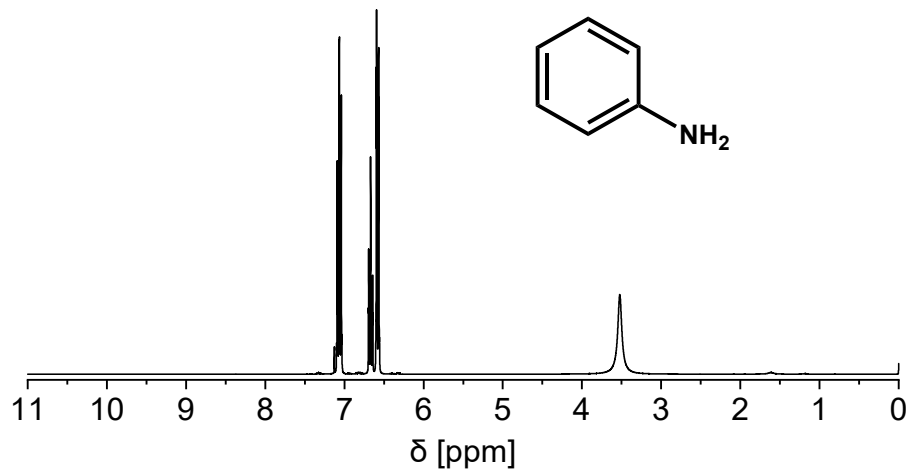


Fig. S21a ^1H NMR spectra (CDCl_3 , 25 °C) of spectrum of aniline. δH (300 MHz, CDCl_3 , 25°C): 7.06 (2H, t, Ph), 6.66 (1H, t, Ph), 6.57 (2H, d, Ph), 3.52 (2H, s, NH_2).

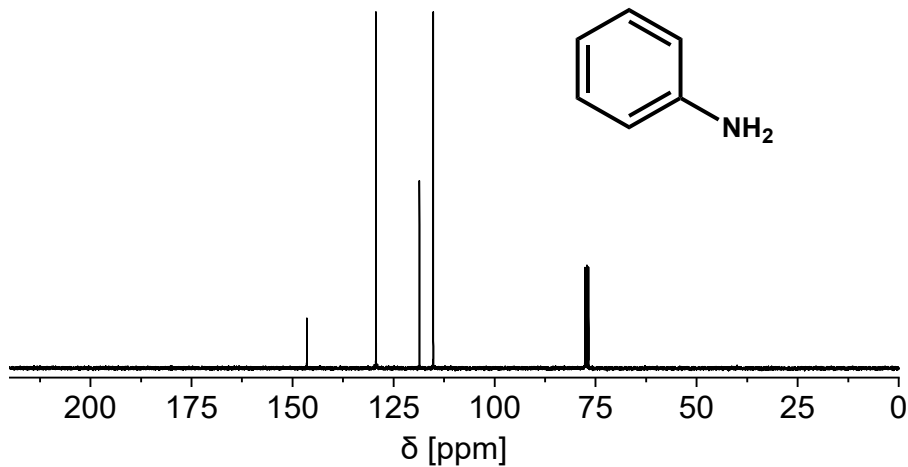


Fig. S21b ^{13}C NMR (broadband decoupled, CDCl_3 , 25 °C) spectrum of aniline. δC (75 MHz, CDCl_3): 146.47 (q, Ph), 129.35 (t, Ph), 118.59 (t, Ph), 115.17 (t, Ph).

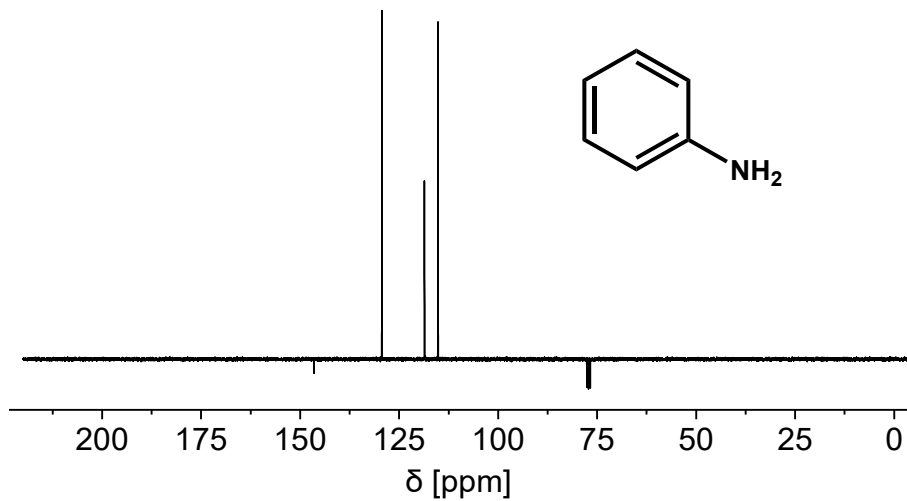


Fig. S21c ^{13}C NMR (DEPTQ-135, CDCl_3 , 25 °C) spectrum of aniline.

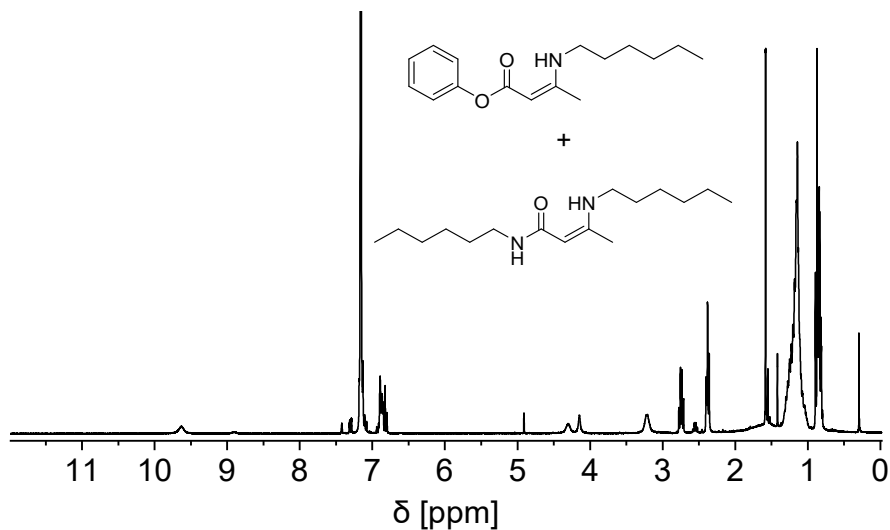


Fig. S22a ^1H NMR spectra (benzene-d₆, 25 °C) of spectrum of the synthesized mixture of Phe-VUT-Hex and Hex-VUA-Hex. Phenyl-3-(hexylamino)but-2-enoate (Phe-VUT-Hex) δH (300 MHz, benzene-d₆, 298 K): 8.90 (1H, s, NH), 4.90 (1H, s, CH), 2.54 (2H, dd, CH_2) 1.41 (3H, s, CH_3), 1.33–1.03 (8H, m, CH_2), 0.89–0.78 (6H, t, CH_3). N-hexyl-3-(hexylamino)but-2-enamide (Hex-VUA-Hex) δH (300 MHz, benzene-d₆, 298 K): 9.68 (1H, s, NH), 4.63 (1H, t, NH), 4.25 (1H, s, CH), 3.26 (2H, d, CH_2), 2.77 (2H, dd, CH_2), 1.61 (3H, s, CH_3), 1.42–1.02 (16H, m, CH_2 , 0.84 (3H, t, CH_3), 0.83 (3H, t, CH_3).

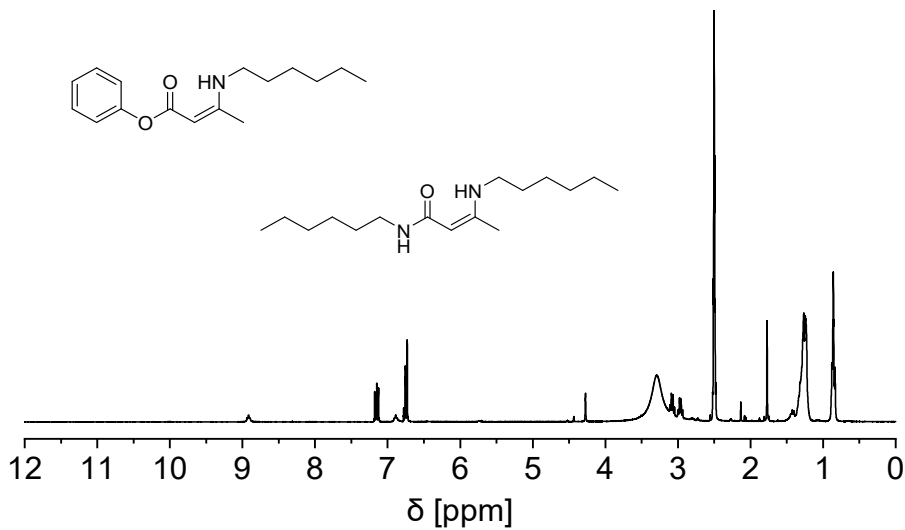


Fig. S22b ^1H NMR spectra (DMSO-d6, 25 °C) of spectrum of the synthesized mixture of Phe-VUT-Hex and Hex-VUA-Hex. Hex-VUA-Hex: δH (300 MHz, DMSO-d6, 298 K): δH (300 MHz, DMSO-d6, 298 K): 8.92 (1H, t, NH), 6.89 (1H, t, NH), 4.28 (1H, s, CH), 3.08 (2H, dd, CH_2), 2.97 (2H, dd, CH_2), 1.77 (3H, s, CH_3), 1.51–1.05 (16H, m, CH_2), 0.86 (3H, t, CH_3), 0.85 (3H, t, CH_3). Phe-VUT-Hex: δH (300 MHz, DMSO-d6, 298 K): 8.52 (1H, s, NH), 7.19–7.06 (2 H, m, Ph), 6.79–6.66 (3H, m, Ph), 4.57 (s, 1H; CH), 3.23 (2H, m, CH_2) 1.77 (3H, s, CH_3), 1.57–1.40 (2H, m, CH_2), 1.35–1.14 (6H, m, CH_2), 0.90–0.78 (3H, t, CH_3). Acetic acid: 8.8 (COOH), 1.77 (3H, s, CH_3).

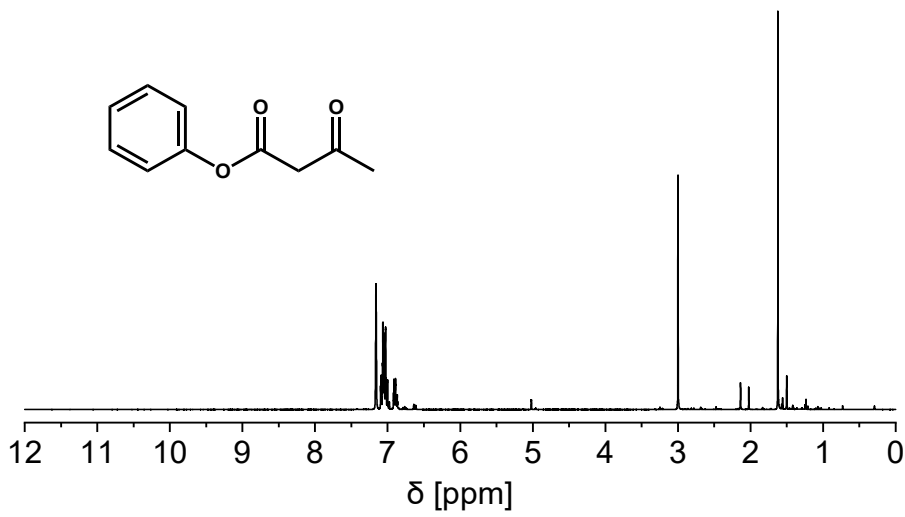


Fig. S22c ^1H NMR spectra (benzene-d6, 25 °C) of spectrum of the synthesized monomer PH. δH (300 MHz, benzene-d6, 298 K): 7.11–6.97 (4H, m, Ph), 6.92–6.85 (1H, m, Ph), 3.00 (2H, s, CH_2), 1.62 (3H, s, CH_3).

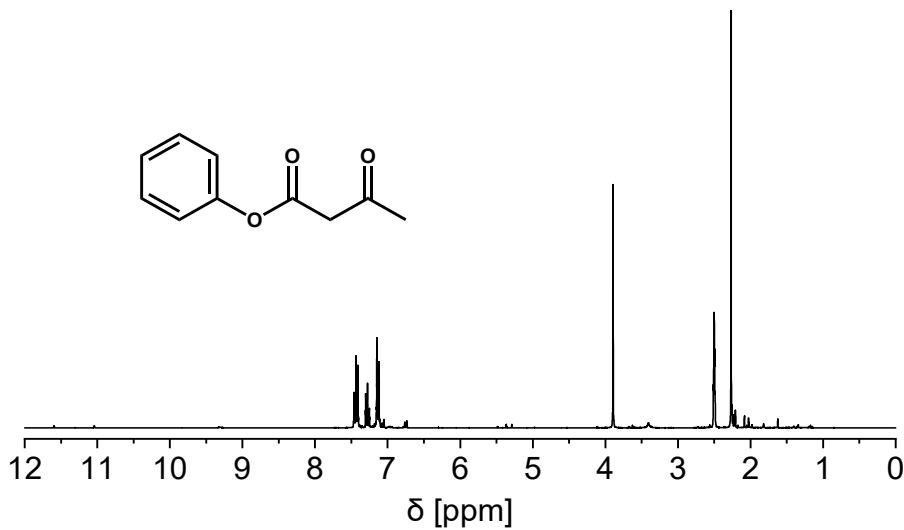


Fig. S22d ^1H NMR spectra (DMSO-d₆, 25 °C) of spectrum of the synthesized monomer PH. δH (300 MHz, DMSO-d₆, 298K): 7.47–7.39 (2H, m, Ph), 7.31–7.24 (1H, m, Ph), 7.16–7.10 (2H, m, Ph), 3.89 (2H, s, CH_2), 2.27 (3H, s, CH_3).

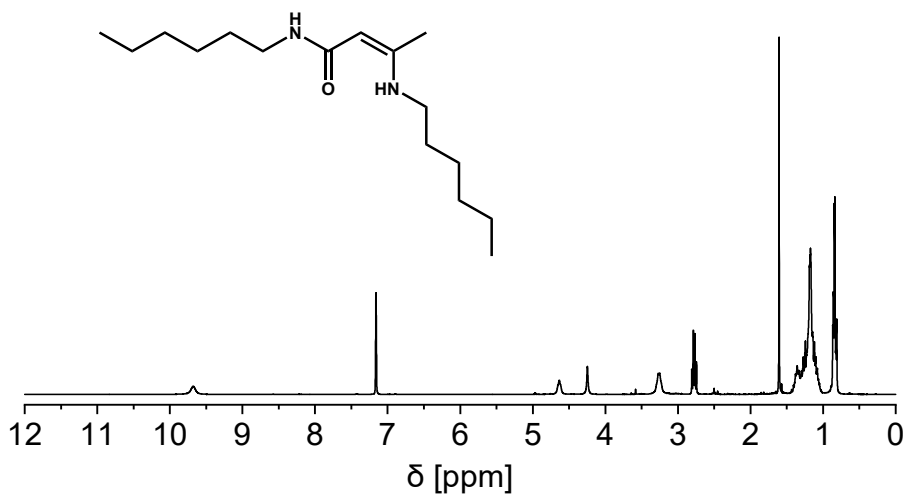


Fig. S22e ^1H NMR spectra (benzene-d₆, 25 °C) of spectrum of the synthesized vinylogous urea reference compound N-hexyl-3-(hexylamino)but-2-enamide (Hex-VUA-Hex). δH (300 MHz, benzene-d₆, 298 K): 9.68 (1H, s, NH), 4.63 (1H, t, NH), 4.25 (1H, s, CH), 3.26 (2H, d, CH_2), 2.77 (2H, dd, CH_2), 1.61 (3H, s, CH_3), 1.42–1.02 (16H, m, CH_2), 0.84 (3H, t, CH_3), 0.83 (3H, t, CH_3).

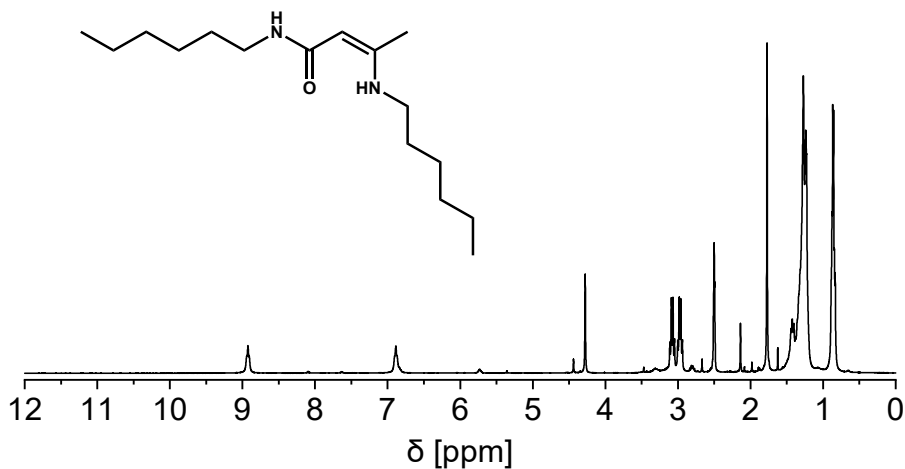


Fig. S22f ¹H NMR spectra (DMSO-d₆, 25 °C) of spectrum of the synthesized vinylogous urea reference compound N-hexyl-3-(hexylamino)but-2-enamide (Hex-VUA-Hex). δH (300 MHz, DMSO-d₆, 298 K): δH (300 MHz, DMSO-d₆, 298 K): 8.92 (1H, t, NH), 6.89 (1H, t, NH), 4.28 (1H, s, CH), 3.08 (2H, dd, CH₂), 2.97 (2H, dd, CH₂), 1.77 (3H, s, CH₃), 1.51–1.05 (16H, m, CH₂), 0.86 (3H, t, CH₃), 0.85 (3H, t, CH₃).

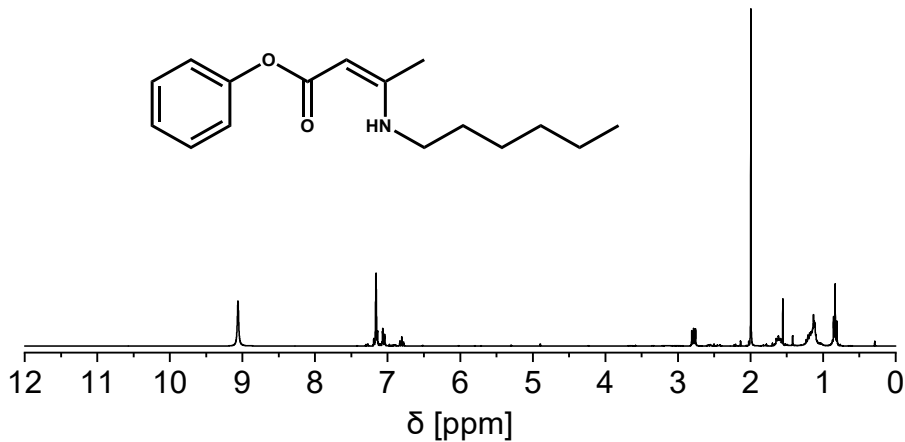


Fig. S22g ¹H NMR spectra (benzene-d₆, 25 °C) of spectrum of the synthesized vinylogous urethane reference compound Phe-VUT-Hex. δH (300 MHz, benzene-d₆, 298 K): 8.90 (1H, s, NH), 4.90 (1H, s, CH), 2.54 (2H, dd, CH₂), 1.41 (3H, s, CH₃), 1.33–1.03 (8H, m, CH₂), 0.89–0.78 (6H, t, CH₃).

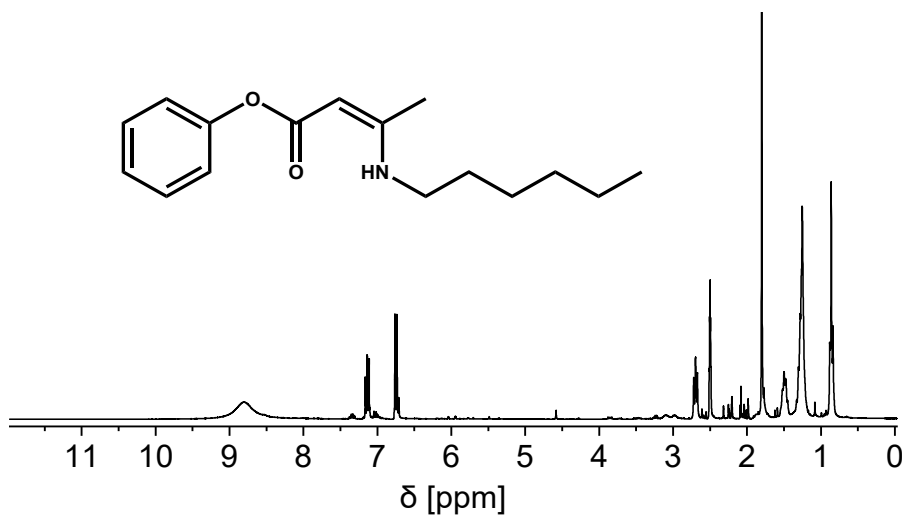


Fig. S22h ¹H NMR spectra (DMSO-d₆, 25 °C) of spectrum of the synthesized vinylogous urethane reference compound (Phe-VUT-Hex). δH (300 MHz, DMSO-d₆, 298 K): 8.52 (1H, s, NH), 7.19–7.06 (2 H, m, Ph), 6.79–6.66 (3H, m, Ph), 4.57 (s, 1H; CH), 3.23 (2H, m, CH₂) 1.77 (3H, s, CH₃), 1.57–1.40 (2H, m, CH₂), 1.35–1.14 (6H, m, CH₂), 0.90–0.78 (3H, t, CH₃). Acetic acid: 8.8 (COOH), 1.77 (3H, s, CH₃).

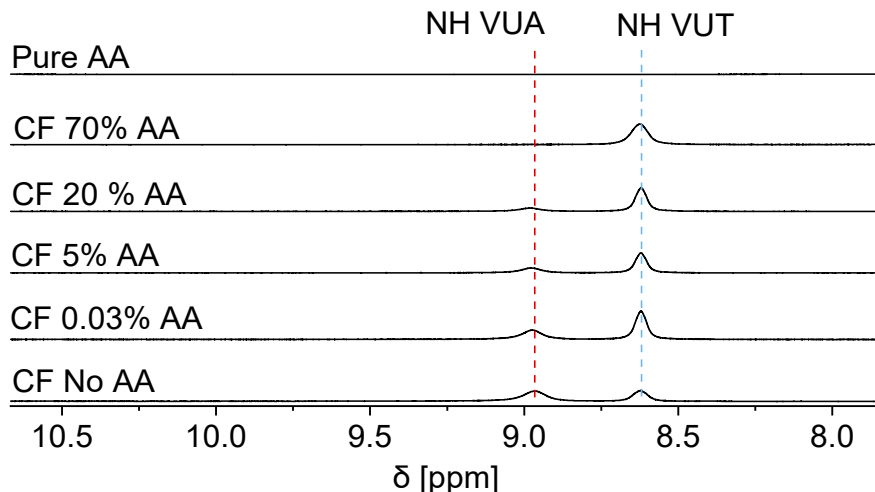


Fig. S23a ¹H NMR spectra (CDCl₃, 25 °C) showing the final ratio of the VUA und VUT compounds by using different amounts of acetic acid (mol %). The ratio was determined by the characteristic NH chemical shifts at 8.98 (VUA) and 8.62 ppm (VUT).

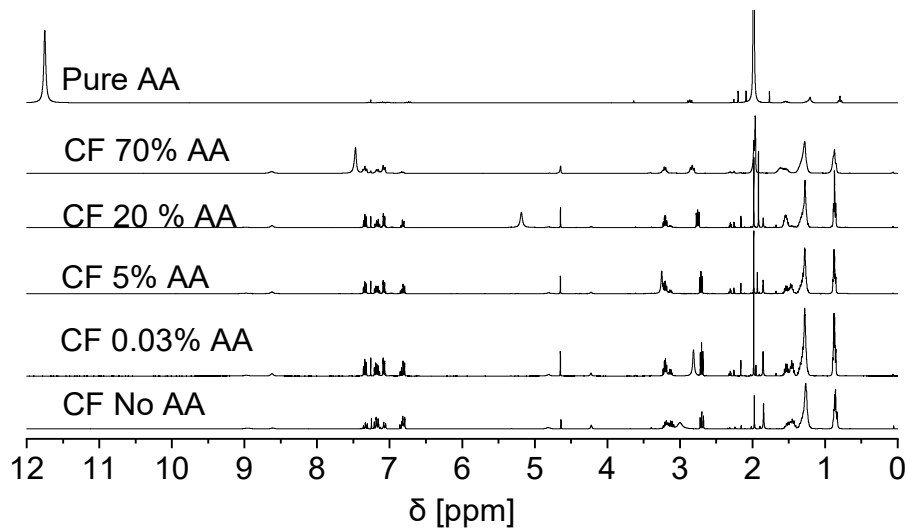


Fig. S23b ^1H NMR spectra (CDCl_3 , 25 °C) showing the final ratio of the VUA und VUT compounds by using different amounts of acetic acid (mol %).

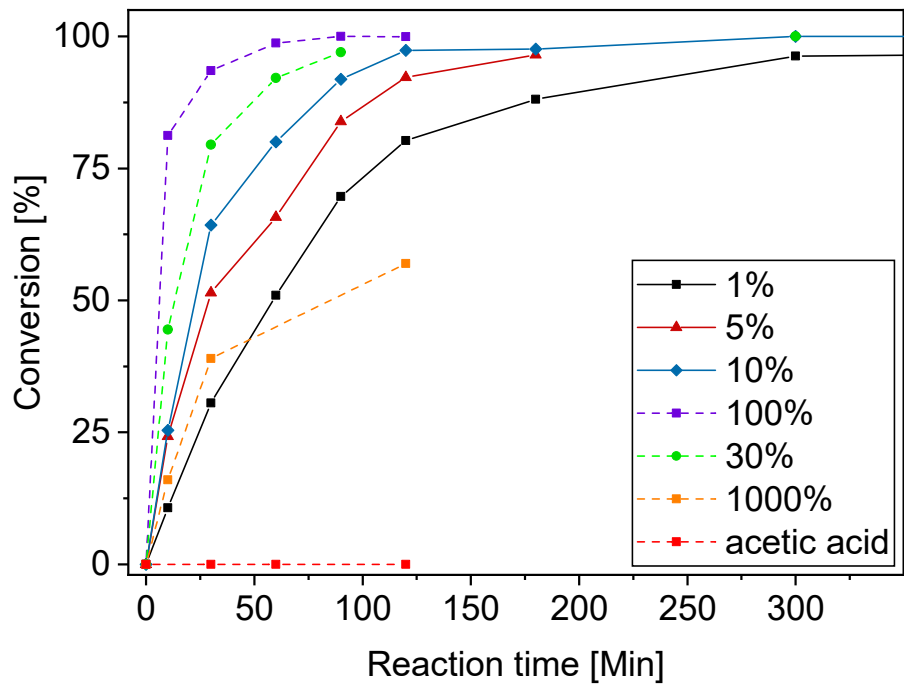


Fig. S24 Conversions of the reaction of phenylacetoacetate (PH) and 2 equivalents of hexylamine in chloroform with different amounts of acetic acid (mol %). The conversion rates are highly increased by using the catalyst, while with higher amount the reaction is slowed down and finally totally inhibited due to protonation of all nucleophilic amines in pure acetic acid.

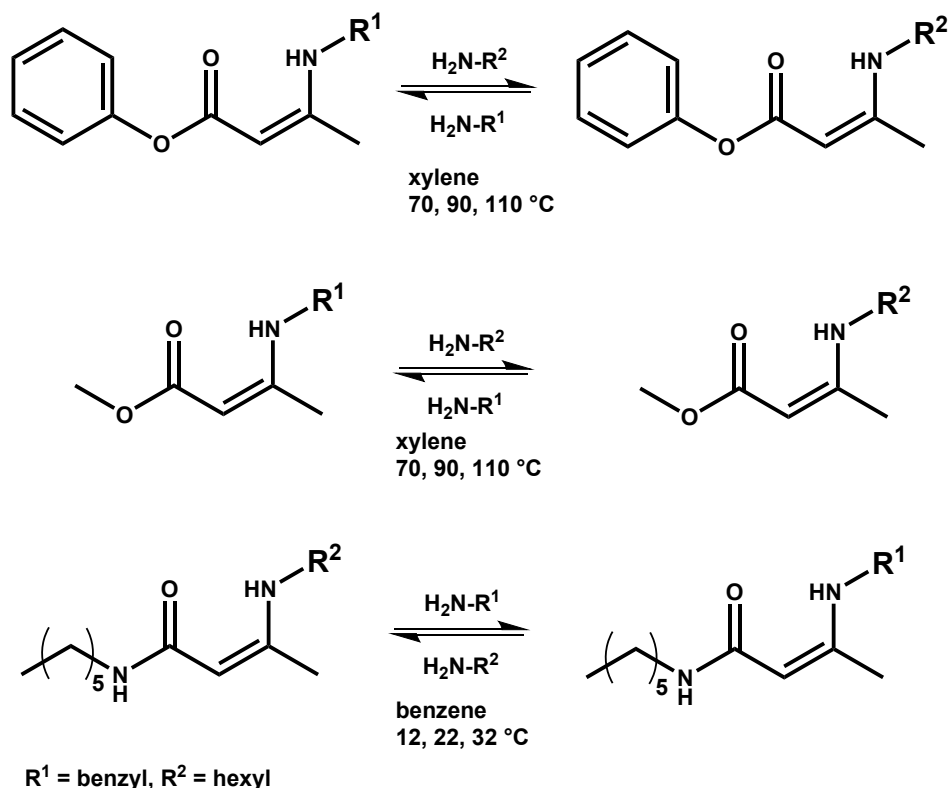


Fig. S25 Overview of the conducted exchange reactions. The transamination reaction of the aromatic vinylogous urethane compounds (top), the aliphatic vinylogous urethane compounds (middle) and the vinylogous urea compounds were investigated (bottom).

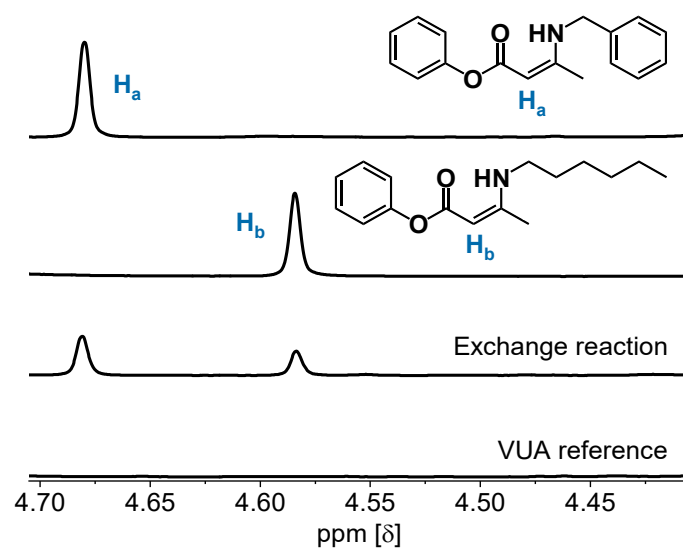


Fig. S26a ^1H NMR spectra (CDCl_3 , 25 °C) showing the characteristic vinylic protons of the reference compounds Phe-VUT-Hex and Phe-VUT-Bz in comparison to the spectrum after the exchange reaction. The signals clearly show the appearance of both signals.

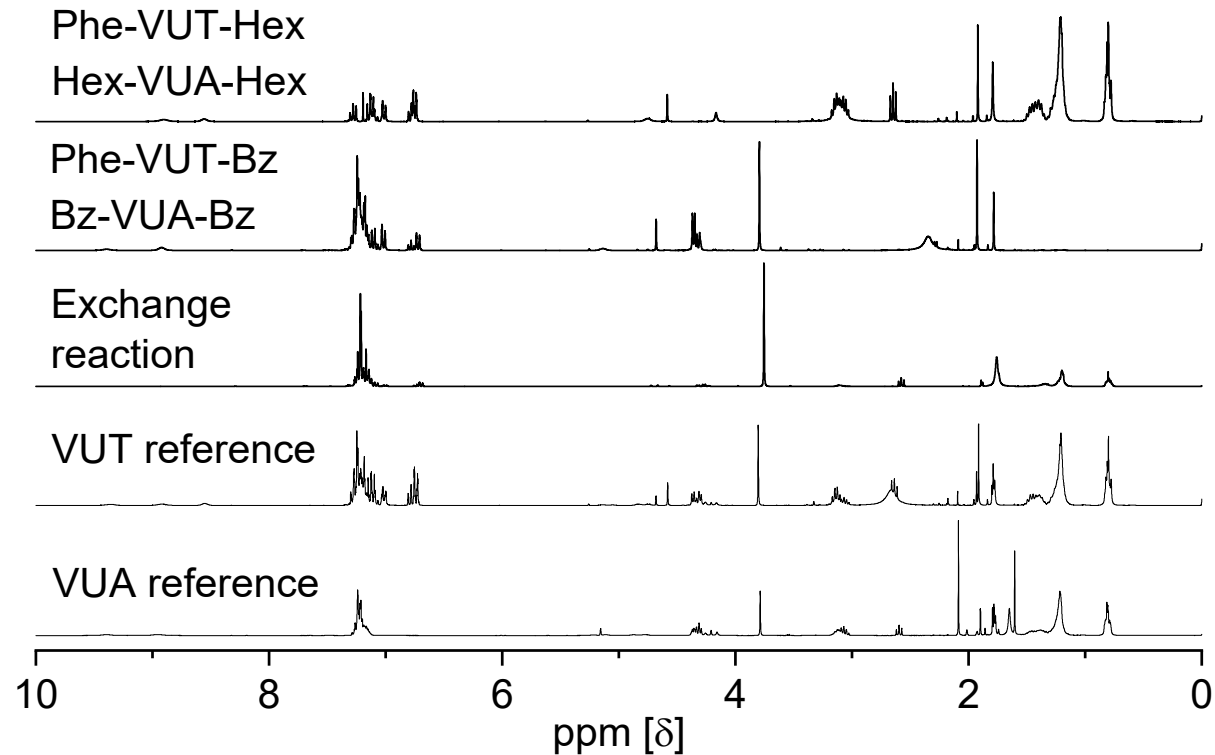


Fig. S26b ^1H NMR spectra (CDCl_3 , 25 °C) showing the signals of the vinylogous urethane compounds Phe-VUT-Hex and Phe-VUT-Bz and the resulting spectra after the exchange reaction, proving the exchange reaction by showing the presence of both signals. ^1H NMR spectra of the characteristic NH protons before and after the exchange reaction in comparison to the vinylogous urethane and urea compounds Phe-VUT-Hex, Phe-VUT-Bz, Hex-VUA-Hex and Hex-VUA-Bz, proving the exchange reaction of the vinylogous urea compounds.

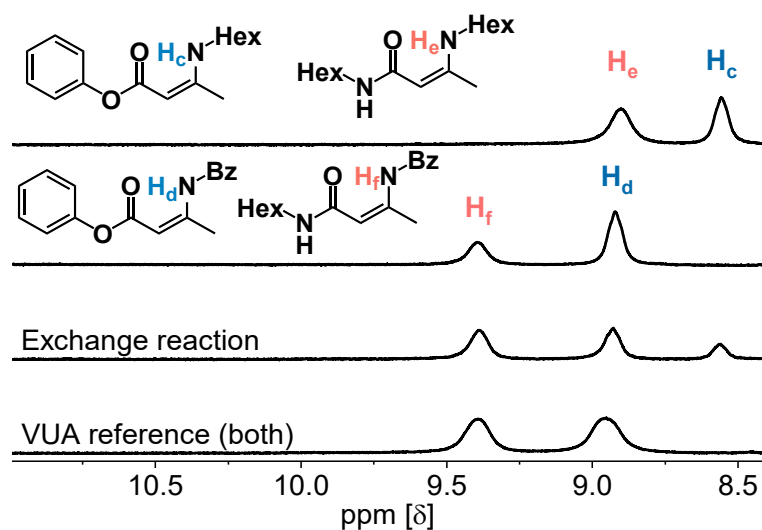


Fig. S27 ^1H NMR spectra (CDCl_3 , 25 °C) of the characteristic NH protons before and after the exchange reaction in comparison to the vinylogous urethane and urea compounds Phe-VUT-Hex, Phe-VUT-Bz, Hex-VUA-Hex and Hex-VUA-Bz, proving the exchange reaction of the vinylogous urea compounds.

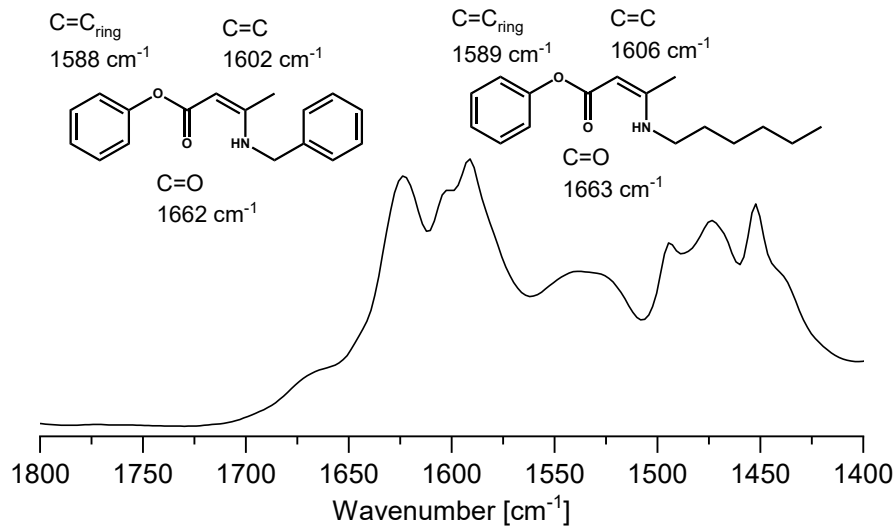


Fig. 28 ATR-FT-IR spectra did not show a visible significant shift in the $\text{C}=\text{O}$ ester or $\text{C}=\text{C}$ bands after the exchange reaction.

Calculation of the activation energy (E_a) via an Arrhenius law:

The decrease of the reactant concentration as a function of time is described by:^[33]

$$[R] = 1 - c_p + c_p * e^{\frac{-kt}{c_p}}$$

$[R]$	concentration reactant
c_p	equilibrium ratio of the
	products (5)
k	initial rate (fitted)
t	reaction time [s]

Equation S1: Exponential fit for the conversion of the reactant to determine the initial rate k .

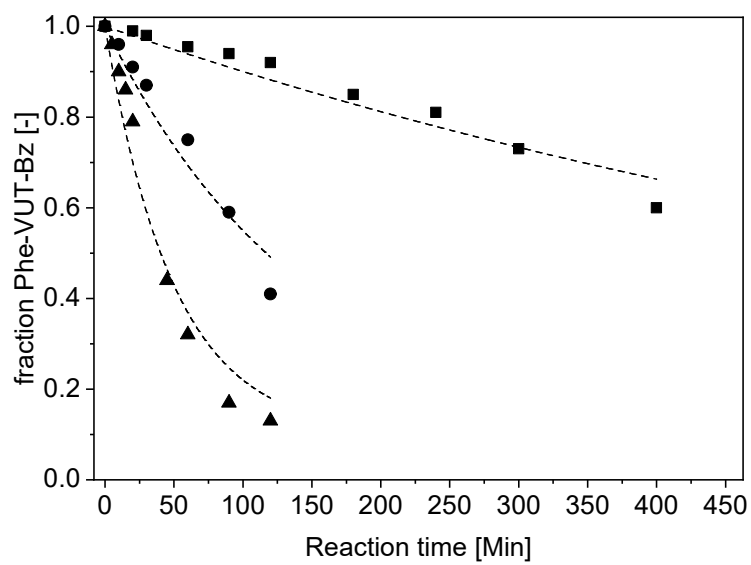


Fig. S29a Monitoring the decay of the vinylogous urethane compound Phe-VUT-Bz at 70, 90 and 110 °C during the exchange reaction with hexylamine.

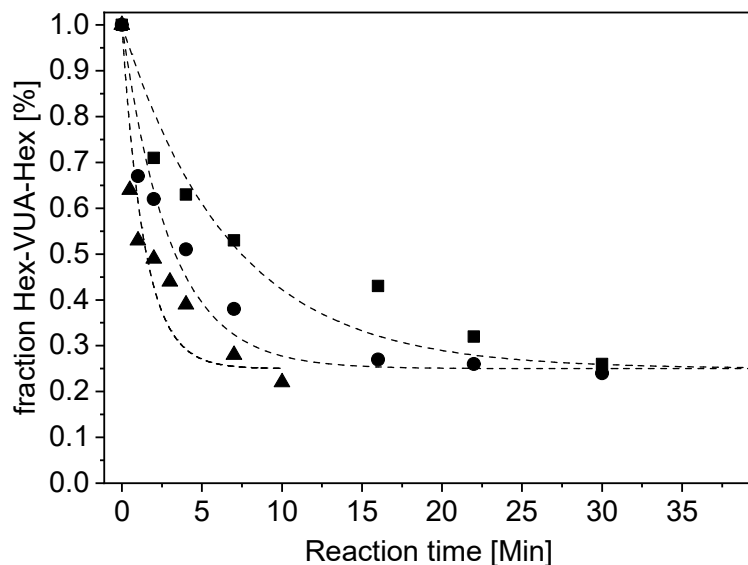


Fig. S29b Monitoring the decay of the vinylogous urea compound Hex-VUA-Hex at 12, 22 and 32 °C during the exchange reaction with benzylamine.

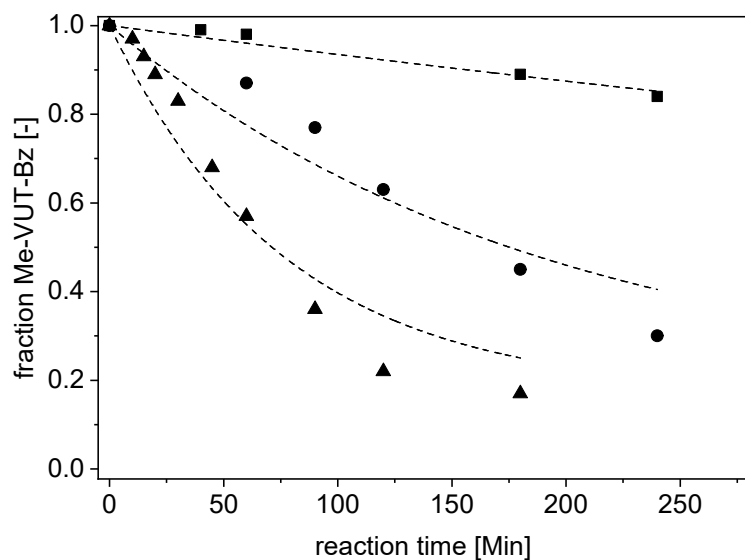


Fig. S29c Monitoring the decay of the vinylogous urethane compound Methyl-VUT-Bz at 70, 90 and 110 °C during the exchange reaction with hexylamine.

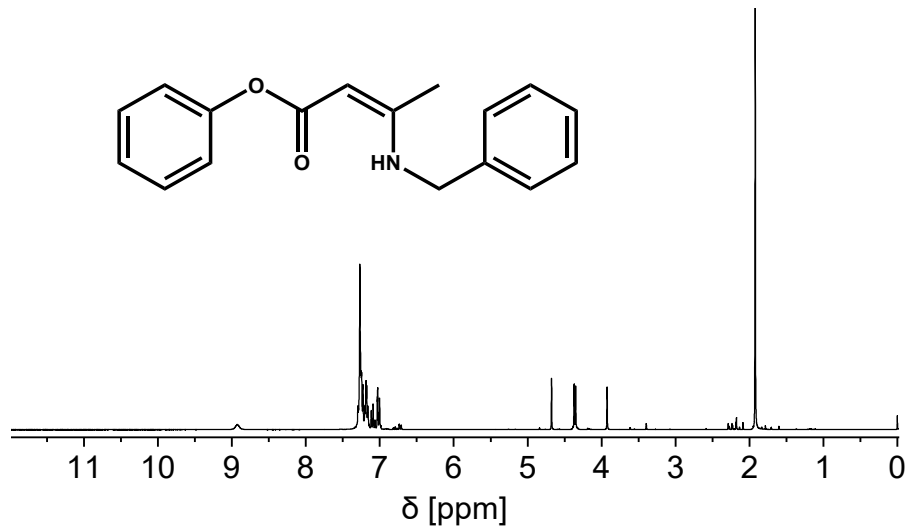


Fig. S30a ^1H NMR spectra (CDCl_3 , 25 °C) of spectrum of the synthesized vinylogous urethane reference compound (Phe-VUT-Bz). δH (300 MHz, CDCl_3 , 298 K): 8.98 (1H, t, NH), 7.33–7.03 (10H, m, Ph), 4.72 (1H, s, CH), 4.36 (2H, d, CH_2), 1.94 (s, 3H, CH_3).

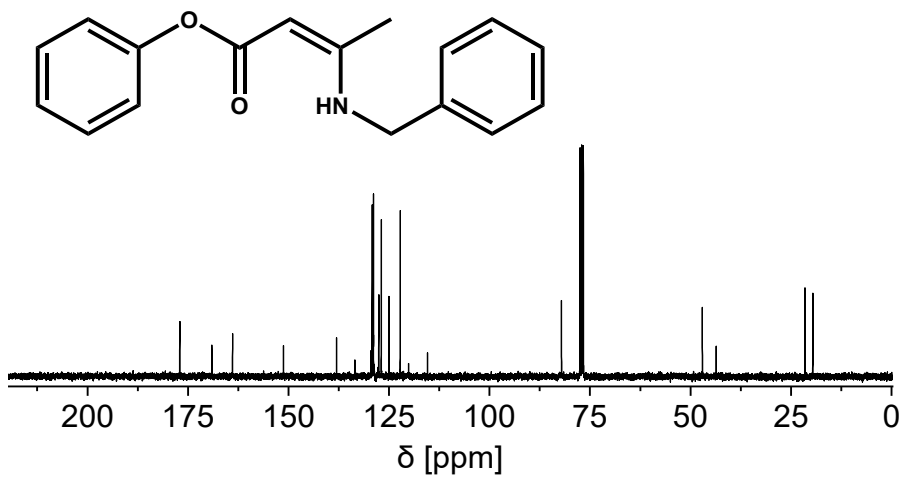


Fig. S30b ^{13}C NMR (broadband decoupled, CDCl_3 , 25 °C) spectrum of the synthesized vinylogous urethane reference compound Phe-VUT-Bz. δC (75 MHz, CDCl_3 , Me_4Si): 169.16 (q, COO), 164.08 (q, C=C), 151.54 (q, Ph-O), 129.28 (t, Ph), 124.96 (t, Ph), 122.32 (t, Ph), 80.82 (t, CH), 43.38 (s, CH_2), 31.59 (s, CH_2), 31.32 (s, CH_2), 26.62 (s, CH_2), 22.49 (s, CH_2), 31.6 (p, C- CH_3) 14.11 (p, $\text{CH}_2\text{-CH}_3$).

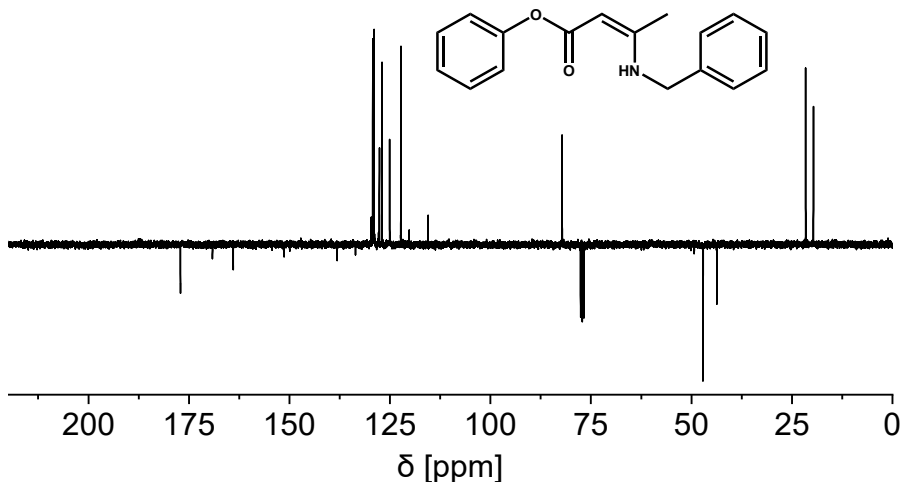


Fig. S30c ^{13}C NMR (DEPTQ-135, CDCl_3 , 25 °C) spectrum of the synthesized vinylogous urethane reference compound Phe-VUT-Bz. δC (75 MHz, CDCl_3 , Me_4Si): 169.16 (q, COO), 164.08 (q, C=C), 151.54 (q, Ph-O), 129.28 (t, Ph), 124.96 (t, Ph), 122.32 (t, Ph), 80.82 (t, CH), 43.38 (s, CH_2), 31.59 (s, CH_2), 31.32 (s, CH_2), 26.62 (s, CH_2), 22.49 (s, CH_2), 31.6 (p, C- CH_3) 14.11 (p, $\text{CH}_2\text{-CH}_3$).

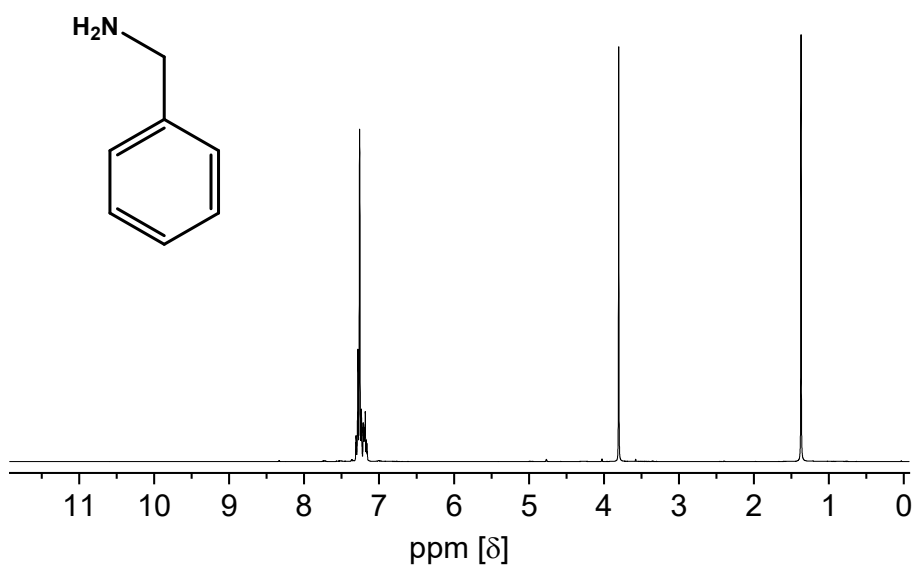


Fig. S30d ^1H NMR spectra (CDCl_3 , 25 °C) of spectrum of benzylamine. δH (300 MHz, CDCl_3): δH (300 MHz, CDCl_3 , 25°C): 7.31–7.15 (5H, m, Ph), 3.80 (2H, s, CH_2), 1.37 (2H, s, NH_2).

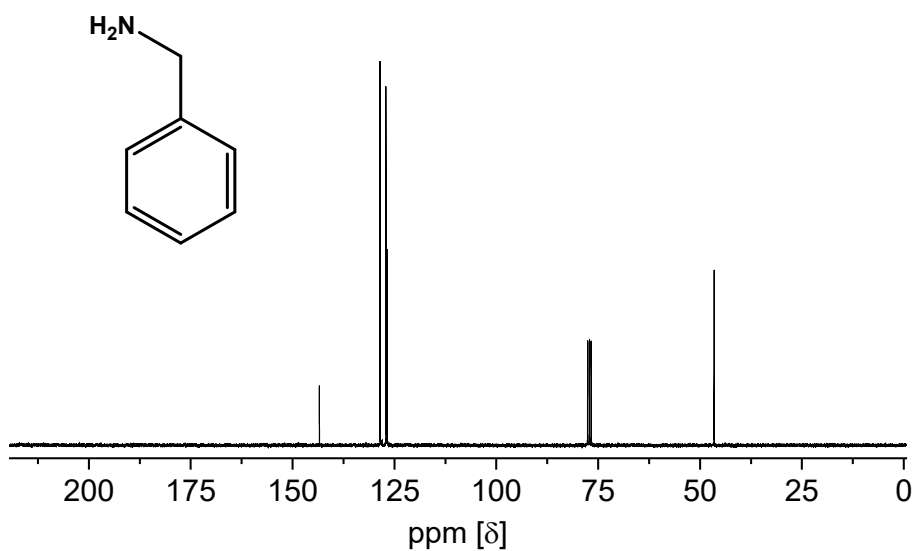


Fig. S30e ^{13}C NMR (broadband decoupled, CDCl_3 , 25 °C) spectrum of benzylamine. δC (75 MHz, CDCl_3): 143.42 (q, Ph), 128.56 (t, Ph), 127.08 (t, Ph), 126.79 (t, Ph), 46.56 (s, CH_2).

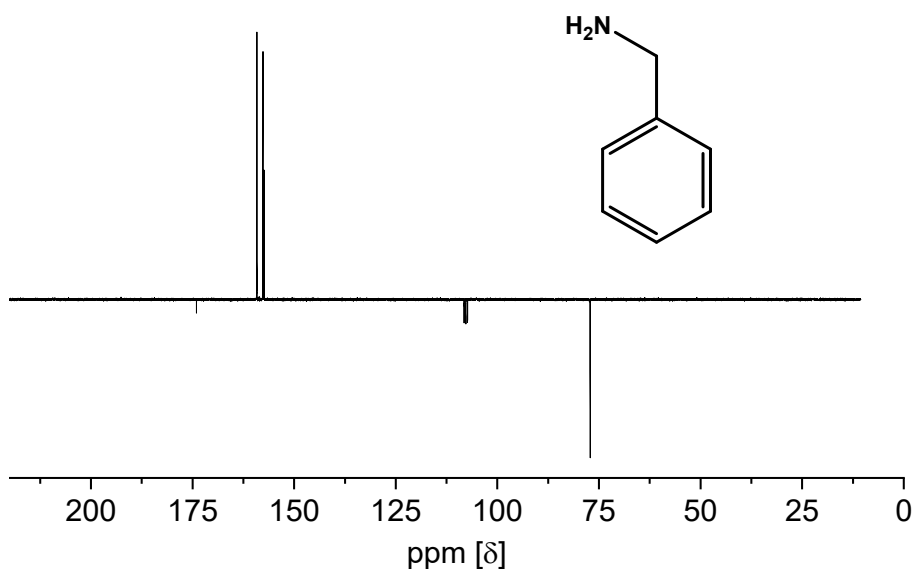


Fig. S30f ^{13}C NMR (DEPTQ-135, CDCl_3 , 25 °C) spectrum of benzylamine. δC (75 MHz, CDCl_3): 143.42 (q, Ph), 128.56 (t, Ph), 127.08 (t, Ph), 126.79 (t, Ph), 46.56 (s, CH_2).

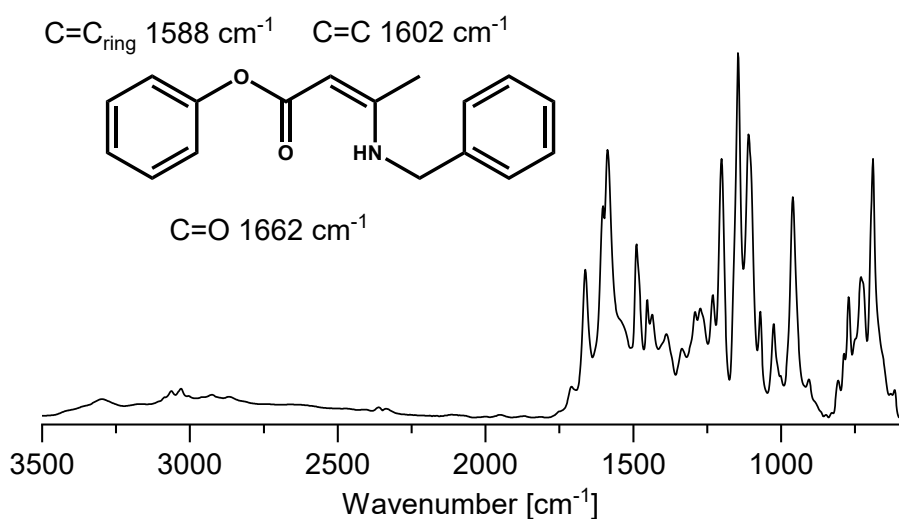


Fig. S31 ATR-FT-IR spectrum of the vinylogous vinylogous urethane reference compound Phe-VUT-Bz with the characteristic C=O ester band at 1662 cm^{-1} and C=C band at 1602 cm^{-1} .

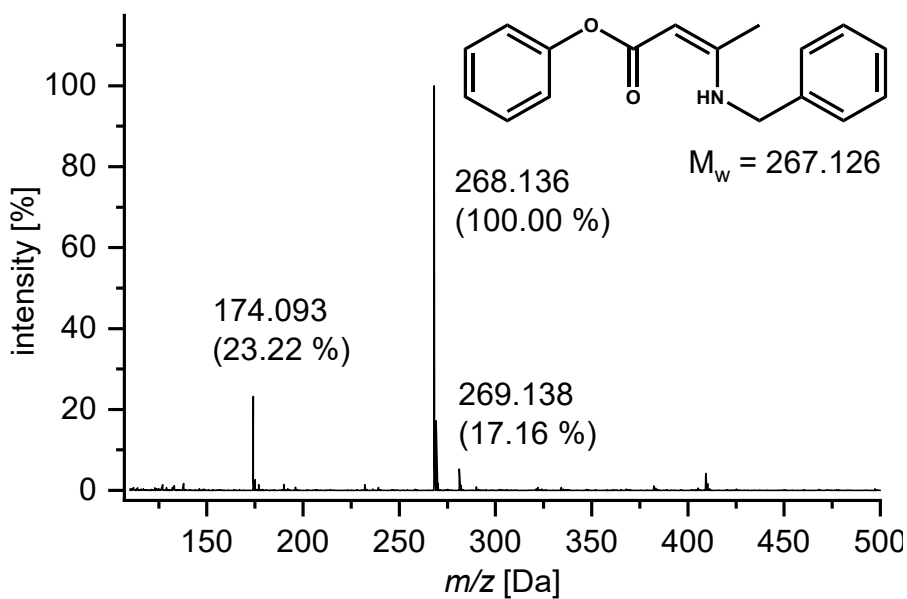


Fig. S32 ESI-MS spectrum of the synthesized vinylogous urethane compound Phe-VUT-Bz showing the characteristic molecule ion peak $m/z = 268.136$ ($M^+ + 1$) and $m/z = 269.138$ ($M^+ + 2$).

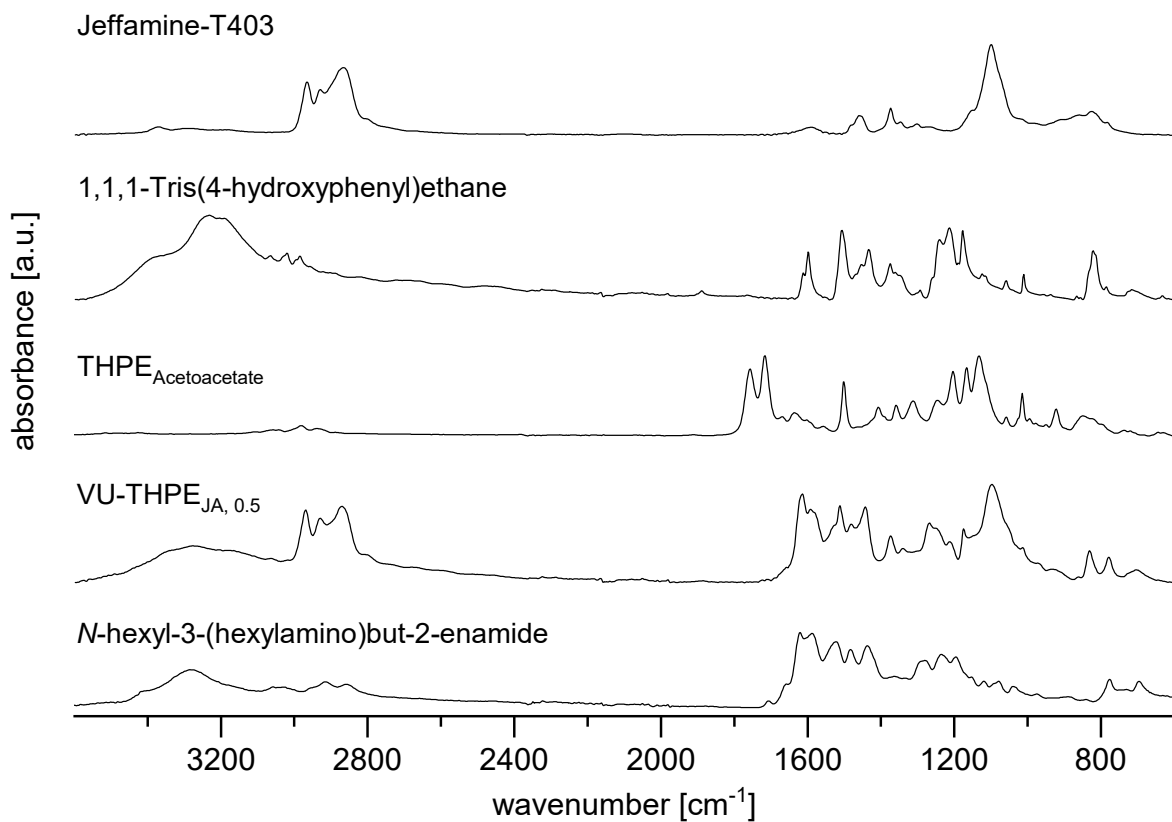


Fig. S33 ATR-FT-IR spectra of the reactants Jeffamine-T403, 1,1,1-Tris(4-hydroxyphenyl)ethane, the acetoacetate monomer THPE_{AcAc}, the vinylogous urea reference N-hexyl-3-(hexylamino)but-2-enamide and the product VU-THPE_{JA, 0.5}.

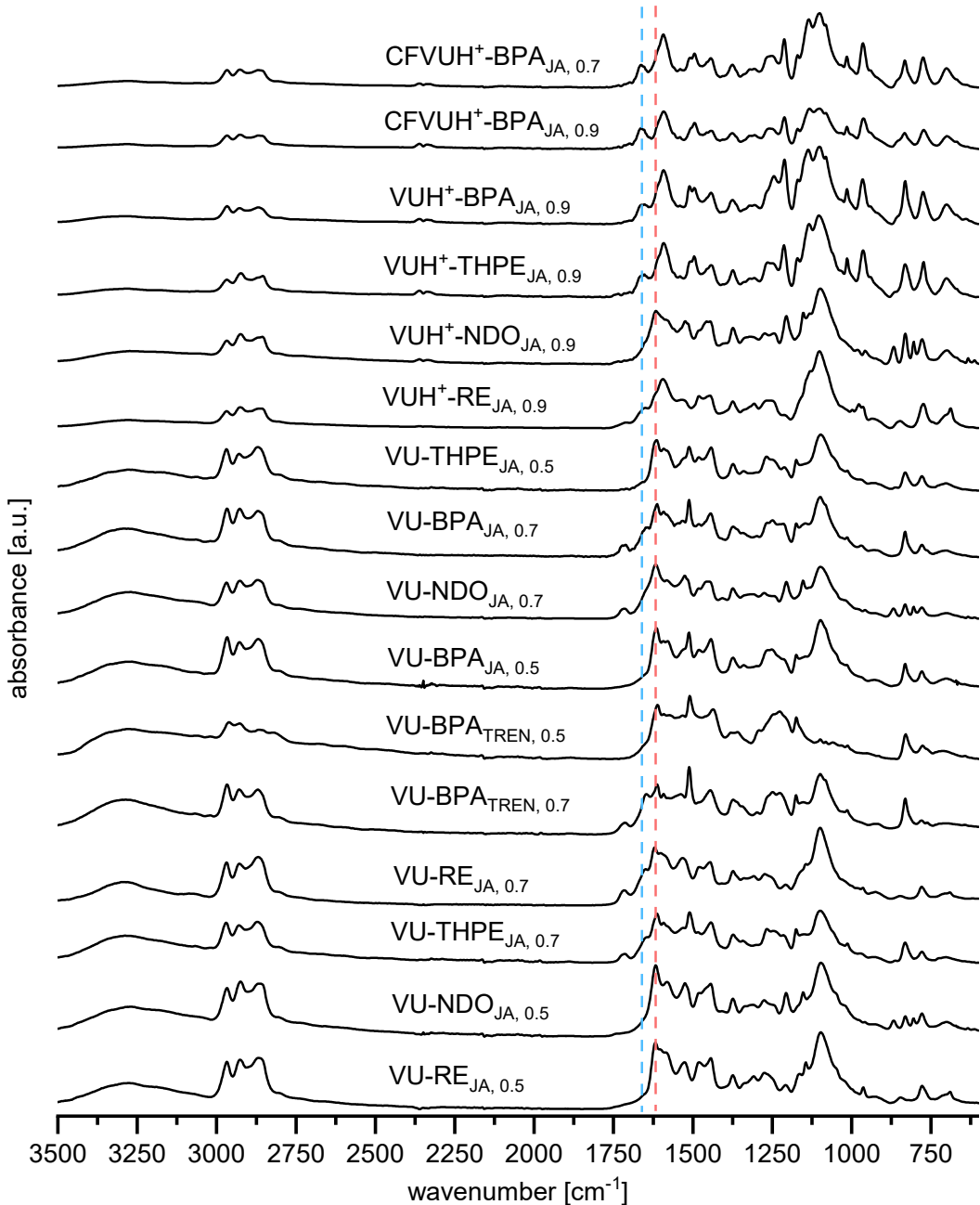


Fig. S34a ATR-FT-IR spectra of all synthesized blended poly (vinylidene urethane/urea) vitrimer networks derived from RE, NDO, BPA and THPE cured with JA or TREN with and without acetic acid in a bulk or solvent-based polymerization. The blue line marks the

characteristic VUT C=O ester band, while the red line marks the characteristic VUA C=O amid band.

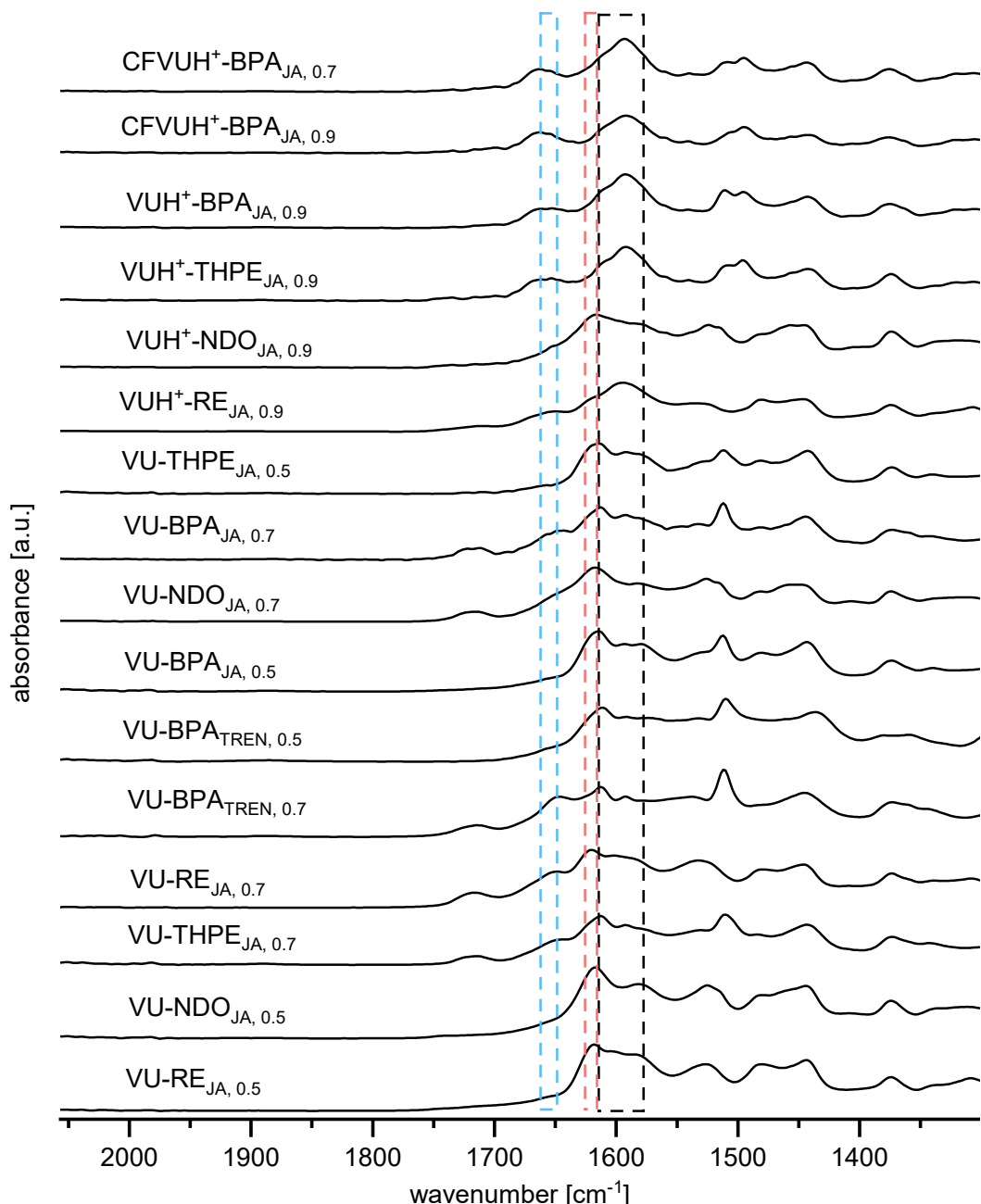


Fig. S34b ATR-FT-IR spectra of all synthesized blended poly (vinylogous urethane/urea) vitrimer networks derived from RE, NDO, BPA and THPE cured with JA or TREN with and without acetic acid in a bulk or solvent-based polymerization. The blue line marks the

characteristic VUT C=O ester band, while the red line marks the characteristic VUA C=O amid band. The black line marks the area of C=C stretching bands.

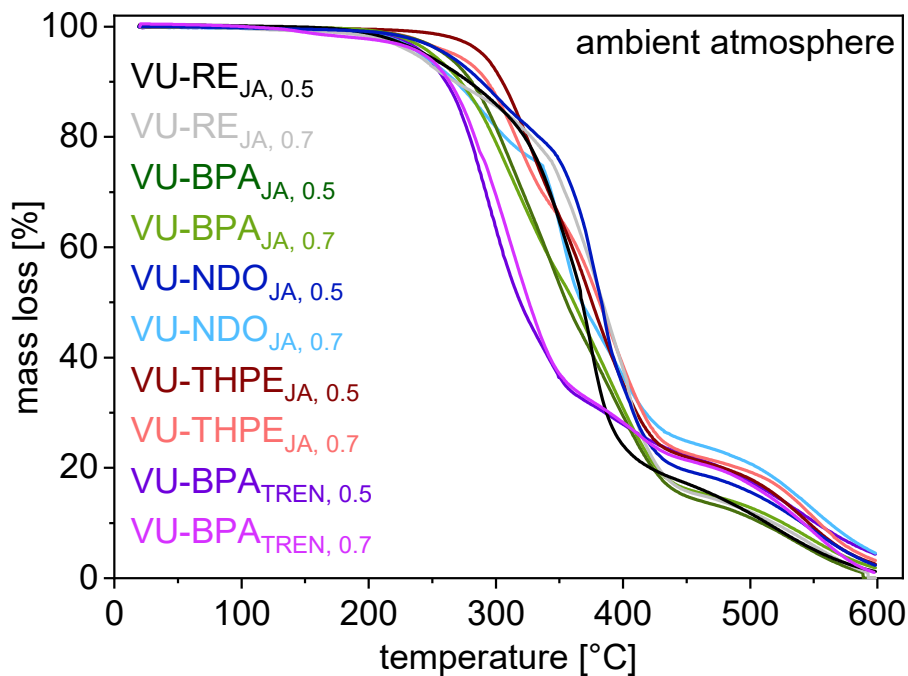


Fig. S35a Thermogravimetric analysis (TGA) measurements of the vitrimers cured without additional catalyst and acetoacetate to amine ratios of 0.5 and 0.7. The thermal degradation points were determined at 5 % mass loss.

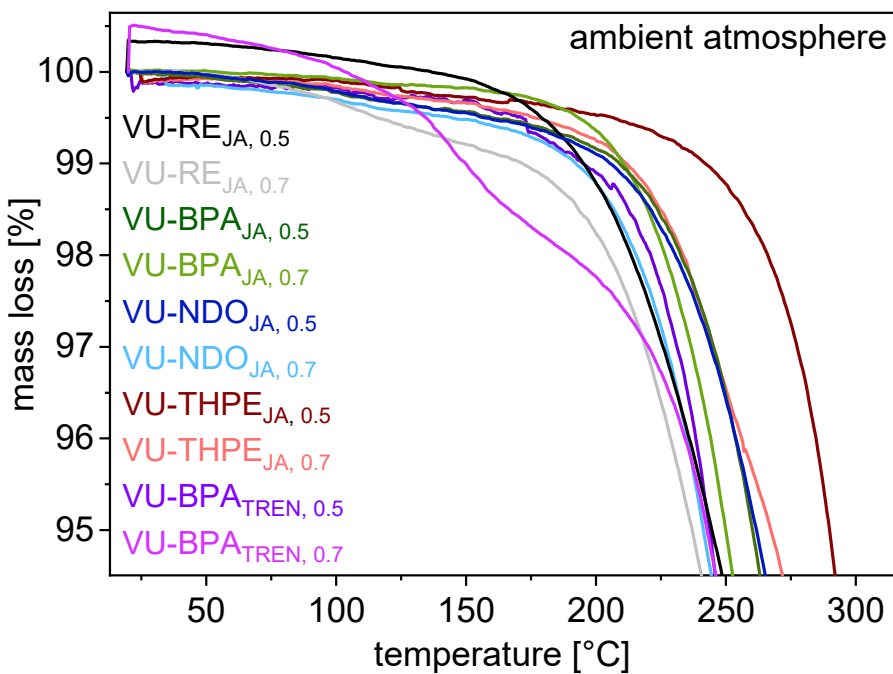


Fig. S35b Details of the thermogravimetric analysis (TGA) measurements of the vitrimers cured without additional catalyst and acetoacetate to amine ratios of 0.5 and 0.7. The thermal degradation points were determined at 5 % mass loss.

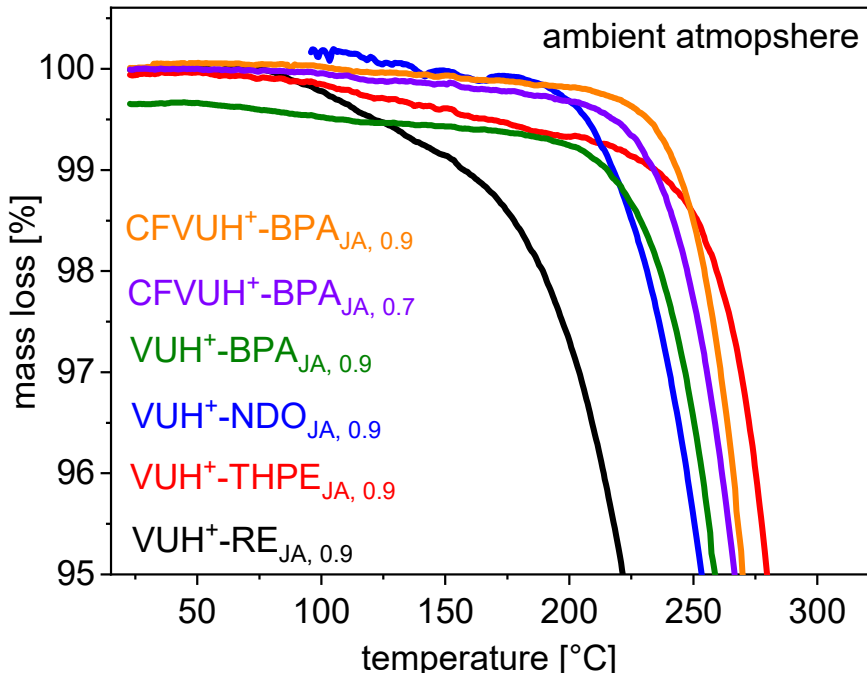


Fig. S35c Details of the thermogravimetric analysis (TGA) measurements of the vitrimers cured with additional acetic acid and/or chloroform as solvent. The thermal degradation points were determined at 5 % mass loss.

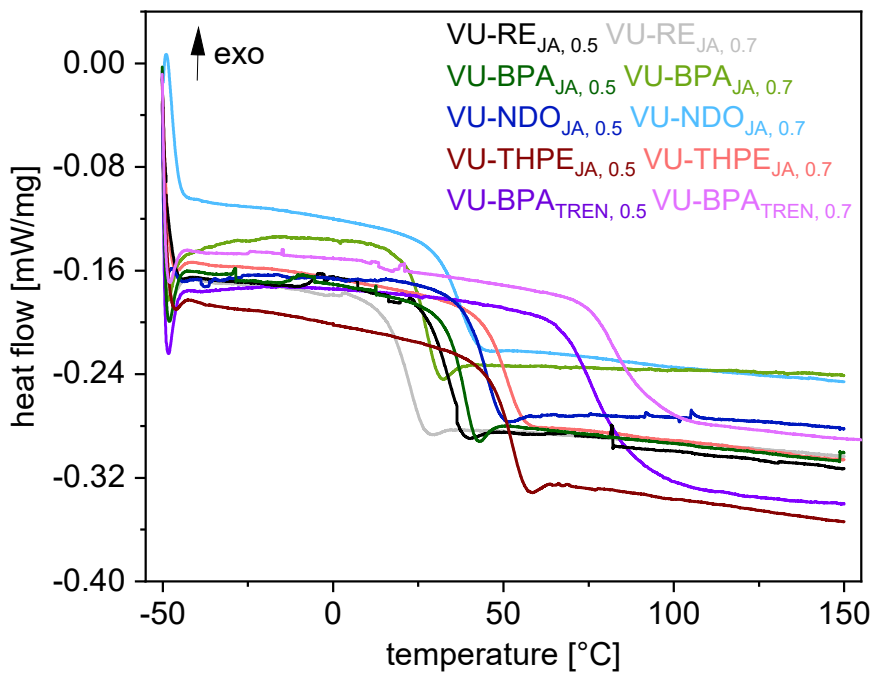


Fig. S36a Differential scanning calorimetrerie (DSC) measurements of the vitrimers polymerized with JA or TREN and acetoacetate to amine ratios of 0.5 or 0.7 and without catalyst.

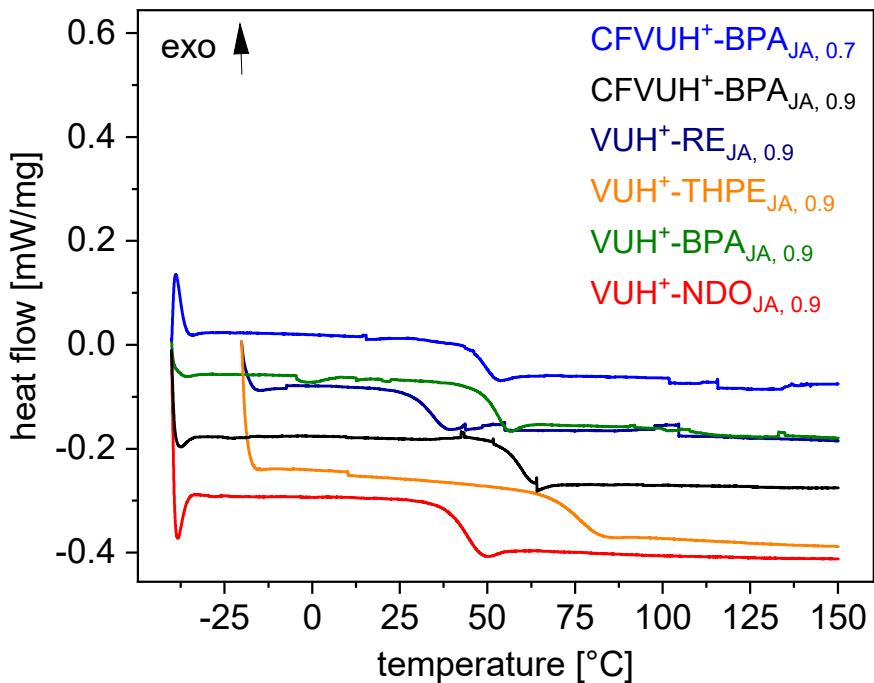


Fig. S36b Differential scanning calorimetrerie (DSC) measurements of the vitrimers polymerized with JA and an acetoacetate to amine ratios of 0.7 or 0.9 with acetic acid as catalyst.

Calculation of the activation energy (E_a) by stress relaxation experiments:^[1]

The stress relaxation times as a function of temperature can be described by an Arrhenius law:

$$\tau(T) = \tau_0 e^{\frac{E_a}{RT}}$$

τ	stress relaxation time (37 %)	[s]
τ_0	Stress relaxation time	[s]
	(normalized 0,1)	
E_a	activation energy	[kJ mol ⁻¹]
R	gas constant	[J K ⁻¹ mol ⁻¹]
T	temperature	[K]

Equation S2: Arrhenius law for calculating the activation energy by stress-relaxation times according to Maxwell law for viscoelastic fluids (37%, 1/e) as a function of temperature.

The activation energy was calculated by plotting $\ln k$ versus $1000/T$.

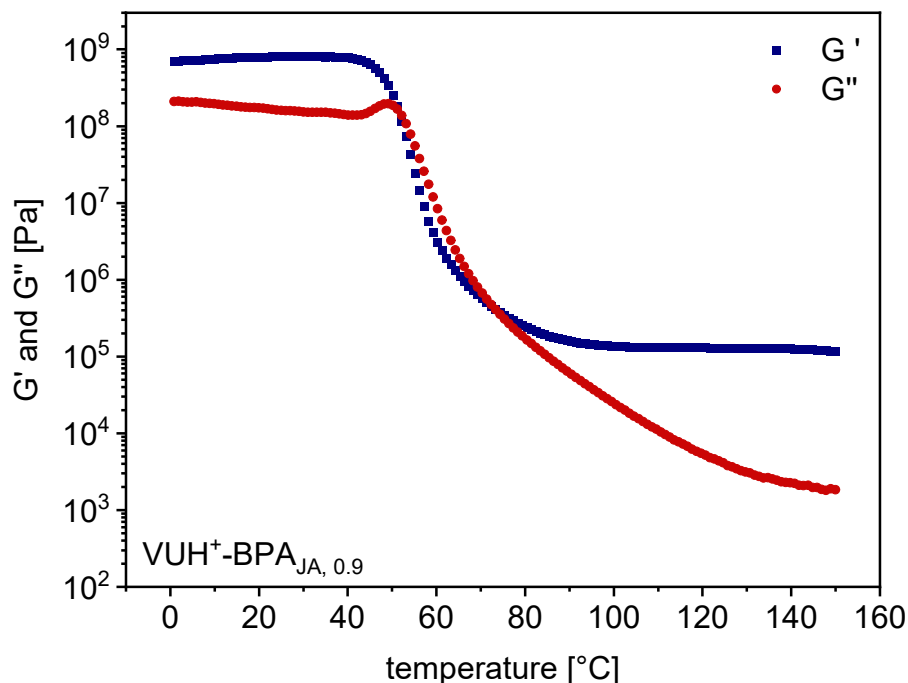


Fig. S37a Temperature-dependent DMA measurement ($\omega = 10$ rad/s, $y = 0.1\%$) of VUH⁺-BPA_{JA, 0.9} in the temperature range of 0–150 °C, showing the storage- and loss modulus (G' and G'') with the characteristic rubbery plateau of the cross-linked material at elevated temperatures up to 150 °C.

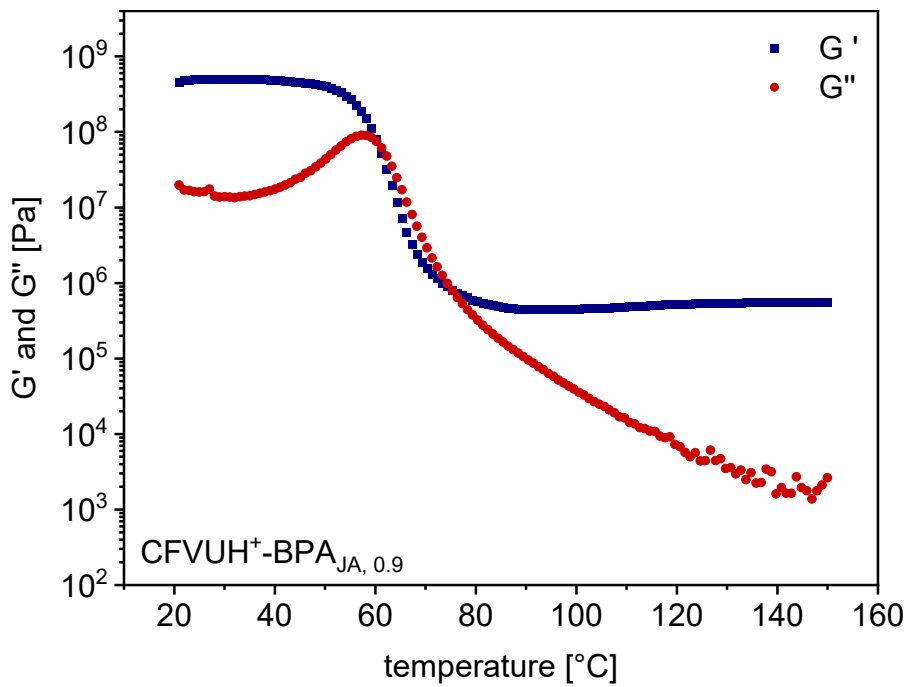


Fig. S37b Temperature-dependent DMA measurement ($\omega = 10 \text{ rad/s}$, $y = 0.1 \%$) of CFVUH⁺-BPA_{JA, 0.9} in the temperature range of 20–150 °C, showing the storage- and loss modulus (G' and G'') with the characteristic rubbery plateau of the cross-linked material at elevated temperatures up to 150 °C.

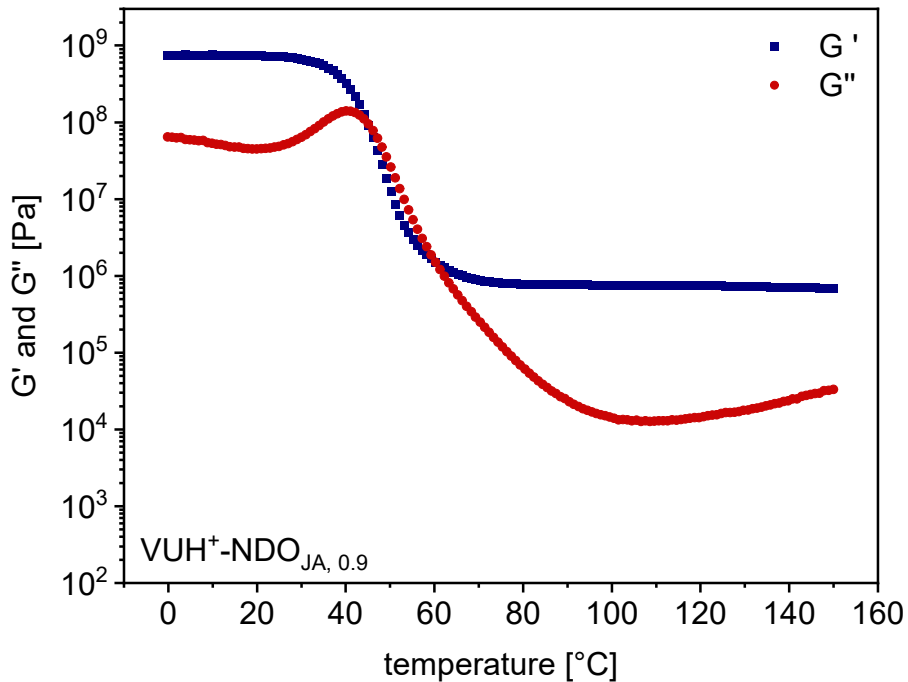


Fig. S37c Temperature-dependent DMA measurement ($\omega = 10 \text{ rad/s}$, $y = 0.1 \%$) of VUH⁺-NDO_{JA, 0.9} in the temperature range of 0–150 °C, showing the storage- and loss modulus (G' and G'') with the characteristic rubbery plateau of the cross-linked material at elevated temperatures up to 150 °C.

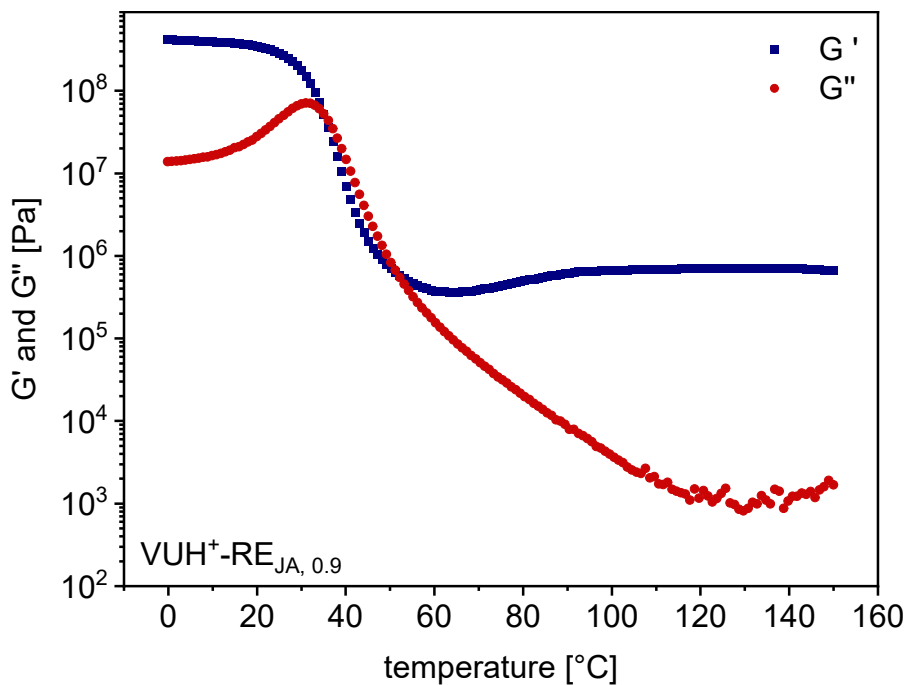


Fig. S37d Temperature-dependent DMA measurement ($\omega = 10 \text{ rad/s}$, $y = 0.1 \%$) of $\text{VUH}^+ \text{-RE}_{\text{JA}, 0.9}$ in the temperature range of 0–150 °C, showing the storage- and loss modulus (G' and G'') with the characteristic rubbery plateau of the cross-linked material at elevated temperatures up to 150 °C.

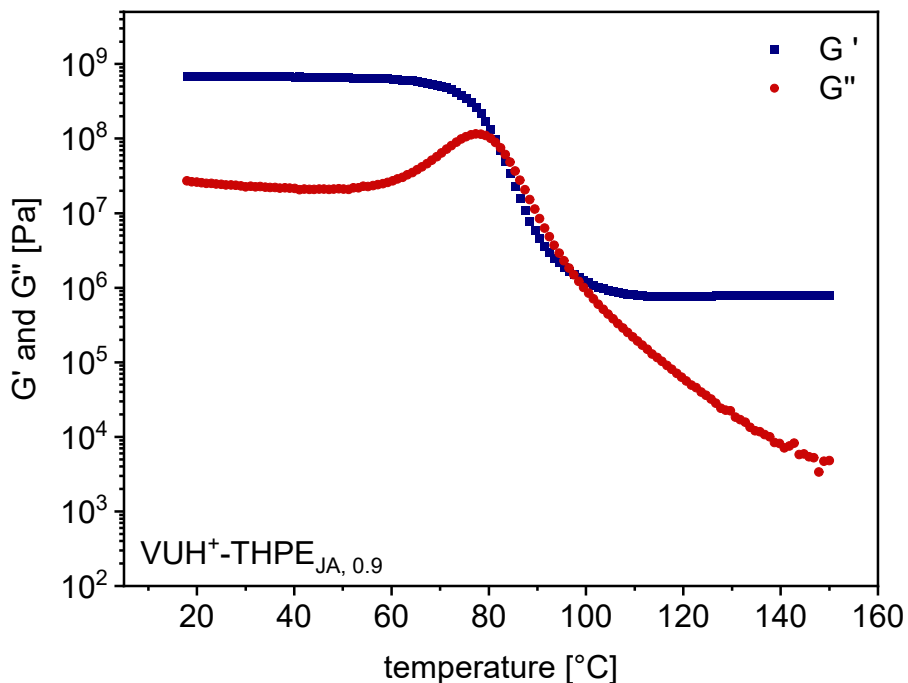


Fig. S37e Temperature-dependent DMA measurement ($\omega = 10 \text{ rad/s}$, $y = 0.1 \%$) of $\text{VUH}^+ \text{-THPE}_{\text{JA}, 0.9}$ in the temperature range of 20–150 °C, showing the storage- and loss modulus (G' and G'') with the characteristic rubbery plateau of the cross-linked material at elevated temperatures up to 150 °C.

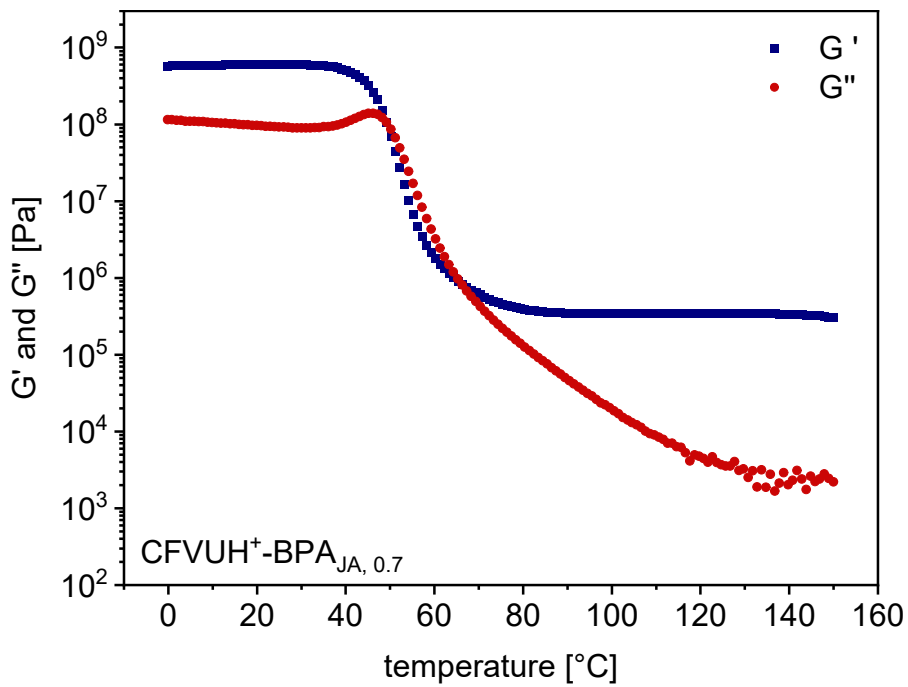


Fig. S37f Temperature-dependent DMA measurement ($\omega = 10 \text{ rad/s}$, $y = 0.1 \%$) of $\text{VUH}^+ \text{-BPA}_{\text{JA}, 0.7}$ in the temperature range of 0–150 $^\circ\text{C}$, showing the storage- and loss modulus (G' and G'') with the characteristic rubbery plateau of the cross-linked material at elevated temperatures up to 150 $^\circ\text{C}$.

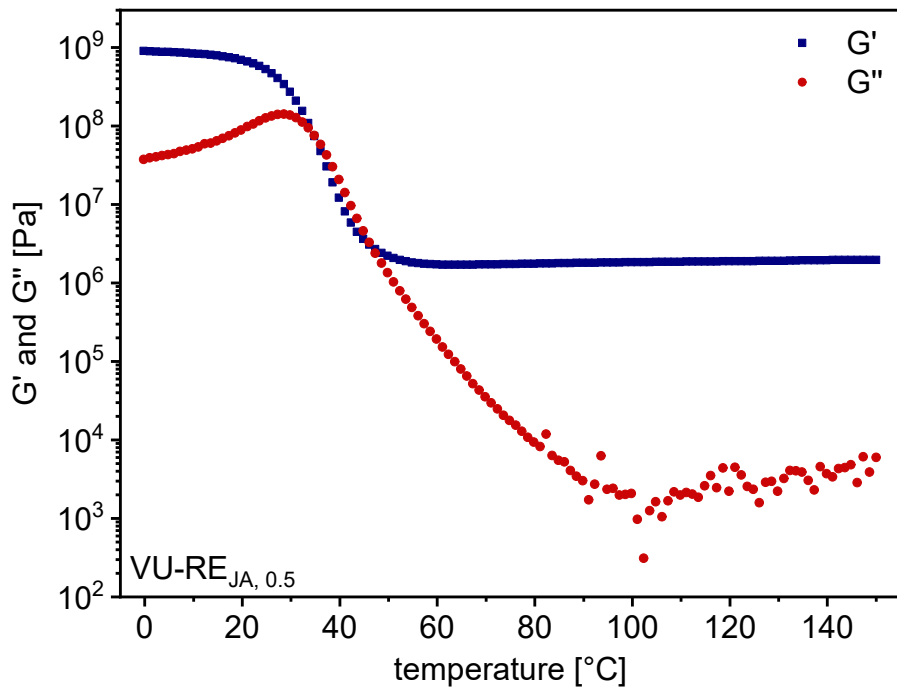


Fig. S37g Temperature-dependent DMA measurement ($\omega = 10 \text{ rad/s}$, $y = 0.1 \%$) of $\text{VU-RE}_{\text{JA}, 0.5}$ in the temperature range of 0–150 $^\circ\text{C}$, showing the storage- and loss modulus (G' and G'') with the characteristic rubbery plateau of the cross-linked material at elevated temperatures up to 150 $^\circ\text{C}$.

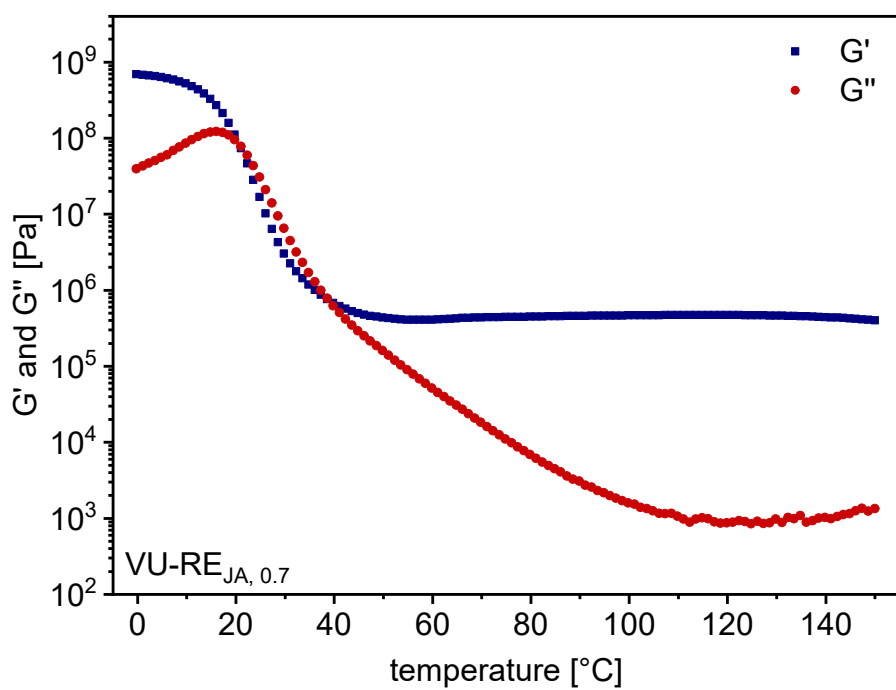


Fig. S37h Temperature-dependent DMA measurement ($\omega = 10 \text{ rad/s}$, $y = 0.1 \%$) of VU-RE_{JA}, 0.7 in the temperature range of 0–150 °C, showing the storage- and loss modulus (G' and G'') with the characteristic rubbery plateau of the cross-linked material at elevated temperatures up to 150 °C.

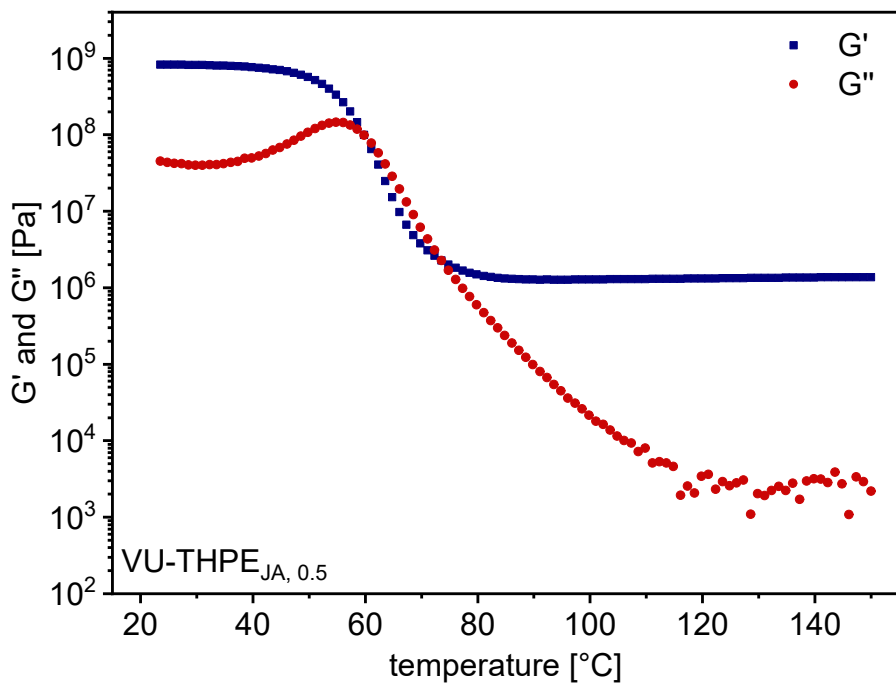


Fig. S37i Temperature-dependent DMA measurement ($\omega = 10 \text{ rad/s}$, $y = 0.1 \%$) of VU-THPE_{JA}, 0.5 in the temperature range of 20–150 °C, showing the storage- and loss modulus (G' and G'') with the characteristic rubbery plateau of the cross-linked material at elevated temperatures up to 150 °C.

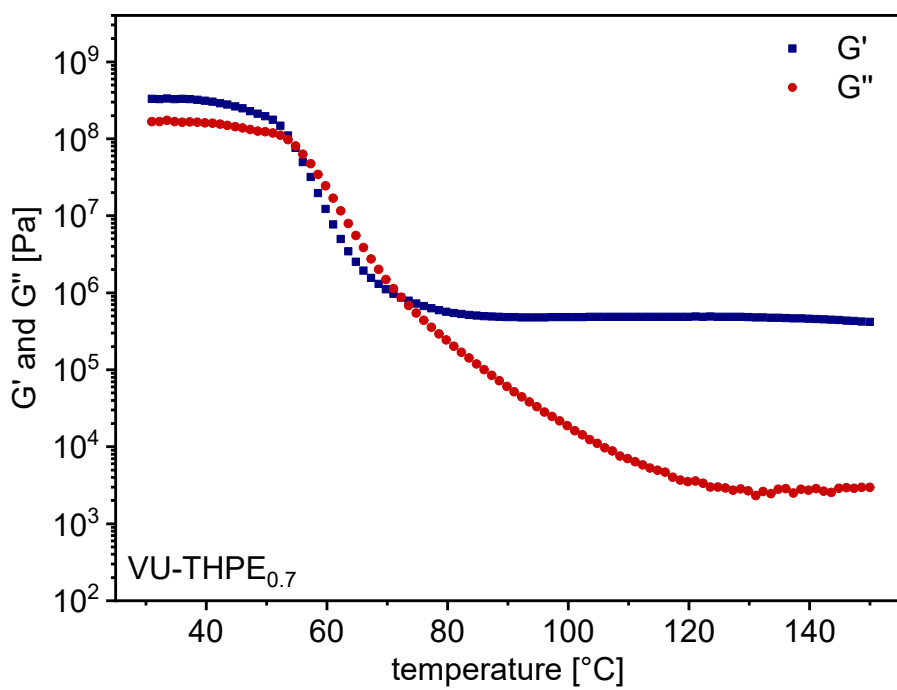


Fig S37j Temperature-dependent DMA measurement ($\omega = 10 \text{ rad/s}$, $\gamma = 0.1 \%$) of VU-THPE_{JA, 0.7} in the temperature range of 20–150 °C, showing the storage- and loss modulus (G' and G'') with the characteristic rubbery plateau of the cross-linked material at elevated temperatures up to 150 °C.

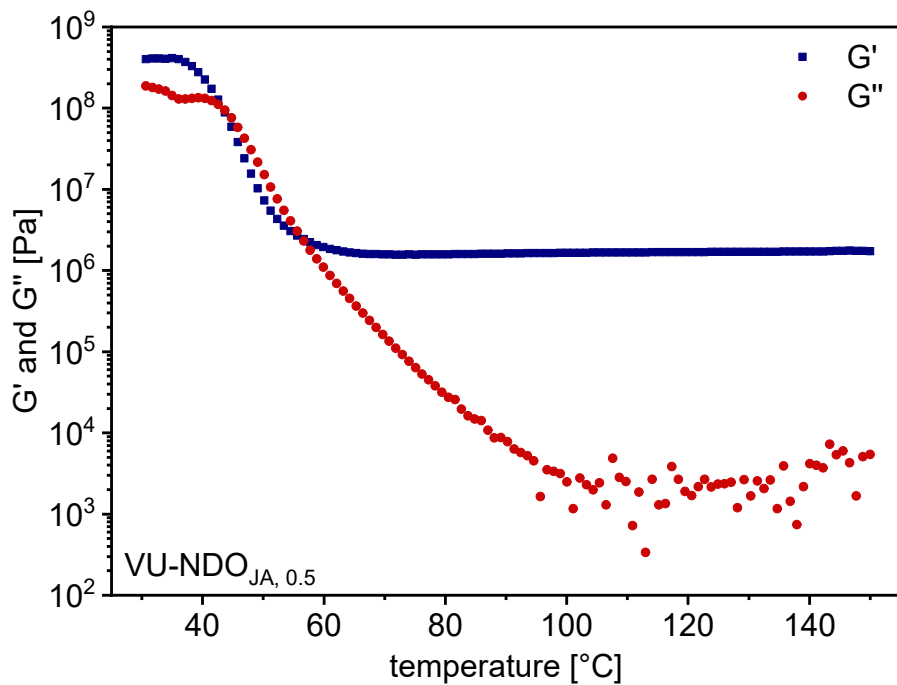


Fig. S37k Temperature-dependent DMA measurement ($\omega = 10 \text{ rad/s}$, $\gamma = 0.1 \%$) of VU-NDO_{JA, 0.5} in the temperature range of 30–150 °C, showing the storage- and loss modulus (G' and G'') with the characteristic rubbery plateau of the cross-linked material at elevated temperatures up to 150 °C.

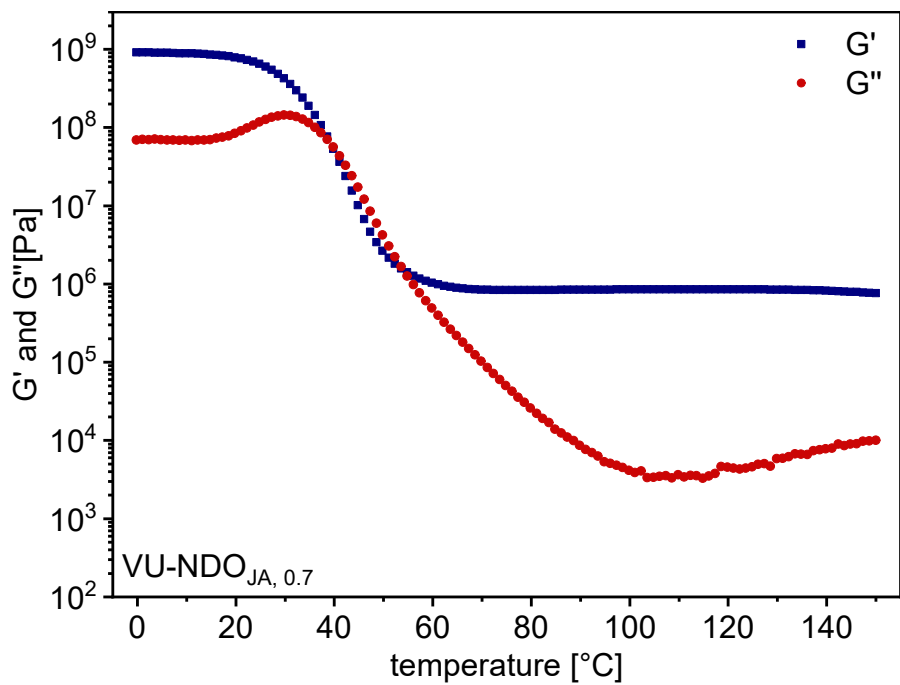


Fig. S37l Temperature-dependent DMA measurement ($\omega = 10 \text{ rad/s}$, $y = 0.1 \%$) of VU-NDO_{JA}, 0.7 in the temperature range of 0–150 °C, showing the storage- and loss modulus (G' and G'') with the characteristic rubbery plateau of the cross-linked material at elevated temperatures up to 150 °C

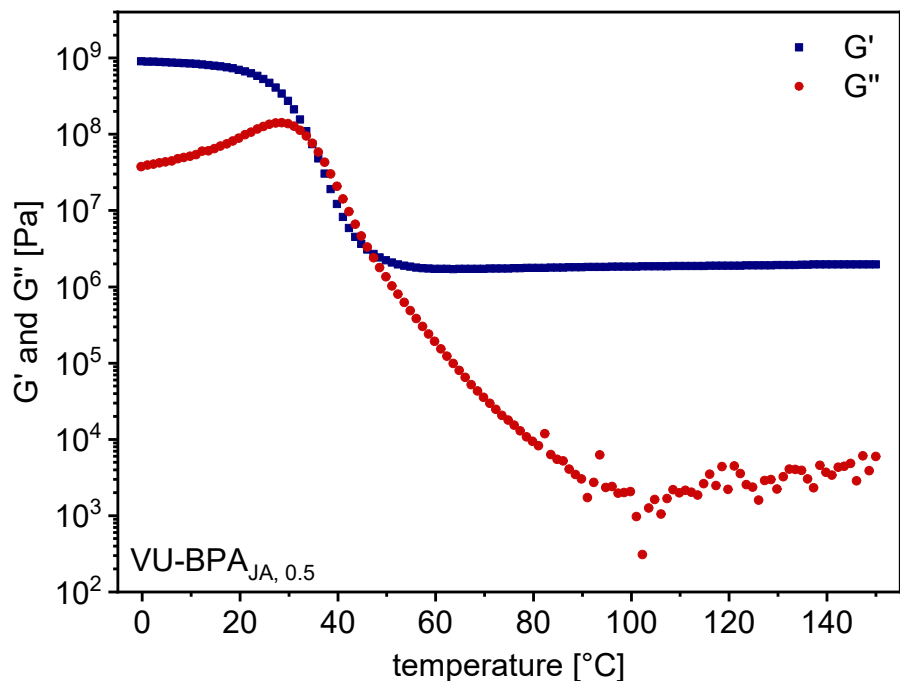


Fig. S37m Temperature-dependent DMA measurement ($\omega = 10 \text{ rad/s}$, $y = 0.1 \%$) of VU-BPA_{JA}, 0.5 in the temperature range of 0–150 °C, showing the storage- and loss modulus (G' and G'') with the characteristic rubbery plateau of the cross-linked material at elevated temperatures up to 150 °C.

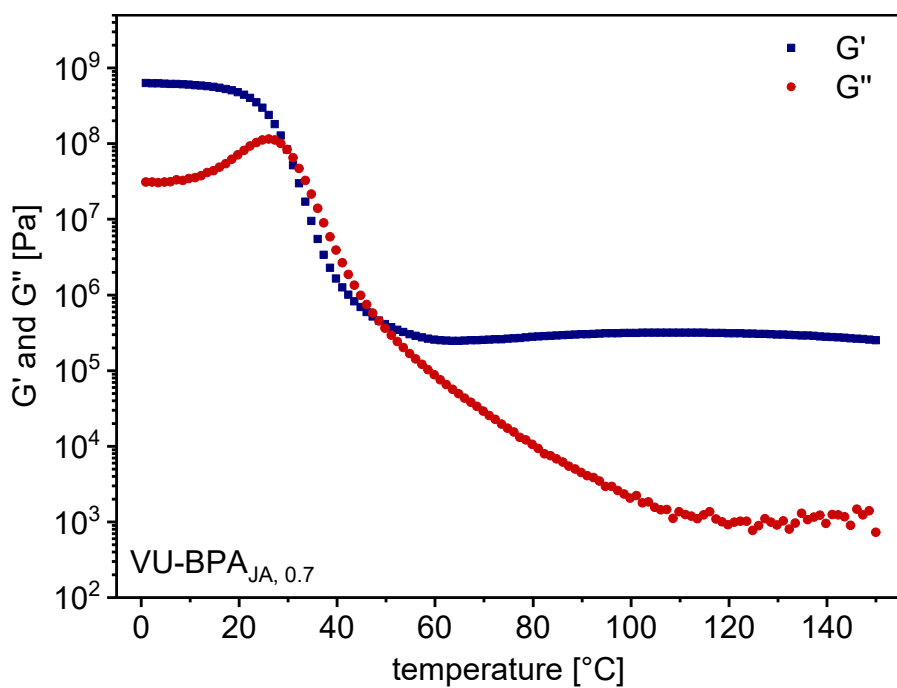


Fig. S37n Temperature-dependent DMA measurement ($\omega = 10 \text{ rad/s}$, $y = 0.1 \%$) of VU-BPA_{JA}, 0.7 in the temperature range of 0–150 °C, showing the storage- and loss modulus (G' and G'') with the characteristic rubbery plateau of the cross-linked material at elevated temperatures up to 150 °C.

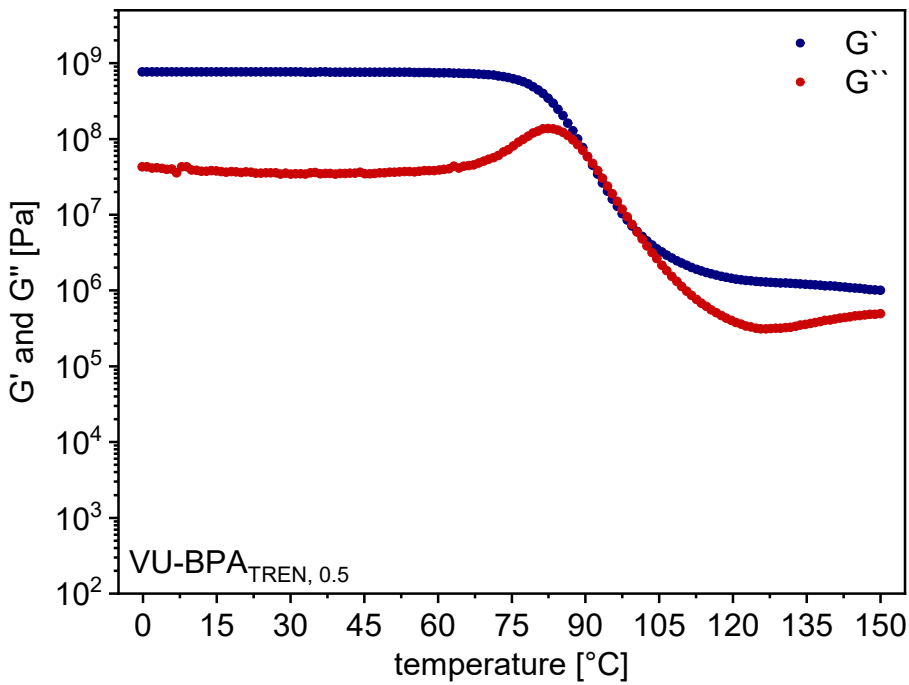


Fig. S37o Temperature-dependent DMA measurement ($\omega = 10 \text{ rad/s}$, $y = 0.1 \%$) of VU-BPA_{TREN}, 0.5 in the temperature range of 75–150 °C, showing the storage- and loss modulus (G' and G'') with the characteristic rubbery plateau of the cross-linked material at elevated temperatures up to 150 °C.

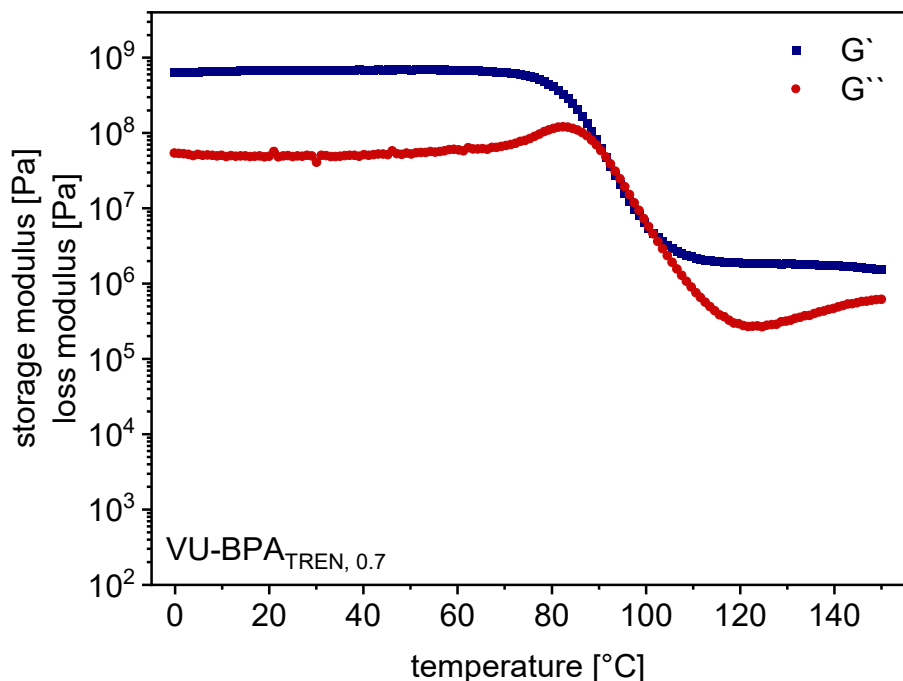


Fig. S37p Temperature-dependent DMA measurement ($\omega = 10$ rad/s, $y = 0.1\%$) of VU-BPA_{TREN, 0.7} in the temperature range of 75–150 °C, showing the storage- and loss modulus (G' and G'') with the characteristic rubbery plateau of the cross-linked material at elevated temperatures up to 150 °C.

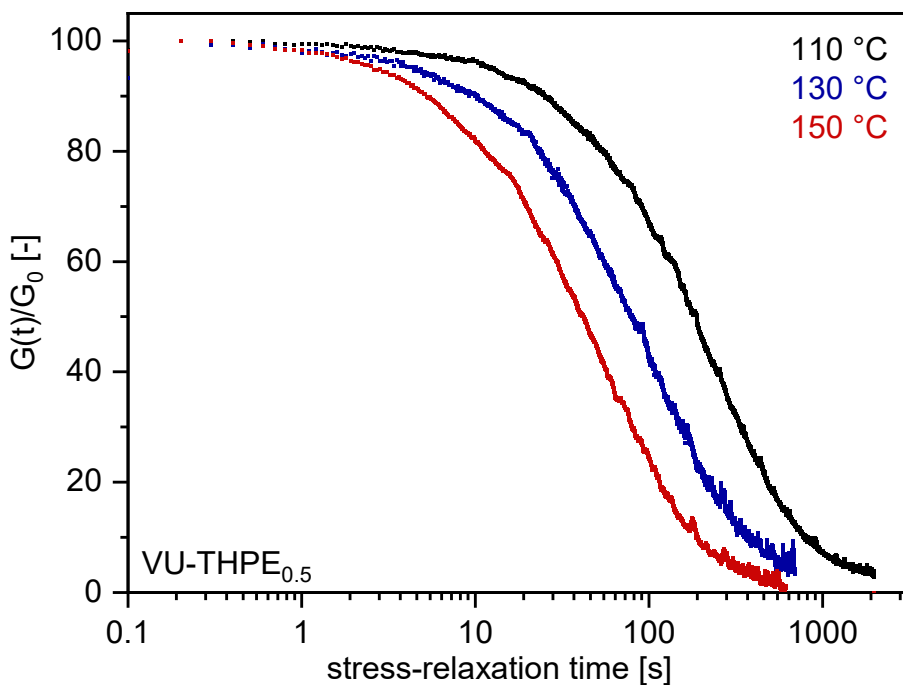


Fig. S38a Stress relaxation experiment of VU-THPE_{JA, 0.5}, plotting the normalized stress relaxation against the stress-relaxation time (DMA) measured at temperatures of 110, 130 and 150 °C.

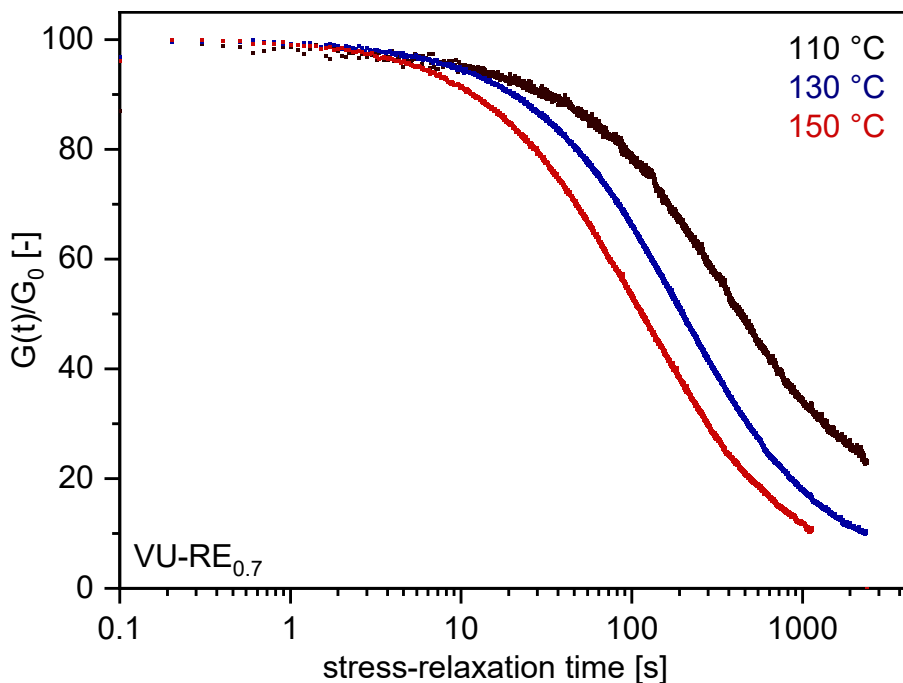


Fig. S38b Stress relaxation experiment of $\text{VU-RE}_{\text{JA}, 0.7}$, plotting the normalized stress relaxation against the stress-relaxation time (DMA) measured at temperatures of 110, 130 and 150 °C.

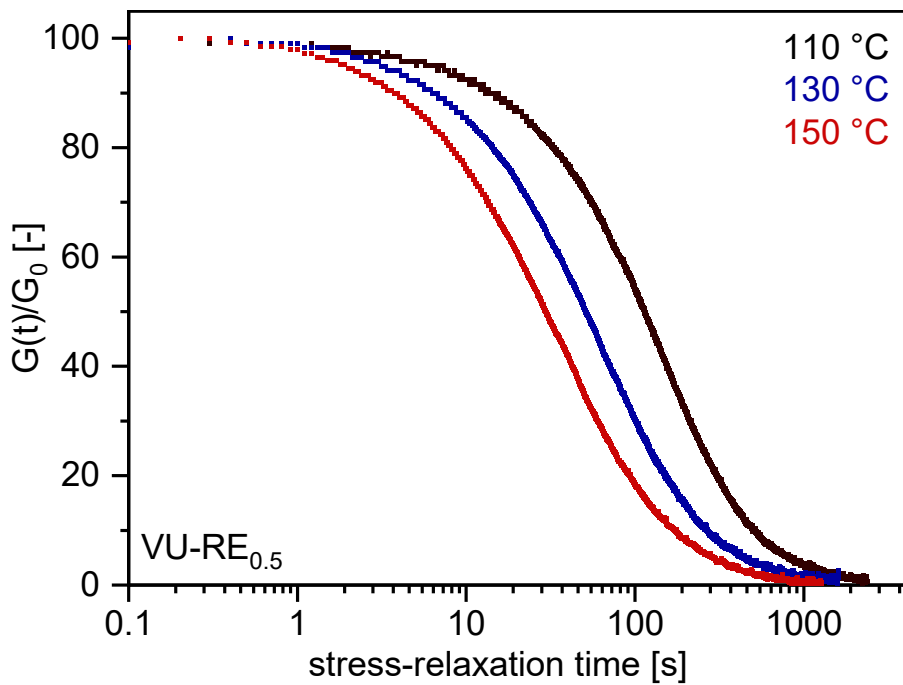


Fig. S38c Stress relaxation experiment of $\text{VU-RE}_{\text{JA}, 0.5}$, plotting the normalized stress relaxation against the stress-relaxation time (DMA) measured at temperatures of 110, 130 and 150 °C.

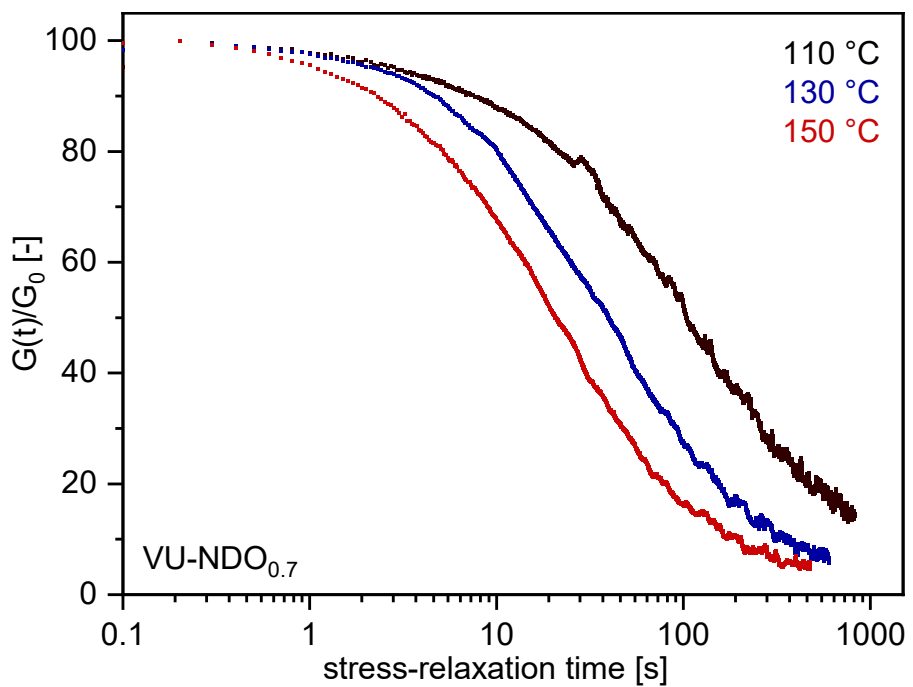


Fig. S38d Stress relaxation experiment of VU-NDO_{0.7}, plotting the normalized stress relaxation against the stress-relaxation time (DMA) measured at temperatures of 110, 130 and 150 °C.

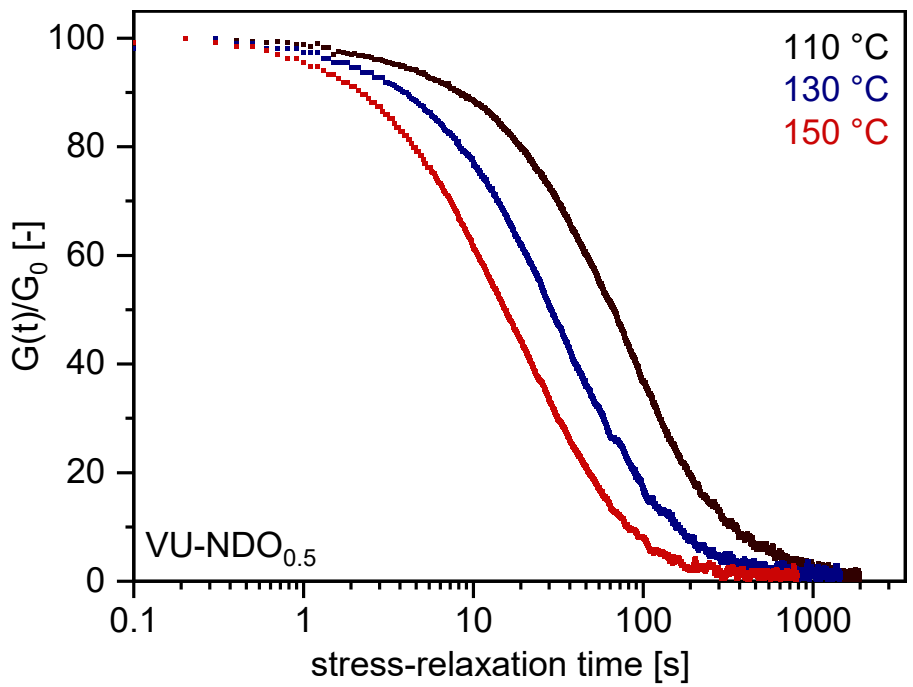


Fig. S38e Stress relaxation experiment of VU-NDO_{0.5}, plotting the normalized stress relaxation against the stress-relaxation time (DMA) measured at temperatures of 110, 130 and 150 °C.

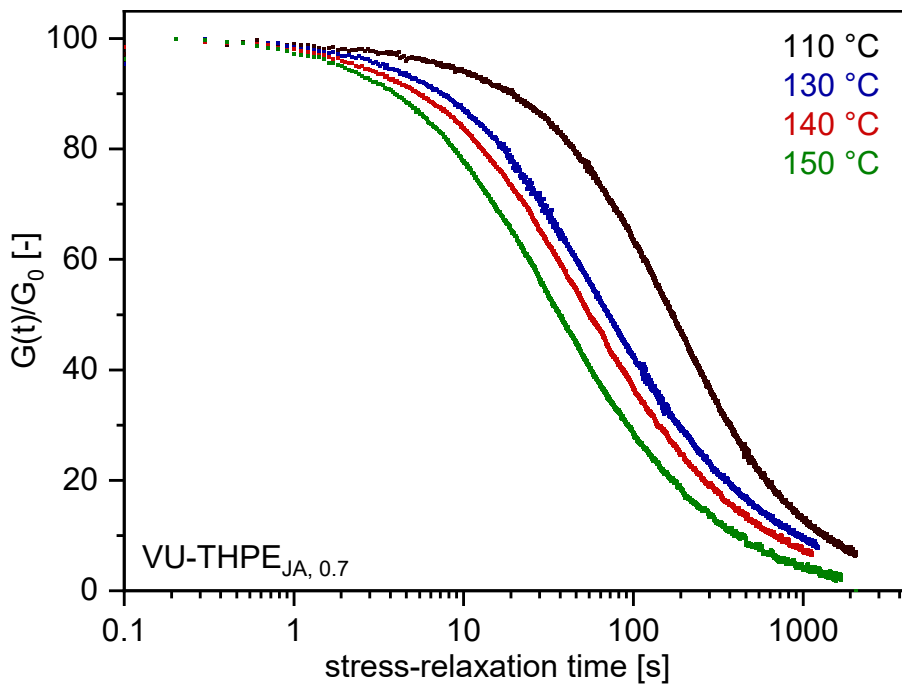


Fig. S38f Stress relaxation experiment of VU-THPE_{JA, 0.7}, plotting the normalized stress relaxation against the stress-relaxation time (DMA) measured at temperatures of 110, 130, 140 and 150 °C.

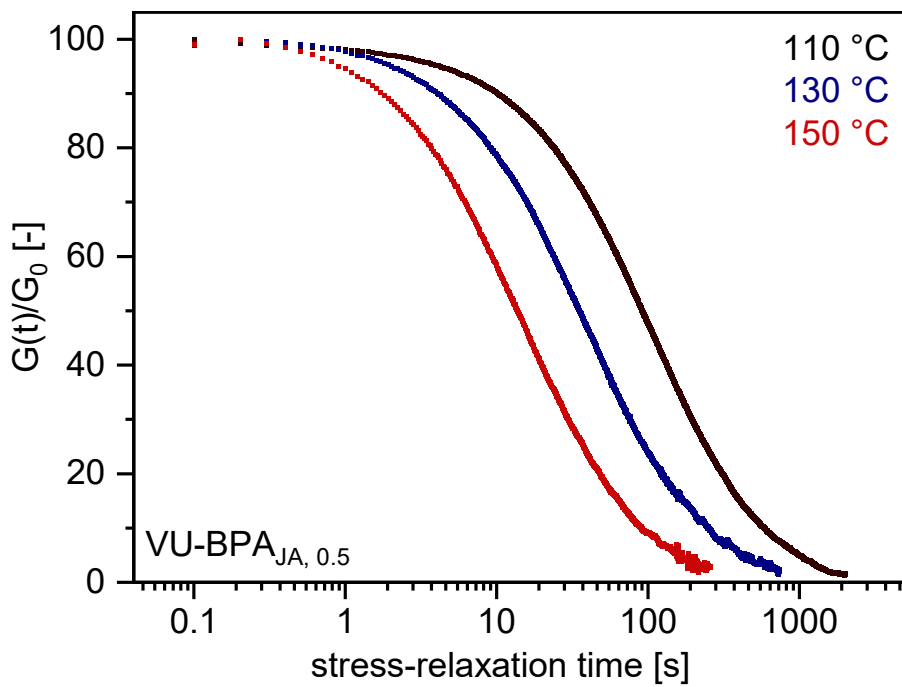


Fig. S38g Stress relaxation experiment of VU-BPA_{JA, 0.5}, plotting the normalized stress relaxation against the stress-relaxation time (DMA) measured at temperatures of 110, 130 and 150 °C.

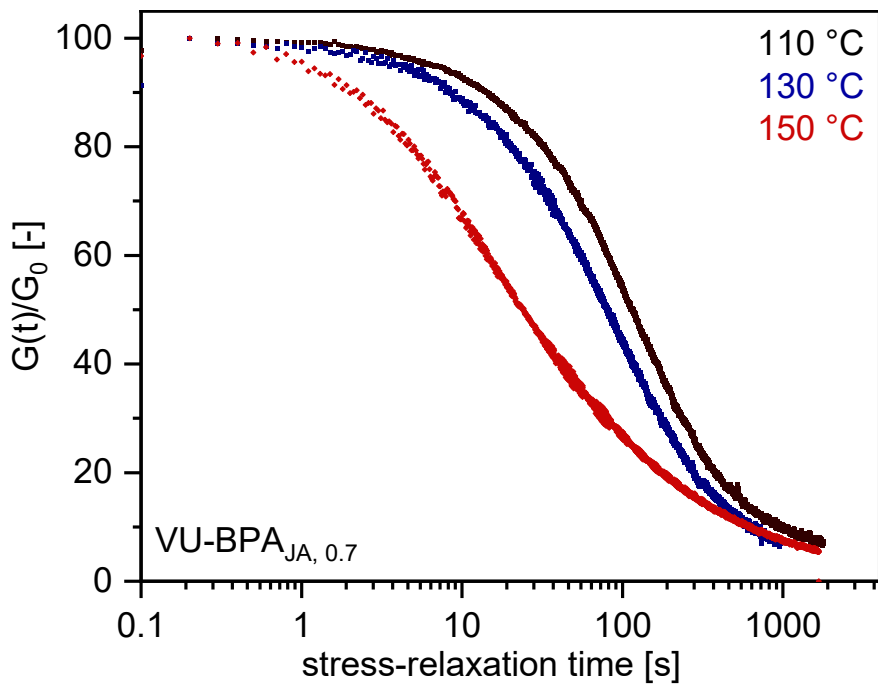


Fig. S38h Stress relaxation experiment of $\text{VU-BPA}_{\text{JA}, 0.7}$, plotting the normalized stress relaxation against the stress-relaxation time (DMA) measured at temperatures of 110, 130 and 150 °C

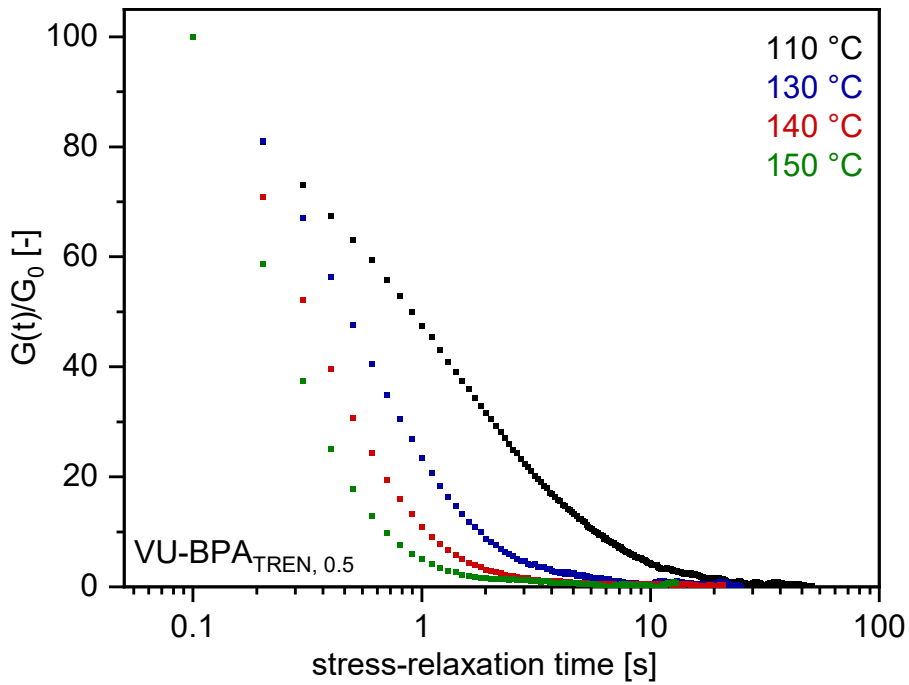


Fig. S38i Stress relaxation experiment of $\text{VU-BPA}_{\text{TREN}, 0.5}$, plotting the normalized stress relaxation against the stress-relaxation time (DMA) measured at temperatures of 110, 130 and 150 °C.

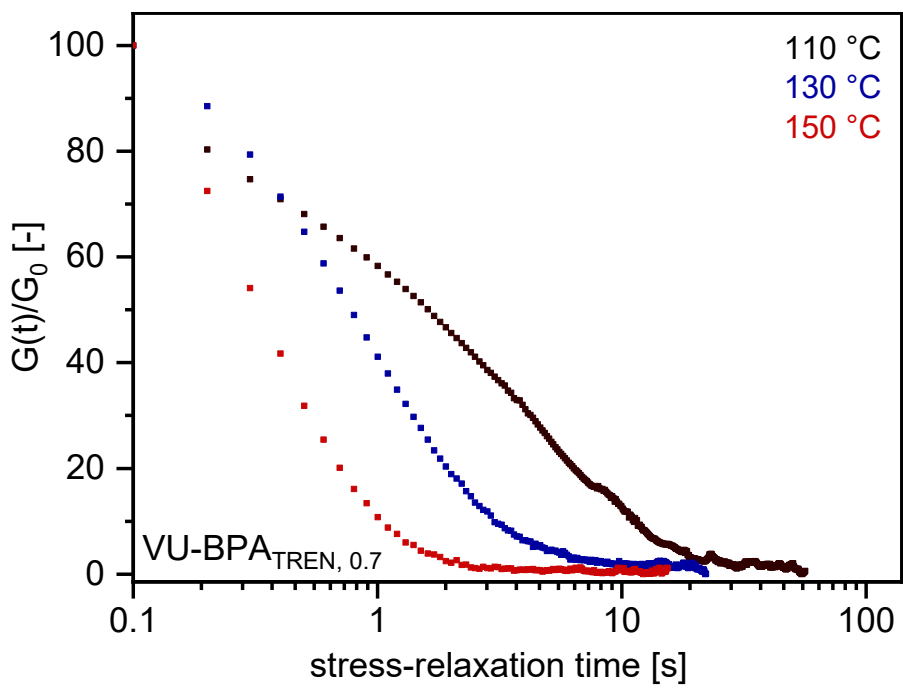


Fig. S38j Stress relaxation experiment of $\text{VU-BPA}_{\text{TREN}, 0.7}$, plotting the normalized stress relaxation against the stress-relaxation time (DMA) measured at temperatures of 110, 130 and 150 °C.

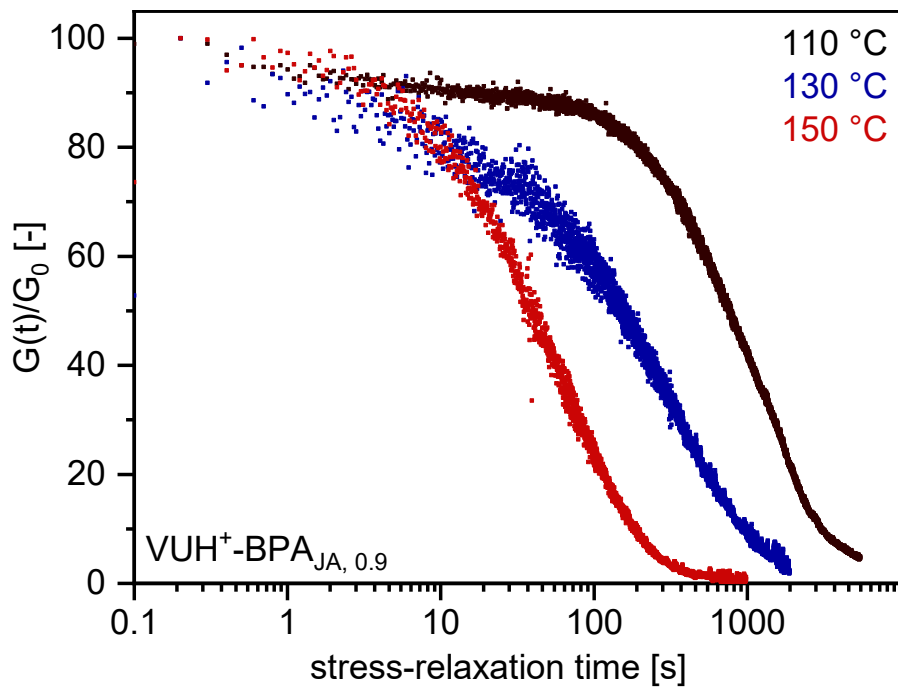


Fig. S38k Stress relaxation experiment of $\text{VUH}^+ \text{-BPA}_{\text{JA}, 0.9}$, plotting the normalized stress relaxation against the stress-relaxation time (DMA) measured at temperatures of 110, 130 and 150 °C.

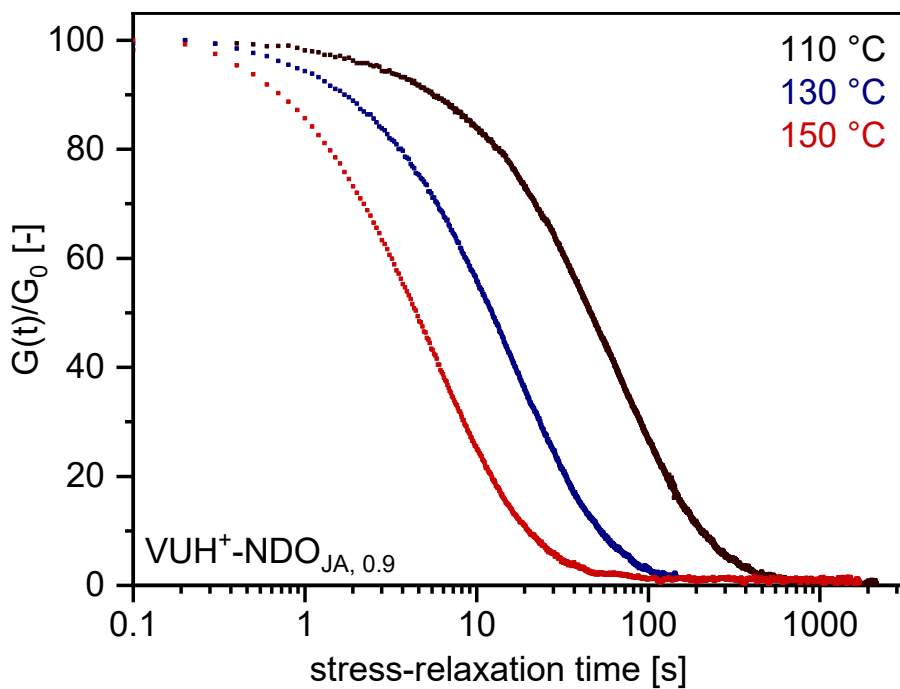


Fig. S38l Stress relaxation experiment of $\text{VUH}^+ \text{-NDO}_{\text{JA}, 0.9}$, plotting the normalized stress relaxation against the stress-relaxation time (DMA) measured at temperatures of 110, 130 and 150 °C.

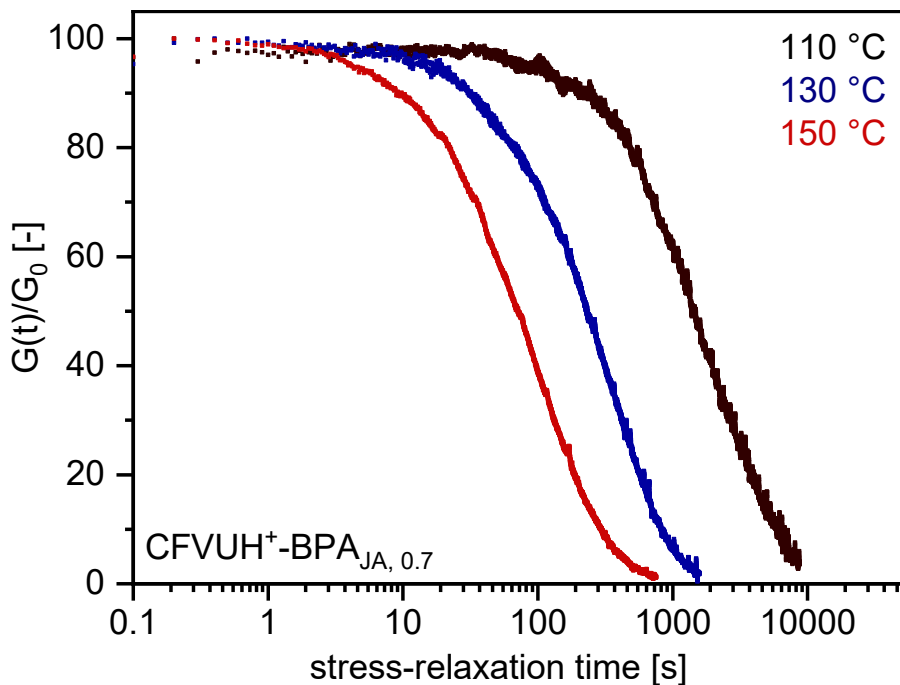


Fig. S38m Stress relaxation experiment of $\text{CFVUH}^+ \text{-BPA}_{\text{JA}, 0.7}$, plotting the normalized stress relaxation against the stress-relaxation time (DMA) measured at temperatures of 110, 130 and 150 °C.

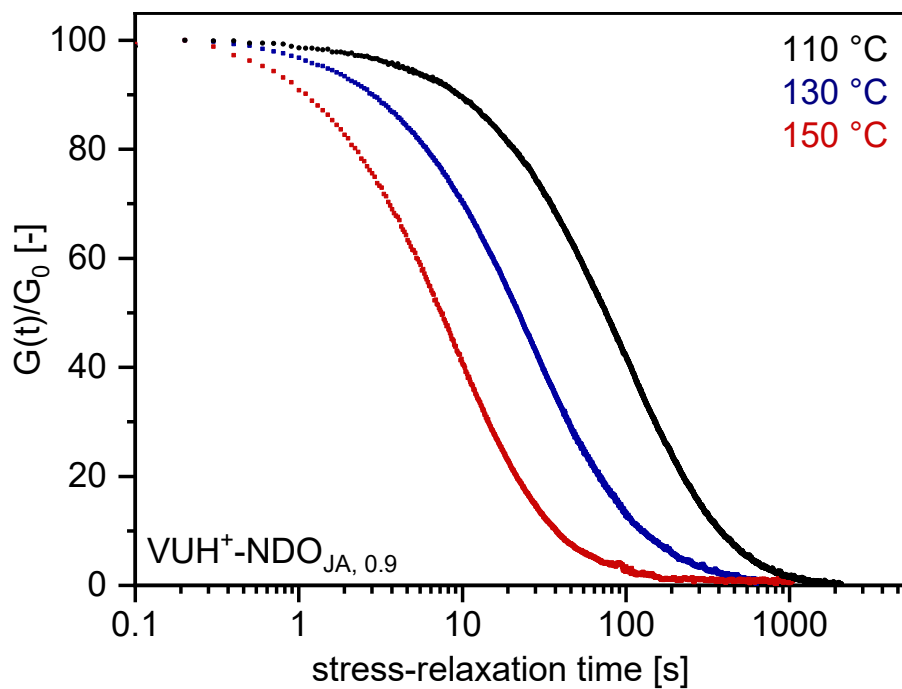


Fig. S38n Stress relaxation experiment of $\text{VUH}^+ \text{-NDO}_{\text{JA}, 0.9}$, plotting the normalized stress relaxation against the stress-relaxation time (DMA) measured at temperatures of 110, 130 and 150 °C.

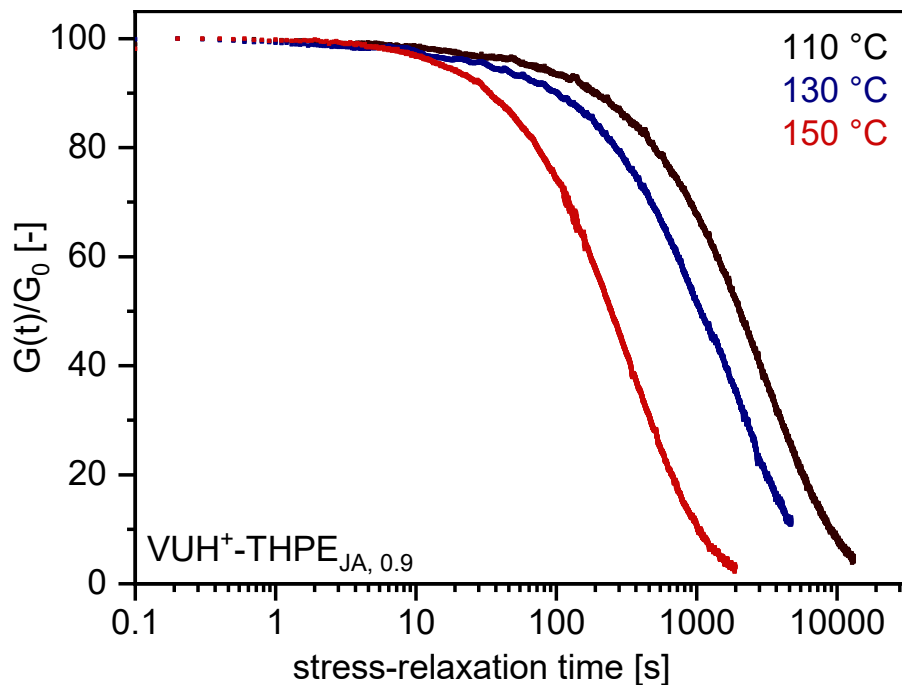


Fig. S38o Stress relaxation experiment of $\text{VUH}^+ \text{-THPE}_{\text{JA}, 0.9}$, plotting the normalized stress relaxation against the stress-relaxation time (DMA) measured at temperatures of 110, 130 and 150 °C.

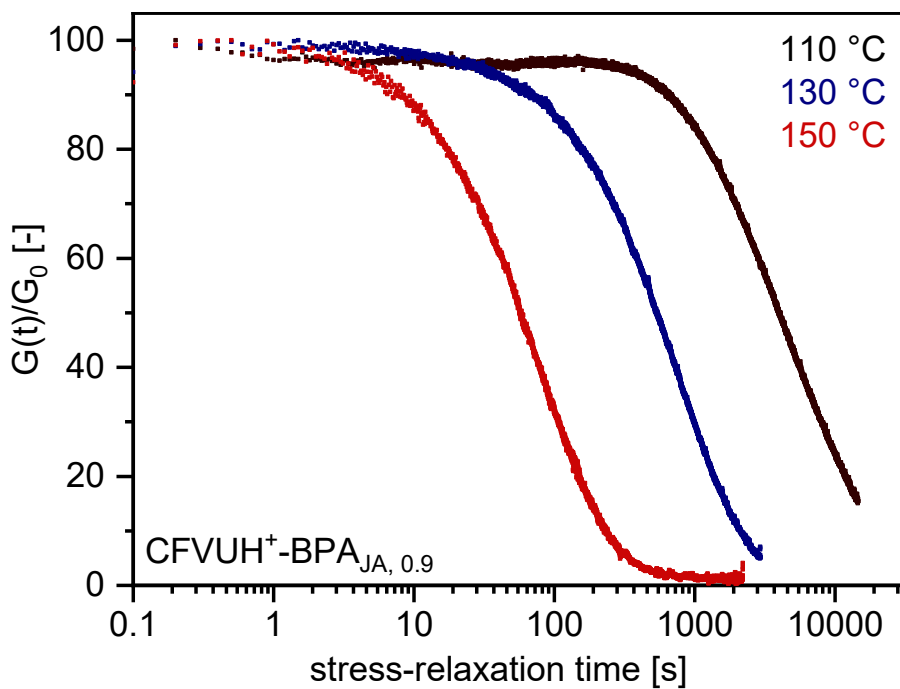


Fig. S38p Stress relaxation experiment of $\text{CFVUH}^+ \text{-BPA}_{\text{JA}, 0.9}$, plotting the normalized stress relaxation against the stress-relaxation time (DMA) measured at temperatures of 110, 130 and 150 °C.

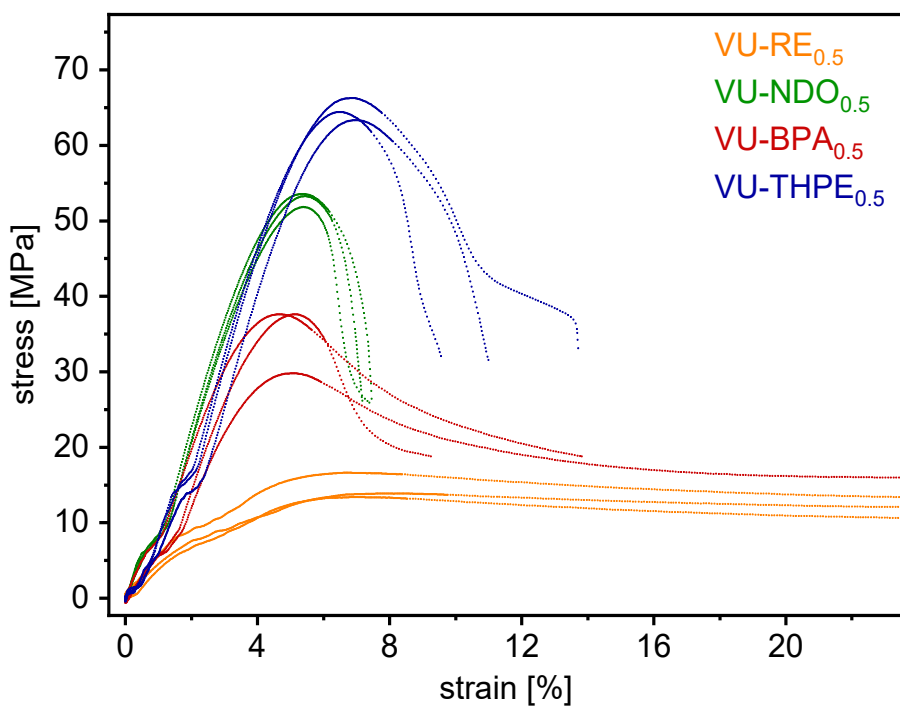


Fig. S39a Stress-strain measurements of the vitrimers $\text{VU-RE}_{\text{JA}, 0.5}$, $\text{VU-NDO}_{\text{JA}, 0.5}$, $\text{VU-BPA}_{\text{JA}, 0.5}$ and $\text{VU-THPE}_{\text{JA}, 0.5}$ with an acetoacetate to amine ratio of 0.5 at room temperature (the test was carried out at 10 mm min^{-1}).

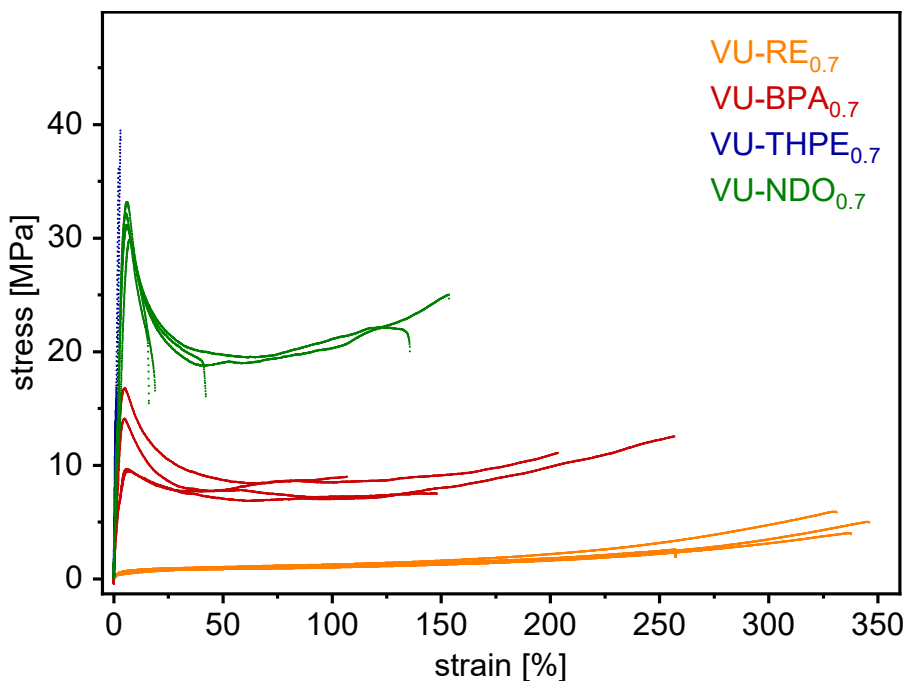


Fig. S39b Stress-strain measurements of the vitrimers VU-RE_{JA, 0.5}, VU-NDO_{JA, 0.5}, VU-BPA_{JA, 0.5} and VU-THPE_{JA, 0.5} with an acetoacetate to amine ratio of 0.7 at room temperature (the test was carried out at 10 mm min⁻¹).

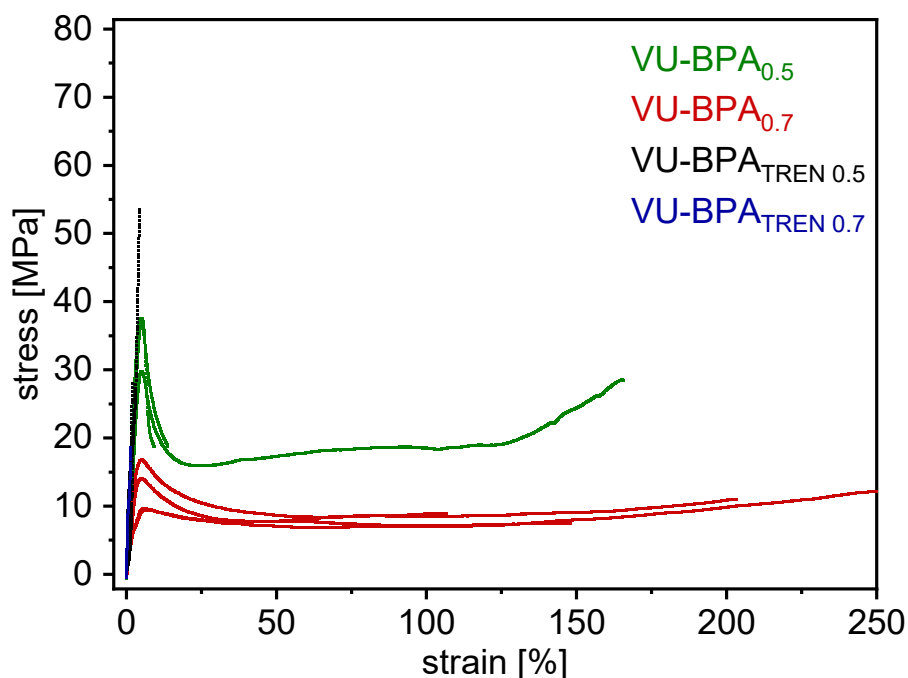


Fig. S39c Stress-strain measurements of the vitrimers VU-BPA cured with JA or TREN and acetoacetate to amine ratio of 0.5 or 0.7 at room temperature (the test was carried out at 10 mm min⁻¹).

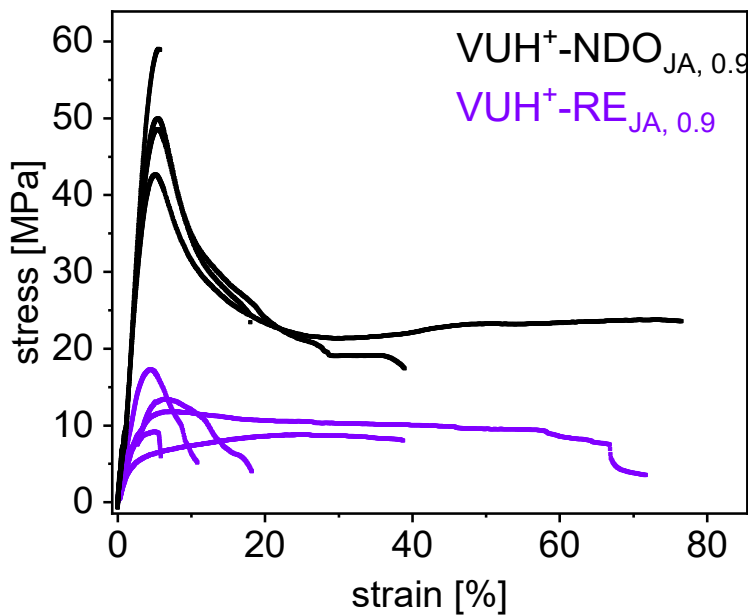


Fig. S39d Stress-strain measurements of the vitrimers $\text{VUH}^+ \text{-NDO}_{\text{JA}, 0.9}$ and $\text{VUH}^+ \text{-RE}_{\text{JA}, 0.9}$.

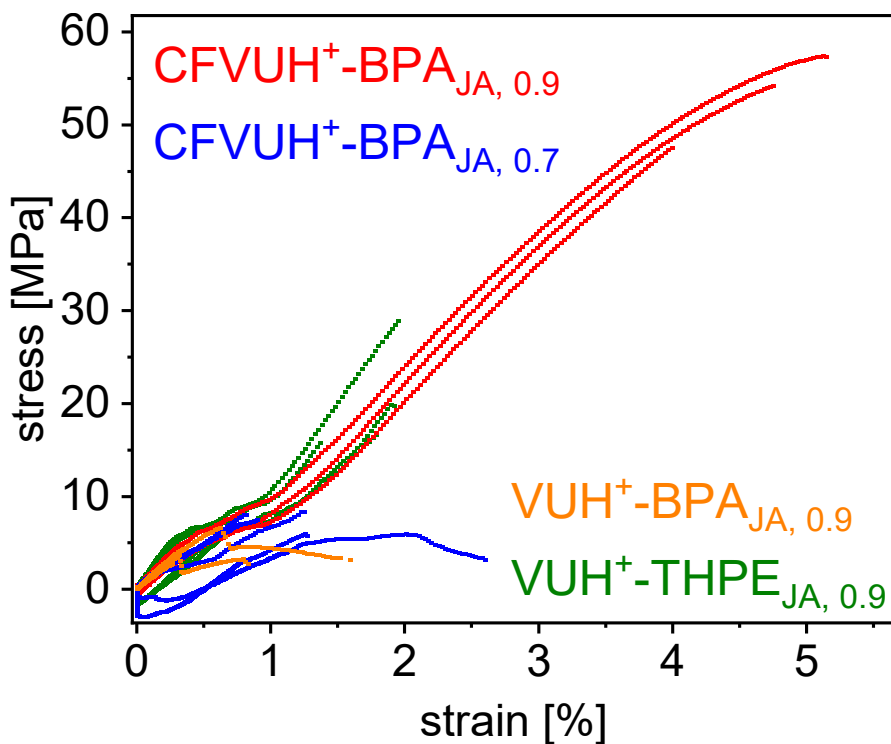


Fig. S39e Stress-strain measurements of the vitrimers $\text{CFVUH}^+ \text{-BPA}_{\text{JA}, 0.9}$, $\text{CFVUH}^+ \text{-BPA}_{\text{JA}, 0.7}$, $\text{VUH}^+ \text{-BPA}_{\text{JA}, 0.9}$ and $\text{VUH}^+ \text{-THPE}_{\text{JA}, 0.9}$.

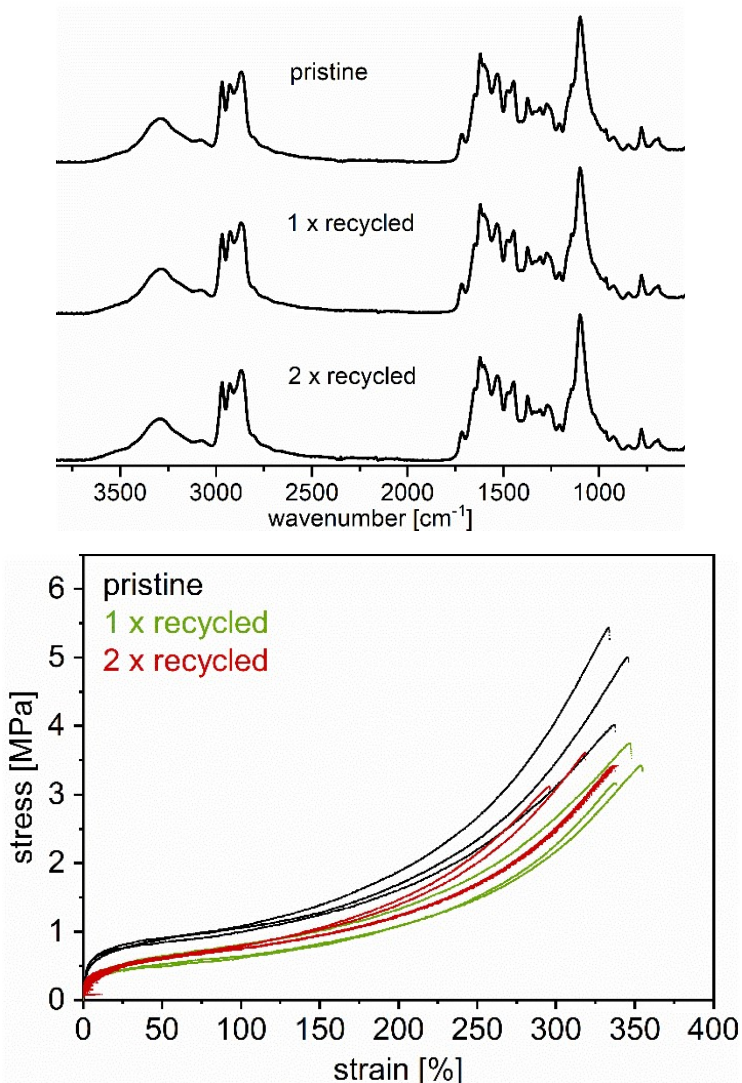


Fig. S40 Reprocessing cycles of the vitrimers by consecutive grinding and compression molding ($150\text{ }^\circ\text{C}$, 300 s), generating homogeneous, transparent, and bubble-free films (specimen) (top). Repetitive ATR-FT-IR spectra of the exemplary reprocessing cycles of the elastomeric vitrimer VU-RE_{0.7}, showing similar spectra after each cycle (middle). Repetitive stress-strain measurements of the exemplary reprocessing cycles of the elastomeric vitrimer VU-RE_{0.7}, showing a stable stress and strain behavior after a slight decrease after the first cycle (bottom).

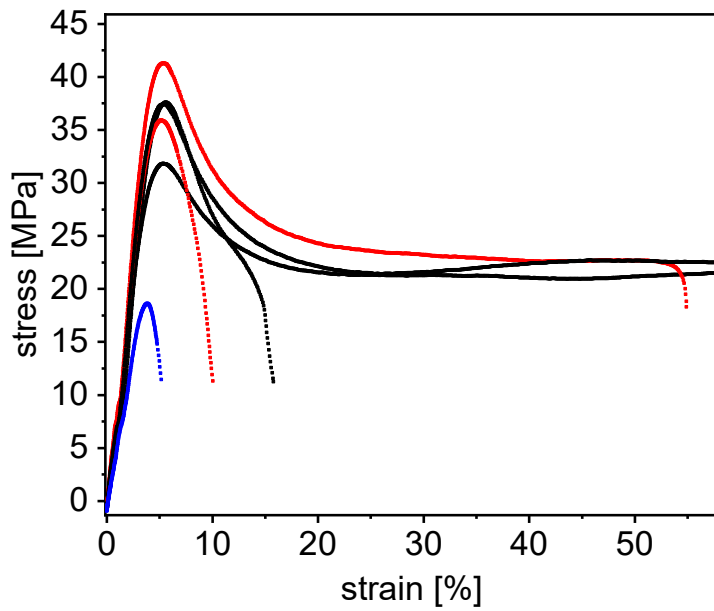


Fig. S41 Self-healing, exemplary showed for VU-RE_{JA, 0.5}. The DIN 5B bones were cut half and put into the oven for 30 minutes at 150 °C. Tensile tests show almost full recovery after the self-healing process (black: original, red: self-healed). The blue curve represents a sample which was not cured after cutting, showing significantly lower stress resistant.

References

- [1] W. Denissen, G. Rivero, R. Nicolaÿ, L. Leibler, J. M. Winne, F. E. Du Prez, *Advanced Functional Materials* **2015**, 25, 2451.